applied sciences

MDPI

Review

Nanomaterials in Photocatalysis: An In-Depth Analysis of Their Role in Enhancing Indoor Air Quality

Enrico Greco [1,2,3,4,*], Alessia De Spirt [1], Alessandro Miani [4,5], Prisco Piscitelli [6], Rita Trombin [7], Pierluigi Barbieri [1] and Elia Marin [8]

[1] Department of Chemical and Pharmaceutical Sciences, University of Trieste, via L. Giorgieri 1, 34127 Trieste, Italy; despirt.alessia@gmail.com (A.D.S.); barbierp@units.it (P.B.)
[2] National Interuniversity Consortium of Materials Science and Technology (INSTM), via G. Giusti 9, 50121 Firenze, Italy
[3] Institute for the Advanced Study of Culture and the Environment (IASCE), University of South Florida, 4202 E Fowler Avenue, Tampa, FL 33620, USA
[4] Società Italiana di Medicina Ambientale (SIMA), Viale di Porta Vercellina, 9, 20123 Milano, Italy; alessandro.miani@gmail.com
[5] Department of Environmental Science and Policies, University of Milan, via G. Celoria, 2, 20133 Milan, Italy
[6] Department of Experimental Medicine, University of Salento, via Monteroni, 73100 Lecce, Italy; prisco.piscitelli@unisalento.it
[7] Italian Academy of Biophilia (AIB), Lungadige Galtarossa 21, 37133 Verona, Italy; r.trombin@aibitalia.org
[8] Biomedical Engineering Laboratory, Kyoto Institute of Technology, Matsugasaki, Kyoto 606-8585, Japan; elia-marin@kit.ac.jp
* Correspondence: enrico.greco@units.it

Abstract: Since people spend most of their time in indoor environments, they are continuously exposed to various contaminants that threaten human health. The air quality in these settings is therefore a crucial factor in maintaining health safety. In order to reduce the concentration of indoor air pollutants and improve air quality, photocatalytic oxidation has drawn the attention of researchers. This study aims to provide a comprehensive view of the nanomaterials used in the photocatalytic oxidation of the most common pollutants in indoor environments. The effects of various parameters like humidity, airflow, deposition time, and light intensity were also evaluated, as they can significantly influence photocatalytic reactions. The most common nanomaterials used in photocatalysis are TiO_2-based and, in this study, they were classified and examined based on their morphology. TiO_2 doping with metals and non-metals has demonstrated an enhancement of its adsorption properties and photocatalytic efficiency for the removal of several pollutants. The role of carbon-based nanomaterials in photocatalysis was also evaluated due to their adsorption capabilities towards various pollutants. In addition, other less common photocatalysts such as ZnO, MnO_2, WO_3, CeO_2, and CdS also exhibited high photocatalytic activity for pollutant degradation. Applications of these photocatalysts in air purifiers, paints, and building materials e.g., concrete, glass, and wallpapers, lead to efficient reduction of pollutants in indoor settings.

Keywords: photocatalysis; nanomaterials; indoor air quality (AIQ); titanium dioxide (TiO_2); volatile organic compounds (VOCs); photocatalytic oxidation; doping techniques; reactive oxygen species (ROS); environmental remediation; semiconductor photocatalysis

Academic Editors: Xiaosi Qi and Changyong Lan

Received: 8 January 2025
Revised: 28 January 2025
Accepted: 4 February 2025
Published: 6 February 2025

Citation: Greco, E.; De Spirt, A.; Miani, A.; Piscitelli, P.; Trombin, R.; Barbieri, P.; Marin, E. Nanomaterials in Photocatalysis: An In-Depth Analysis of Their Role in Enhancing Indoor Air Quality. *Appl. Sci.* **2025**, *15*, 1629. https://doi.org/10.3390/app15031629

1. Introduction

Indoor environments, such as homes, schools, and offices, account for approximately 90% of the time spent by individuals [1], making indoor air quality (IAQ) [2] a critical factor

for human health. Prolonged exposure to various gaseous compounds in these settings has necessitated a deeper understanding of IAQ to ensure health safety. Indoor spaces are characterized by a wide range of pollutant sources that continuously release contaminants, including volatile organic compounds (VOCs) [3], nitrogen oxides (NO_x) [4], non-biological particulate matter (PM) [5], and biological agents like bacteria and fungi [6,7]. These pollutants, even at low concentrations, can accumulate over time and contribute to a decline in IAQ, posing significant risks to human health. Long-term exposure to these hazardous compounds can lead to mild symptoms such as headaches, nausea, and skin irritation, while higher exposure levels have been linked to severe respiratory and cardiovascular diseases, organ damage, cancer, and even premature mortality [8–10]. As such, maintaining IAQ in indoor environments is essential to safeguard human well-being [11].

A variety of strategies have been developed to mitigate the risks associated with poor IAQ, with photocatalytic oxidation emerging as a promising approach due to its ability to degrade pollutants using light irradiation and photocatalytic materials [12]. This process has gained considerable attention for its potential to effectively eliminate diverse indoor air contaminants. Research has predominantly focused on the development of nanomaterials that serve as efficient photocatalysts, with titanium dioxide (TiO_2) standing out among semiconductors for its remarkable properties in the oxidative degradation of VOCs and NO_x [13]. Studies have extensively investigated the photocatalytic activity of TiO_2, examining its various morphologies—such as nanoparticles, nanotubes, and nanosheets—and the impact of modifications like doping and heterojunction formation on enhancing its pollutant degradation capabilities [14].

Beyond TiO_2, other nanomaterials have been explored for their roles in photocatalytic oxidation, either as pollutant adsorbents or as active photocatalysts. Carbon-based nanomaterials [15], including carbon nanotubes and graphene, have garnered significant interest due to their exceptional adsorption properties and versatile structural characteristics. Furthermore, less commonly used nanomaterials, such as zinc oxide (ZnO) [16] and tungsten oxide (WO_3) [17], have also been investigated to expand the range of photocatalytic oxidation applications.

The integration of these nanomaterials into real-world applications, such as building materials, paints, and air purification systems, has demonstrated their efficacy in reducing indoor pollutants and providing antimicrobial benefits. By making use of these innovative materials, substantial improvements in IAQ can be achieved, promoting healthier indoor environments.

2. Indoor Environments

Sick Building Syndrome (SBS) has become an increasingly recognized health issue, affecting individuals who experience a range of symptoms such as headaches, nausea, skin irritation, and general weakness [18–20]. These symptoms are commonly linked to prolonged exposure to poor indoor air quality (IAQ), highlighting the significance of building environments on human well-being. Pollutants contributing to SBS can originate from both indoor and outdoor sources, with outdoor contaminants—such as vehicle emissions [21], dust re-suspension [22], and combustion fumes [23]—often being transported into buildings, further degrading IAQ. While similar pollutant concentrations might be observed indoors and outdoors due to air exchange, indoor environments frequently have poorer air quality due to the presence of additional contaminants emitted from building materials [24], furnishings [25], and human activities.

The IAQ of indoor environments is also greatly influenced by factors such as their geographic location and structural design. Urban areas, with their dense road traffic and specific building materials, tend to have higher pollution levels. The compact layout of

urban buildings can create a stagnation effect that hinders air circulation, leading to the accumulation of pollutants. In contrast, rural areas experience different IAQ challenges, primarily stemming from the burning of biomass and coal for cooking and heating. These variations underscore the complex dynamics of IAQ, which depend on both external and internal factors within different settings. These variations underscore the complex dynamics of IAQ, which depend on both external and internal factors within different settings. To better understand the influence of these factors, it is essential to examine IAQ across a range of specific environments, including residential spaces like houses and apartments [26], offices [27] and commercial buildings [28], industrial environments [29], public indoor spaces such as museums [30], hospitals [31], and schools [32], and public transportation systems like buses [33], trains [34], and airplanes [35].

The main indoor environments, the key points about the air quality and relative references are presented in Table 1:

Table 1. Category of indoor environments, key points, and relevant references.

Category	Key Points	Ref.
Residential	Key factors include heating systems, building materials, age of buildings, and ventilation systems.	[24,36–43]
	Urban homes are prone to outdoor pollutants (e.g., NO_x, SO_2, PM) infiltrating indoor spaces.	
	Poor Indoor Air Quality (IAQ) results from both indoor and outdoor pollutants, including vehicle emissions, dust, and combustion fumes.	
	COVID-19 lockdowns increased indoor pollutant exposure (e.g., VOCs, particulate matter, microbes).	
	Prolonged confinement and remote work highlighted the need for healthy IAQ and pollutant control in homes	
Offices and commercial settings	Like for residential buildings, IAQ in offices affects health and well-being, but also productivity.	[44–51]
	Common pollutants include VOCs from office equipment (e.g., printers, copiers), PM, CO_2, and biological contaminants.	
	Pollutant sources include furnishings, cleaning agents, air fresheners, and external urban pollutants.	
	Poorly maintained HVAC systems, more common in commercial settings, exacerbate IAQ issues.	
	Good IAQ improves cognitive function, reduces absenteeism, and aligns with corporate social responsibility goals.	
	Investment in IAQ offers health and economic benefits	
Industrial Environments	High pollutant concentrations due to manufacturing, machinery, and chemical use.	[52–57]
	Key pollutants: PM, VOCs, heavy metals, CO, SO_2, NO_x, and biological contaminants.	
	PM originates from material handling, grinding, cutting, and welding.	
	VOCs are released during painting, coating, and solvent use.	
	Combustion processes emit CO and NO_x, posing severe health risks.	
	Strategies include compliance with occupational health standards and improved air quality management.	

Table 1. *Cont.*

Category	Key Points	Ref.
Publication transportation	IAQ in public transport depends on factors like vehicle type (e.g., buses, trains, subways), ventilation, passenger density, and outdoor pollution exposure.	[58–63]
	Pollutants: PM, CO_2, VOCs, NO_x, and biological contaminants.	
	Subways in particular have higher levels of PM due to friction from brakes, wheels, and rails.	
	Buses and trains are exposed to outdoor pollution often allow infiltration of vehicle emissions.	
	Crowded conditions increase bioaerosol concentrations (e.g., bacteria, viruses).	
	Solutions include effective ventilation, air purification systems, and regular cleaning.	

3. Common Volatile Organic Compounds

Volatile Organic Compounds (VOCs) constitute a broad category of organic chemicals distinguished by their high volatility, making them predominantly present in the gaseous state at room temperature [36]. Common VOCs identified in indoor environments include carbonyl compounds (e.g., formaldehyde, acetaldehyde, acetone), aliphatic hydrocarbons (e.g., hexane, cyclohexane, isoprene), aromatics (e.g., benzene, toluene, xylene), and alcohols (e.g., ethanol, methanol, isopropanol). These compounds represent the primary pollutants in indoor settings and originate from a variety of sources both indoors and outdoors. Key sources of these pollutants include combustion processes, furniture, building materials, paints, and cleaning products, although specific sources may vary depending on the compound. Indoor concentrations of VOCs are generally higher than those outdoors, particularly during colder seasons when heating use increases, and ventilation decreases [37].

Exposure to VOCs in indoor environments (Table 2) poses significant health risks, especially given that individuals spend a substantial portion of their time indoors. Research has established that VOCs can exert a profound impact on human health, causing symptoms ranging from eye and throat irritation, headaches, and nausea to more severe effects such as respiratory issues and cancer [38].

Table 2. List of common VOCs that can be found in indoor environments, along with their most common known effects on health.

Substance	Found in	Effects	References
Benzene	Cigarette smoke, cleaning products, building materials, furniture, heating systems	Headaches, insomnia, nausea, fatigue, acute myeloid leukemia and genotoxic effects. Chronic exposure can be fatal	[39–41]
Ethylene glycol	Antifreeze and de-icing solutions, paints, cleaning agents	Headaches, dizziness, metabolic acidosis, kidney damage. Chronic exposure can lead to respiratory issues and central nervous system effects	[42–44]
Formaldehyde	Combustion, wooden furniture, textiles, insulating materials, paints, wallpapers, and adhesives	Headaches, dizziness, nausea, eye and skin irritation, nasal tumors, chronic bronchitis	[45–47]
Acetaldehyde	silvering of mirrors, chemical in the paper industry, fuel mixtures, glue production and denaturant for alcohol	Irritation of eyes, nose, throat and respiratory tract, drunkenness, chronic respiratory irritation, upper respiratory tract cancer, chemical burns	[48–50]

Table 2. *Cont.*

Substance	Found in	Effects	References
Methylene chloride	Paint strippers, adhesives, and aerosol products	Dizziness, headaches, nausea, central nervous system depression and cancer	[51–53]
Tetrachloroethylene	Solvent in dry cleaning and degreasing	Dizziness, headaches, nausea respiratory problems, kidney damage and cancer	[54–56]
Toluene	Solvent in coatings and paints	Nausea, headache, vertigo, detrimental effects on the nervous system, kidney and liver	[57–59]
Xylene	solvent used in the printing, rubber, and leather industries, paints, varnishes, and cleaning agents	Headaches, dizziness, and respiratory issues upon exposure. May affect the central nervous system, liver and kidney damage	[60–62]
1,3-Butadiene	used in the production of synthetic rubber and plastics	respiratory irritation and headaches, increased risk of cancer	[63–65]
Glycol Ethers	solvents commonly found in paints, cleaning agents, and coatings	respiratory irritation and reproductive toxicity	[66–68]
Limonene and other "green" products	fragrances, cleaning products, solvents	Respiratory irritation, allergic reactions	[69–71]
NO_x	combustion of fossil fuels	Respiratory irritation, decreased lung function, increase susceptibility to infections, chronic respiratory diseases, cardiovascular problems	[72–74]

4. Photocatalytic Oxidation

Among the various methods available to reduce pollutant concentrations in indoor environments, photocatalytic oxidation has emerged as a particularly promising approach in recent years [75,76]. This technique is a type of advanced oxidation process (AOP) that utilizes the high reactivity of oxygen species in oxidation/reduction reactions. These reactions are facilitated through the interaction of the target pollutant with a photocatalyst and light irradiation, offering the advantage of not requiring the addition of external compounds like H_2O_2. Heterogeneous photocatalysis, in particular, has been extensively studied for its application in purifying indoor air, as it typically involves the removal of gaseous pollutants using the surface of a semiconductor, such as transition metal oxides [77]. In semiconductors, the valence band and the conduction band are separated by a specific band gap width. When the semiconductor surface is irradiated with light of sufficient energy, electrons are excited from the valence band to the conduction band, initiating photocatalytic reactions. The effectiveness of photocatalytic oxidation is influenced by the properties of the semiconductor used, such as its adsorption capacity and band gap width. Additionally, external factors like humidity, light intensity, pollutant concentration, and airflow significantly affect the process's efficiency [78].

4.1. Mechanism

Photocatalytic oxidation reactions are activated when the semiconductor surface is irradiated with photons with energy equal to or greater than the semiconductor band gap. The semiconductor absorbs the photons, promoting the excitation of electrons from the valence band to the conduction band of the semiconductor. Consequently, photogenerated electrons are obtained in the conduction band, while positively charged holes are formed in the valence band. These electron-hole pairs are generated within femtoseconds, setting the stage for subsequent chemical reactions [78].

In the second step, the photogenerated electrons are transferred to the semiconductor surface. Electrons and holes can directly react with the pollutants through oxidation/reduction reactions, or they can reduce electron acceptors or oxidize electron donors,

respectively. Specifically, photogenerated electrons and holes can interact with nearby H_2O and O_2 molecules to form reactive oxygen species (ROS) such as hydroxyl radicals and superoxide ions. The reduction of O_2 leads to the formation of the superoxide ion ($O_2 \cdot^-$), while the hydroxyl radical (·OH) is obtained by the ionization of H_2O. Pollutant molecules are then adsorbed onto the active sites on the surface of the photocatalyst, where they can react with these ROS. Pollutants are primarily oxidized by the hydroxyl radicals derived from the oxidation of adsorbed H_2O or adsorbed hydroxide ions (OH^-). The main products of photocatalytic oxidation are CO_2 and H_2O, but it is crucial to limit the formation of minor by-products, as these can also be hazardous compounds or reduce the efficiency of photocatalysis. By-products can occupy the active sites of the photocatalyst, thereby limiting access to the target pollutants [79].

The general photocatalytic oxidation reaction for the degradation of a pollutant can be expressed as described in Table 3 and as follows:

$$\text{Pollutant} + O_2 \rightarrow CO_2 + H_2O + \text{By\_products}$$

Table 3. Reactions occurring during photocatalytic oxidation [80].

Reaction Type	Reaction
Photoexcitation	$\text{Semiconductors} + hv \rightarrow h^+ + e^-$
Oxidation reaction	$OH^- + h^+ \rightarrow \cdot OH$
Reduction reaction	$O_2 + e^- \rightarrow O_2^- \cdot$
Ionization of water	$H_2O \rightarrow OH^- + H^+$
Protonation of superoxide	$O_2^- \cdot + H^+ \rightarrow HOO \cdot$
Formation of H_2O_2	$HOO \cdot + H^+ \rightarrow H_2O_2$

The electron-hole pairs can react with each other through recombination on the surface or within the bulk of the semiconductor. This recombination process reduces the efficiency of photocatalytic reactions because it decreases the number of electrons and holes available for participation in oxidation/reduction reactions that generate reactive oxygen species (ROS) [81]. Recombination of electron-hole pairs occurs within tens of nanoseconds. Hydrogen peroxide (H_2O_2), produced during the reactions, acts as an oxidizing agent capable of trapping photogenerated electrons, thereby diminishing the rate of charge carrier recombination.

When the recombination of charge carriers occurs, it releases a certain amount of energy, which can be detected as a photoluminescence emission spectrum. There are two primary types of photoluminescence: band gap photoluminescence, which pertains to the separation of photogenerated charge carriers [82], and excitonic photoluminescence, which provides insights into oxygen vacancies and surface defects [83]. By analyzing excitonic photoluminescence, researchers can deduce other factors affecting photocatalysis, such as the efficiency of electron trapping and transfer. Consequently, the photoluminescence spectrum serves as an indicator of the recombination rate: a low intensity suggests minimal charge carrier recombination, indicating enhanced photocatalytic activity, while a high intensity signifies a high recombination rate [84].

For example, (Figure 1A), the photoluminescence spectrum of P25 TiO_2 reveals a high recombination rate, as evidenced by the peak's high intensity. In contrast, another sample (USPNT) shows significantly lower photoluminescence intensity, indicating a reduced recombination rate. The largest peak in the photoluminescence spectrum, often associated with band gap photoluminescence, corresponds to the radiation energy nearly equal to the band gap of the sample. Additional peaks within a specific wavelength range may correspond to excitonic photoluminescence associated with surface defects and oxygen vacancies.

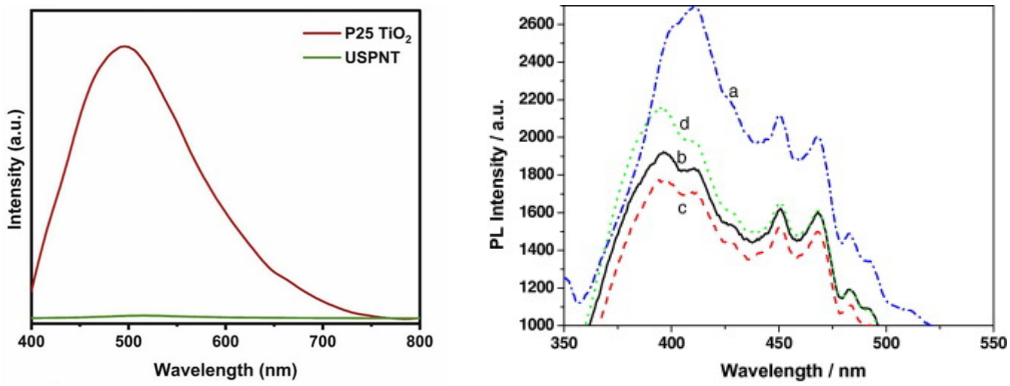

(**A**) (**B**)

Figure 1. (**A**) photoluminescence spectra of P25 TiO_2 and USPNT [85] and (**B**) Photoluminescence spectra of P25 (a) and Au–TiO_2 containing various amounts of Au (b–d) [86].

In another example, the largest peak in the photoluminescence spectrum (Figure 1B) at about 395 nm is associated with the band gap photoluminescence and the corresponding radiation energy is almost equal to the band gap of the sample. The other four peaks between 440 and 500 nm correspond to the excitonic photoluminescence and are associated with the oxygen vacancies and defects of the sample surface.

4.2. Thermodynamics and Kinetics

As previously noted, photocatalysts absorb radiation with sufficient energy to excite electrons from the valence band to the conduction band, resulting in the generation of photogenerated electrons in the conduction band and positively charged holes in the valence band. The transfer of holes from the valence band to water molecules is enhanced when the edge of the valence band is more positive than the oxidation potential of water. Similarly, the transfer of electrons from the conduction band to pollutant molecules is facilitated when the edge of the conduction band is more negative than the reduction potential of the pollutant. Pollutants like acetaldehyde and formaldehyde have reduction potentials that are more positive than the conduction band edge of several semiconductors; thus, water molecules also participate in the oxidation process of pollutants due to their low oxidation potential. Additionally, if a pollutant has a more negative reduction potential than that of the reduction product, this leads to increased production of the reduction product [87].

Kinetically, the degradation of pollutants through photocatalytic oxidation can be described within two steps. In the decay profiles, an initial drop can be observed due to the adsorption and desorption of molecules on the surface of the photocatalyst, followed by a second drop at longer times due to the photocatalytic reactions. The photocatalytic oxidation of a pollutant follows pseudo-first-order kinetics, which can be described by the equation [88]:

$$\ln\left(\frac{C_0}{C_t}\right) = k_d t$$

where C_0 and C_t are the concentrations of the target pollutant at times $t = 0$ and t respectively, and k_d is the apparent photocatalytic degradation rate constant.

Identifying the onset of photocatalysis is not straightforward; it requires consideration of two criteria. First, photocatalysis becomes the predominant process only after the system reaches an initial equilibrium between adsorption and desorption over a certain period. Second, the start of photocatalysis must also take into account the moment when the yield of the product stabilizes, indicating that the photocatalytic degradation of the pollutant is consistent. The photocatalytic process can therefore begin at different times for

various pollutants. For instance, in a study using Mn/TiO_2 and Co/TiO_2, the initial time of photocatalysis was observed at approximately 120 min, while using $Mn/Co/TiO_2$, it was observed at 20 min [88].

The Langmuir-Hinshelwood kinetic model describes heterogeneous photocatalytic reactions. The photocatalytic degradation rate (r_0) of the pollutant can be described by this model with the following equation [89]:

$$r_0 = \frac{kKC_0}{1 + KC_0}$$

where k is the reaction kinetic constant, and K is the equilibrium absorption constant.

4.3. Important Factors Affecting Photo Oxidation

The efficiency of photocatalytic oxidation is influenced by the properties of the photocatalyst and target pollutant, as well as various external parameters, including humidity, light intensity, pollutant concentration, residence time, and airflow rate. These factors significantly impact the photocatalytic process, affecting pollutant adsorption, charge carrier recombination rates, and the radiation interacting with the photocatalyst.

4.4. Humidity

Humidity significantly affects the photocatalytic degradation of volatile organic compounds (VOCs). In high humidity conditions, water molecules can compete with pollutant molecules for active sites on the photocatalyst, thereby reducing adsorption efficiency and photocatalytic reactions. Excess water may also act as recombination centers for charge carriers, diminishing photocatalytic activity [90]. Conversely, high water concentrations can promote the formation of hydroxyl radicals that oxidize pollutants, potentially enhancing photocatalytic efficiency. This dual effect complicates the identification of an optimal humidity level for maximizing the removal efficiency of indoor pollutants. It appears that a specific amount of water is necessary to initiate photocatalysis; however, exceeding this concentration may decrease efficiency due to competition for active sites [91].

Moreover, the impact of humidity on photocatalytic efficiency varies with the type of pollutant. For example, higher humidity levels may enhance the degradation of acetaldehyde but reduce the efficiency of ethanol, benzene, and toluene. This variation is due to the differing interactions between the pollutant molecules and the photocatalyst. Photogenerated electrons can be trapped at the semiconductor's active sites, hindering the direct oxidation of adsorbed carbonyl compounds like acetaldehyde. However, in high humidity, these compounds can be indirectly oxidized by hydroxyl radicals generated from water oxidation. In contrast, pollutants like ethanol efficiently adsorb onto the catalyst's active sites, resulting in reduced oxidation efficiency in the presence of water due to limited interactions with hydroxyl groups [91,92].

This pollutant-specific effect of humidity underscores the challenges of applying photocatalysts in indoor environments where multiple pollutants may coexist. The varying responses necessitate a tailored approach to optimize photocatalytic degradation efficiency for each target pollutant, complicating the implementation of photocatalysis in diverse indoor air quality management scenarios [91,92].

Contradictory results have emerged even when studying the same pollutant. For instance, while one study reported that higher humidity levels decreased the efficiency of photocatalytic oxidation for NO [93], another found an increase in degradation efficiency with rising humidity [77].

Research on the photocatalytic removal of formaldehyde indicates that the optimal relative humidity for TiO_2 is approximately 45% [94] (Figure 2a). In contrast, a study on

g-C_3N_4-TiO_2 revealed that pollutant degradation decreased from 60% to 38% as relative humidity increased from 20% to 80% [95] (Figure 2b).

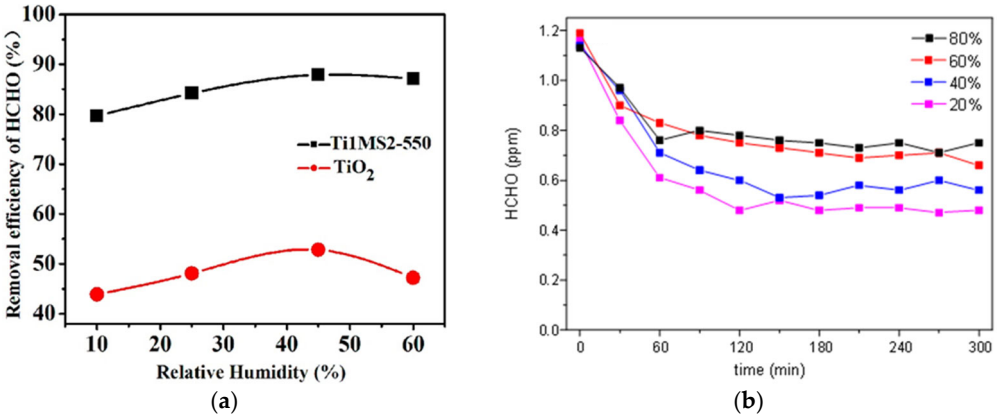

(a) (b)

Figure 2. (**a**) Removal efficiency of formaldehyde using Ti1MS2-550 and TiO_2 increasing the relative humidity [94] and (**b**) degradation of formaldehyde using g-C_3N_4-TiO_2 in different conditions of relative humidity [95].

4.5. Residence Time

Residence time, or contact time, refers to the duration of a gaseous molecule remaining near the catalyst surface. This parameter significantly influences the photocatalytic degradation efficiency of pollutants. Increasing the residence time allows more contact between pollutants and the catalyst, facilitating reactions with hydroxyl radicals and positively charged holes, thus enhancing efficiency. For instance, studies have shown that extending the residence time of formaldehyde from 10 to 40 s increased the conversion rates from 36% to 48%, respectively (Figure 3) [95].

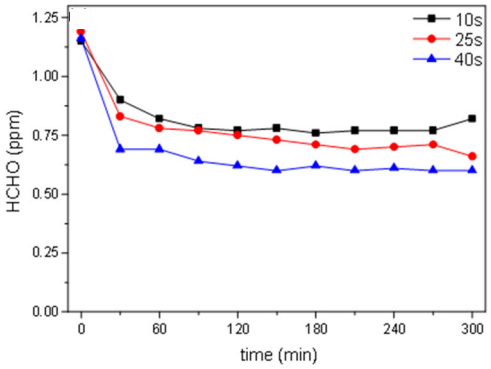

Figure 3. Degradation of formaldehyde using g-C_3N_4-TiO_2 considering different residence times [95].

Most research analyzes photocatalytic oxidation with residence times ranging from seconds to minutes; however, practical indoor conditions often see residence times in the tens to hundreds of milliseconds. Consequently, results from laboratory studies may differ significantly from those obtained in real indoor environments [89].

4.6. Airflow Rate

Airflow rate is another critical factor affecting photocatalytic oxidation. Increased airflow can reduce the residence time of molecules, resulting in decreased photocatalytic efficiency 6. For example, one study found that increasing airflow from 100 to 300 mL/min decreased the conversion rates of toluene, ethylene, and propylene when using TiO_2 nanoparticles (Figure 4) [96].

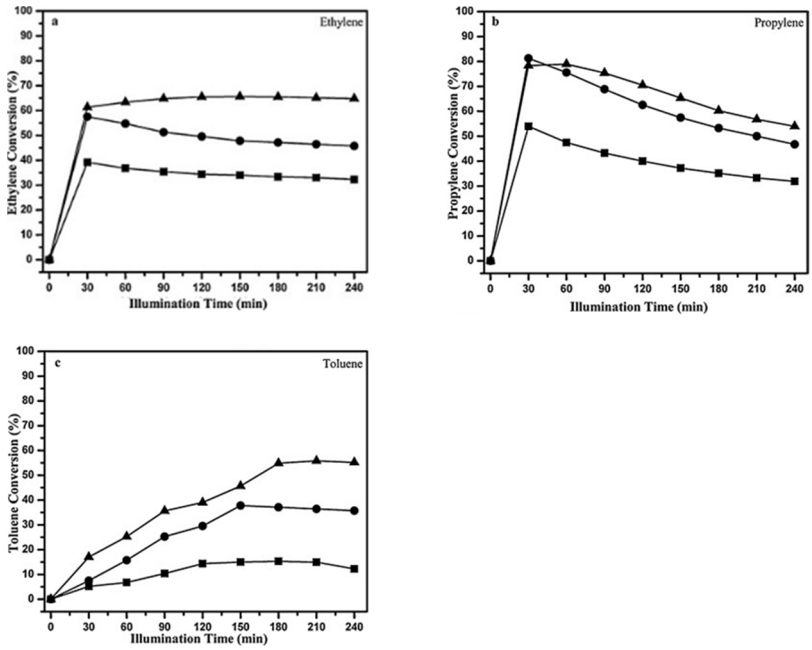

Figure 4. Conversion of ethylene (**a**), propylene (**b**), and toluene (**c**) under various conditions of flow rate: (▲) 100 mL/min; (●) 200 mL/min; (■) 300 mL/min [96].

However, increased airflow also enhances mass transfer between the catalyst and pollutants, potentially increasing conversion rates by reducing concentration gradients between the catalyst bulk and its surface. The effects of airflow rate on pollutant removal are complex and can be categorized into three main conditions:

Low Airflow Rate: High residence time leads to enhanced photocatalytic oxidation due to sufficient contact between the catalyst and pollutants, indicating that mass transfer limits degradation.

Intermediate Airflow Rate: Variations in airflow rate have minimal impact on pollutant removal efficiency.

High Airflow Rate: Increased airflow reduces residence time, decreasing the efficiency of the photocatalytic process [91].

4.7. Light Intensity

Light intensity is crucial for photocatalytic pollutant removal. Higher light intensity increases the photogeneration of charge carriers, enhancing photocatalytic activity [85]. The quantum yield of light absorbed during the photocatalytic process can be expressed as follows:

$$\Phi_{\text{overall}} = \frac{\text{rate of reaction}}{\text{rate of absorption of radiation}}$$

For example, increasing light power from 8 to 24 W improved the photocatalytic efficiency of USPNT for p-xylene removal (Figure 5a) [85]. Additionally, for toluene degradation, increasing infrared irradiation intensity from 95 to 116 mW/cm^2 enhanced the degradation rate for the Pt-rGO-TiO_2 photocatalyst (Figure 5b). Notably, the increase in efficiency was more significant between 95 and 105 W than between 105 and 116 W, suggesting that degradation efficiency does not depend linearly on light intensity [97].

The effects of light intensity can be categorized into three main regimes:

Low Light Intensity: Adsorption of photons is linearly dependent on the light intensity, resulting in constant quantum efficiency.

Intermediate Light Intensity: Quantum efficiency decreases with the square root of light intensity.

High Light Intensity: Photocatalytic efficiency becomes relatively independent of light intensity, as the number of activation sites remains constant, limiting reaction rates despite increased photon activation [98].

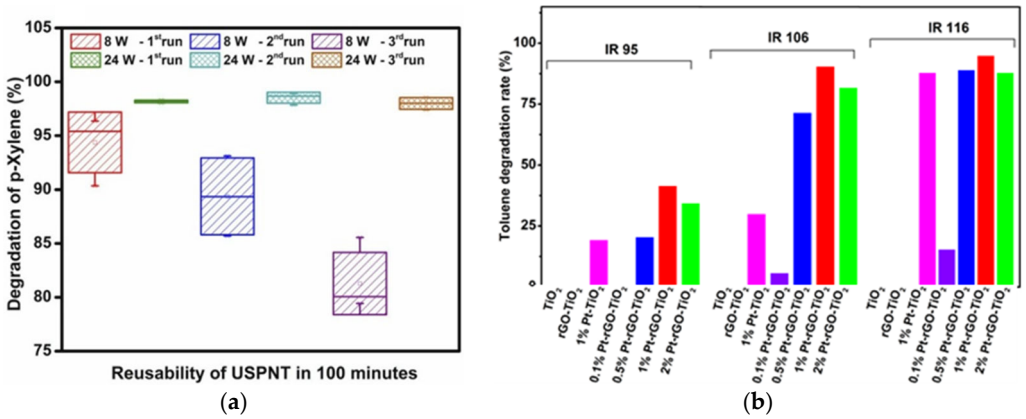

(**a**) (**b**)

Figure 5. (**a**) Degradation of p-xylene using USPNT under different power daylight (8 and 24 W) [85] and (**b**) degradation rate of toluene using Pt-rGO-TiO_2 with different light intensities (95, 106 and 116 mW/cm^2) [97].

4.8. Concentration of Pollutants and Photocatalysts

The initial concentration of the target pollutant can influence photocatalytic oxidation efficiency in various ways. Generally, lower initial concentrations lead to higher degradation rates. High pollutant concentrations can quickly saturate the catalyst's active sites with by-products, limiting efficiency. Additionally, elevated pollutant concentrations can reduce quantum yield by adsorbing or scattering light, thus decreasing the light available to the photocatalyst. For instance, the removal of toluene, ethylene, and propylene using TiO_2 nanoparticles decreased as initial pollutant concentrations rose from 100 to 500 ppm (Figure 6) [96].

Conversely, another study on formaldehyde degradation at initial concentrations of 0.6, 1.2, and 2.4 ppm found that the highest conversion rate occurred at 1.2 ppm. This result suggests that low pollutant concentrations may limit contact with active sites, restricting adsorption [95].

Pollutant adsorption directly impacts photocatalytic oxidation efficiency. When more pollutant molecules are adsorbed on the catalyst surface, the likelihood of reactions between positively charged holes and adsorbed pollutants increases. The non-uniform surface of the photocatalyst features stronger adsorption sites that are filled first at lower concentrations, whereas higher concentrations lead to interactions among adsorbed molecules and gas-phase pollutants. Thus, adsorption sensitivity varies with concentration [89].

At low pollutant concentrations, the adsorption rate on the photocatalyst surface is slower than the reaction rate, making adsorption the limiting factor for photocatalytic oxidation. As initial pollutant concentrations exceed a certain threshold, the adsorption rate can surpass the photocatalysis rate, shifting the limitation to photocatalytic activity. Since indoor pollutant concentrations typically range from parts per billion (ppb) to sub-ppb, while laboratory conditions often test in parts per million (ppm), the efficiency of photocatalysts used in real indoor conditions tends to be lower [89].

Additionally, the concentration of the photocatalyst itself influences photocatalytic activity. For instance, in formaldehyde removal, efficiency increased from 33% to 48% with the amount of g-C_3N_4-TiO_2 rising from 0.05 to 0.25 g (Figure 6). However, this relationship is not linear due to limited contact between pollutant molecules and the catalyst's active sites [95].

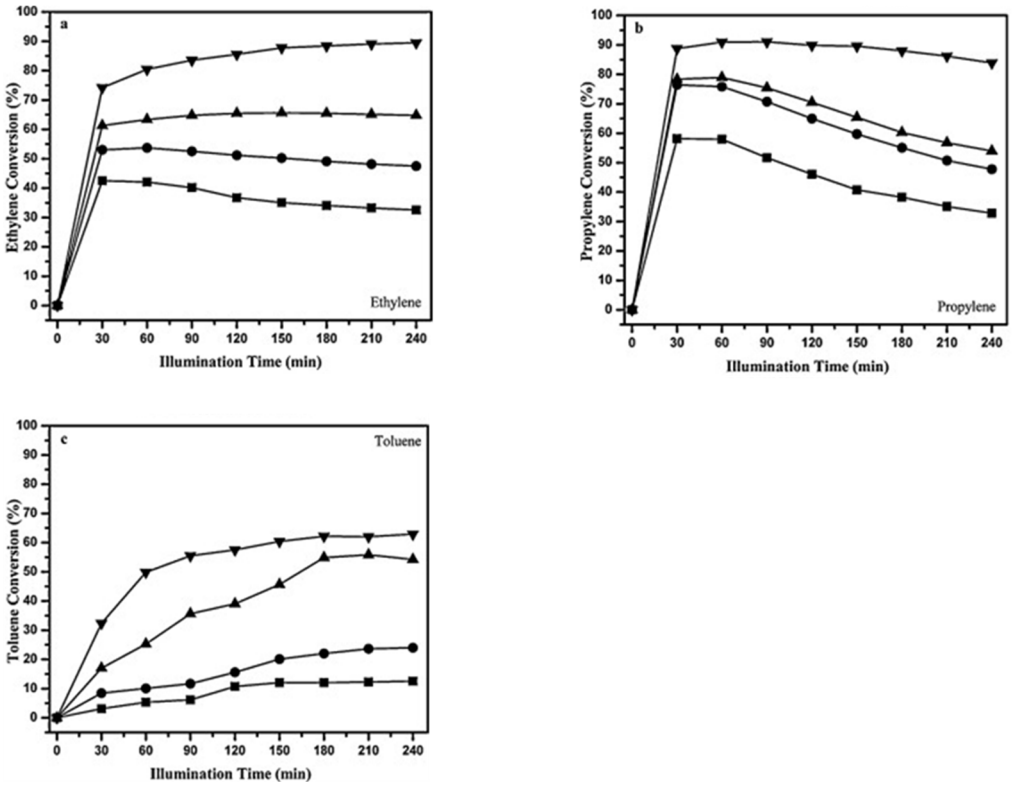

Figure 6. Conversion of ethylene (**a**), propylene (**b**), and toluene (**c**) with different initial concentrations of pollutant: (▼) 100 ppm; (▲) 200 ppm; (●) 300 ppm; (■) 500 ppm [96].

5. Titanium-Based Nanomaterials

Among the various nanomaterials explored as photocatalysts for indoor pollutant removal, titanium-based materials, particularly titanium dioxide (TiO_2), or titania, are the most widely used. TiO_2 is extensively researched due to its high photocatalytic efficiency, stability, low cost, low toxicity, abundance, and environmental friendliness. The morphology of the catalyst significantly impacts the photocatalytic degradation of pollutants, prompting studies on different forms of TiO_2 nanomaterials, such as nanoparticles [99], nanotubes [100], and nanosheets [101], to identify the most effective structure.

During photocatalytic oxidation, TiO_2 absorbs radiation with energy exceeding its band gap, leading to the formation of photogenerated electrons. However, since TiO_2 has a wide band gap (3.2 eV), ultraviolet (UV) light is required to initiate photocatalytic reactions. In indoor environments, where visible and near-infrared (IR) light predominate, this limits TiO_2's photocatalytic applications [102]. To address this challenge, researchers have investigated various doping strategies, using both metal and non-metal materials, to narrow the band gap and enhance TiO_2's efficiency under visible light [103].

In addition to photocatalytic oxidation, UV-irradiated TiO_2 exhibits another photoinduced phenomenon known as super-hydrophilicity [104], which reduces the water contact angle to nearly 0 degrees. This creates a uniform water film that covers the surface, preventing contact between the surface and volatile compounds. As a result, applying TiO_2 coatings on building facades can protect surfaces from volatile compounds and oxidize air pollutants through photocatalytic oxidation [105].

As mentioned earlier, the morphology of the photocatalyst plays a crucial role in determining its properties and photocatalytic activity. TiO_2 nanomaterials are typically classified into four categories based on their dimensionality: nanoparticles (0D) [106], nanotubes (1D) [107], nanosheets (2D) [108], and porous structures (3D) [109]. Each of these structures has been studied to assess which form is the most efficient for photocatalysis. Compar-

isons have been made with the well-known TiO_2 P25, a standard reference photocatalyst composed of 75% anatase and 25% rutile, commonly used in photocatalytic processes [110].

Due to the differences in lattice structures, anatase, and rutile have different structures of the electronic band and therefore different band gaps. For anatase phase TiO_2 the band gap between the valence band and conduction band is 3.2 eV, instead for rutile TiO_2 the band gap is 3.02 eV [111]. Therefore, to overcome this band gap it is necessary the adsorption of a photon with a wavelength of about 388 nm for anatase [80] and 410 nm for rutile [111]. Hence, the adsorption of a photon with $\lambda < 388$ nm is needed to activate the anatase phase TiO_2 semiconductor. Accordingly, TiO_2 does not have a high photocatalytic efficiency in indoor conditions where radiation is mostly in the visible-near IR range. However, when anatase and rutile as nanoparticles, are coupled with a heterojunction, TiO_2 is able to adsorb visible light [80].

The synthesis reactions and doping processes can further influence the morphology of nanomaterials. TiO_2's photocatalytic activity is affected by several factors, including crystallite size, porosity, specific surface area, and crystalline phases. A larger surface area can enhance photocatalytic efficiency by increasing the number of adsorbed molecules. However, it can also introduce more crystal defects, which may promote the recombination of electron-hole pairs, ultimately reducing photocatalytic efficiency [112].

5.1. Nanoparticles and Microspheres

The most common TiO_2 photocatalysts for air purification are zero-dimensional structures such as nanoparticles and microspheres. This kind of structure allows a high photocatalytic efficiency due to its small particle size that causes a high specific surface area and high pore volume. The high specific surface area enhances the exposure of the photocatalyst to radiation and enhances the quantum efficiency. Moreover, the use of nanoparticles implies short charge carrier diffusion distances which reduce the charge carrier's recombination [113]. Therefore, this enhances the adsorption of the target pollutant, the light-harvesting capacity, and the photocatalytic degradation. Despite this, an important problem that influences its photocatalytic activity is the agglomeration of TiO_2 nanoparticles with high Gibbs free energy into larger aggregates leading to a decrease in the active sites of the photocatalyst [114]. Photocatalytic activity is enhanced by the homogeneous distribution of the TiO_2 nanoparticles [115]. To obtain separate nanoparticles is often needed a deagglomeration step [111]. To overcome this limitation, for instance, it has been studied the use of clay mineral-TiO_2 nanocomposites that allow better dispersion of TiO_2 nanoparticles [114].

Particle size significantly influences photocatalytic efficiency since it directly affects the specific surface area of the photocatalyst. It has been demonstrated that there is an optimum particle size of TiO_2 that corresponds to about 10 nm [116]. A smaller radius can reduce the efficiency of the photocatalytic reactions due to the quantum size effect. This term indicates the phenomenon whereby reducing the particle size to a certain value, these particles have discontinuous energy levels of conduction and valence bands resulting in increasing the energy band gap of the material [113].

Mesoporous and porous TiO_2 spheres have been widely studied and presented high photocatalytic efficiency due to the high pore volume and pore size, high specific surface area, and good crystallinity [86,117]. Also, hollow nanospheres have been studied since these structures exploit the multiple scattering of incident light inside the particles increasing the photocatalytic efficiency.

5.2. Nanotubes

One-dimensional structures like TiO_2 nanotubes (TNTs) have been studied due to their high photocatalytic efficiency. These structures have a high specific surface area which provides a high number of adsorbates and channels that enhance electron transfer leading to a reduction of charge carrier recombination especially for nanotubes with thin walls. Furthermore, the length of the TiO_2 nanotubes can increase the photocatalytic efficiency since a longer nanotube implies a greater specific surface area. Moreover, their characteristic structure which contains many hydroxyl groups on the interlayer region of their walls reduces the recombination rate of electron and hole pairs. The recombination rate is lower also because the electrons and positively charged holes can move freely throughout the length of the TNTs [118,119].

In a recent study [119], {001} facet-exposed TiO_2 nanotubes were synthesized and installed on a commercial air cleaner. This study demonstrated that 001-TNT has a high degradation activity for acetaldehyde and formaldehyde under visible light being the first air cleaner that satisfied the Korean air cleaner standards protocol. On the other hand, another sample of TNT whose surface is composed of mainly {101} facets, exhibited only moderate degradation of these pollutants. Furthermore, 001-TNT exhibits a higher efficiency of degradation of toluene than TNT. It has been observed that the 001-TNT also has a greater charge transfer resistance than TNT implying that the charge carriers are transferred at the interface with a higher efficiency. Despite it having been proven that {001} facet exposure is beneficial for photocatalysis, there is an optimum value of exposure of {001} facets on TiO_2 which is about 70%. Over this value, the separation between the charge carriers is not efficient due to the lack of {101} facet TiO_2. It has also been investigated the durability of the two semiconductors, and researchers found that the durability of 001-TNT was almost 9 times greater than that of TNT. This is due to the fact that the photocatalytic activity of 001-TNT has been regenerated by UV irradiation in clear air.

5.3. Nanosheets

TiO_2 nanosheets (TNS) are two-dimensional structures with a thickness of 1–10 nm and a lateral length in the range of μm. The shape of these nanomaterials results in a smooth surface and low turbidity. TNS exhibit photocatalytic properties as the photocatalytic degradation of organic compounds and superhydrophilicity when irradiated with UV radiation. TNS are studied for their advantageous properties of carrier mobility and high adherence with various substrates. TNS do not have great adsorption properties in the visible light range due to their wide band gap and so their applications in indoor environments are limited. Due to their high adherence, TNS is usually used for anti-fouling applications that involve self-cleaning surfaces where photocatalytic reactions happen at the solid-gas interface [113].

To enhance the photocatalytic activity for the degradation of pollutants, high-energy facets TiO_2 can be used. It has been demonstrated that {001} facets TiO_2 are more reactive, adsorb more photons, and have a higher photocatalytic activity than the thermodynamically more stable {101} facets. Therefore, different studies identified nanosheets with high-energy facets in order to enhance the adsorption of pollutants and photocatalytic oxidation [119].

TNS can be doped or form heterojunctions in order to enhance its photocatalytic efficiency. For instance [120], research synthesized N-doped TiO_2 nanosheets/WO_3 composites to observe the photocatalytic removal of hexane. From the UV-vis adsorption spectra, it has been observed that the N doping and the introduction of WO_3 have successfully enhanced the adsorption properties of TiO_2 nanosheets. The photoluminescence spectrum of the composite exhibited a lower intensity indicating a lower recombination rate compared to the TiO_2 nanosheets. Finally, the photocatalytic oxidation of hexane has been observed and

the efficiency of TNS increased due to the N doping and the heterojunction with WO_2 and it has obtained a maximum photocatalytic efficiency of about 44%. The enhancement of the photocatalytic activity is due to the increase in the specific surface area.

5.4. TiO_2 Porous, Supported, and Interconnected Structures

Due to the tendency of TiO_2 nanoparticles to aggregate into larger clusters, they are often supported on various materials or incorporated into porous substrates and ordered interconnected three-dimensional structures [121]. Coupling TiO_2 with adsorbents that have a high specific surface area and strong affinity for pollutants can further enhance its photocatalytic activity. Porous materials like zeolites and ordered mesoporous silica have been commonly used as supports for TiO_2 nanoparticles [122].

Zeolites, in particular, are mesoporous materials with high adsorption efficiency and uniform pore sizes, making them valuable support materials. Recent studies have shown that using waste zeolites can significantly improve photocatalytic efficiency for indoor pollutant removal [95]. Specifically, waste zeolites have been found to increase the adsorption of formaldehyde and reduce the recombination rate of charge carriers. Additionally, waste zeolites enhance the contact between pollutants and the photocatalyst through surface diffusion [95].

Carbon-based support materials have also been utilized to boost photocatalytic activity. For example, carbon nanotubes (CNTs) have been employed as a support for mesoporous TiO_2 in the photocatalytic degradation of CO_2 [123] and acetone [124]. CNTs influence the morphology of TiO_2 aggregates and the size of its crystallites. It has been observed that increasing the CNT content leads to the formation of smaller anatase crystallites and a higher anatase fraction in the composite, thereby improving photocatalytic performance.

Several studies have also suggested that three-dimensional hierarchically porous materials, composed of one-dimensional TiO_2 nanotubes, offer high efficiency in the photocatalytic degradation of pollutants [125]. This structure allows for greater pollutant adsorption due to its large number of pores, enhancing photocatalytic activity. Moreover, the hierarchically porous structure improves light diffusion into the internal regions of the photocatalyst, further increasing its efficiency.

5.5. Doping

As previously mentioned, the major limitation of TiO_2 applications is its restricted range of radiation absorbance. With a wide band gap of 3.2 eV, TiO_2 requires UV light to initiate photocatalytic reactions. To overcome this, doping is employed to induce a bathochromic shift, narrowing the band gap or introducing intermediate energy levels that enhance absorption in the visible light range [126].

Additionally, TiO_2 photocatalysts have a high charge carrier recombination rate, which decreases the efficiency of photocatalytic oxidation. Various dopants are used to reduce this recombination rate. By introducing intermediate energy levels within the band gap, doping enables TiO_2 to be activated by photons in the visible light spectrum [127,128]. These modifications also improve charge carrier separation, thereby reducing recombination and enhancing photocatalytic efficiency [129]. Modifications to TiO_2 can include metal doping, non-metal doping, co-doping (involving different elements), or coupling with other semiconductors [126].

Various metals such as Fe, Cu, Co, Mn, Ag, and Ni have been used as dopants to reduce the band gap of TiO_2. Metal dopants influence photocatalytic oxidation in several ways: they can modify the photocatalyst's light absorption capacity, affect the charge transfer rate at the interface, and improve the adsorption of pollutant molecules on the catalyst surface. When a metal cation is introduced as a dopant in TiO_2, it creates an intermediate energy level near

the valence band, enabling electron transfer from the valence band to the conduction band with less energy than undoped TiO_2. This shift allows the photocatalyst to be activated by visible light. Additionally, metal doping can enhance electron trapping, reducing electron-hole pair recombination, and thus increasing photocatalytic efficiency [128]. However, excessive dopant concentrations can lead to metal aggregation, forming recombination centers that diminish photocatalytic performance [130]. Therefore, factors like dopant type, concentration, and the preparation method of the doped photocatalyst are crucial for optimizing photocatalytic oxidation [80].

Despite the advantages of metal doping, some drawbacks have been identified. Metal dopants can block the porous surface sites of TiO_2, promote nanocrystallite growth, and reduce the specific surface area, all of which lower photocatalytic efficiency [117]. Furthermore, metals deposited on the photocatalyst surface can block photon absorption, leading to increased charge carrier recombination [131].

TiO_2 photocatalysts can be doped with metal ions substitutionally [132] or interstitially [133]. Introducing dopants can enhance conductivity by partially emptying the valence band (with *p-type* dopants) or partially filling the conduction band with electrons (with n-type dopants) [134]. P-type doping, using heterocations with lower valencies than Ti^{4+} (such as Al^{3+} and Cr^{3+}), creates acceptor centers that trap photogenerated electrons, which then attract holes and form charge carrier recombination centers [135]. N-type doping, achieved with heterocations of higher valencies than Ti^{4+} (such as Nb^{5+} and Ta^{5+}), acts as donor centers, increasing electron concentration in the conduction band, which also promotes charge carrier recombination. Combining *p-type* and *n-type* materials can lead to the recombination of electron-hole pairs at the interface [111].

The most commonly used noble metals as dopants for TiO_2 photocatalysts include platinum (Pt) [136], palladium (Pd) [137], silver (Ag) [138], and gold (Au) [139,140]. These dopants enhance the separation of charge carriers and decrease the recombination rate due to the formation of a Schottky barrier at the metal-semiconductor interface. This results in an increased photocatalytic efficiency, leading to a higher pollutant degradation rate. Additionally, noble metal dopants can extend the light absorption capacity of the photocatalyst into the visible light range [140,141].

For example, a study investigated the photocatalytic activity of Ag-doped TiO_2 nanotubes for toluene degradation (Figure 7). Among noble metals, silver is relatively inexpensive and has been shown to improve the photocatalytic efficiency of TiO_2. The Ag-doped TiO_2 achieved a 98% toluene reduction under UV light, outperforming both P25 and undoped TiO_2 nanotubes [142]. This high photocatalytic activity is attributed to the ability of Ag particles to trap photogenerated electrons, limiting the recombination of charge carriers. As a result, the electrons are more efficiently transferred to oxygen adsorbed on the TiO_2 nanotube surface. Moreover, the Ag-doped TiO_2 nanotubes had a porous structure and larger specific surface area, further enhancing their photocatalytic activity. Even under visible light, the Ag-doped TiO_2 nanotubes showed superior photocatalytic performance compared to P25 and undoped TiO_2 nanotubes [142].

In another study (Figure 8) [86], the photocatalytic efficiency of Au-TiO_2 nanocomposite microspheres for formaldehyde removal was examined. The presence of Au nanoparticles inhibited anatase nanocrystal growth, resulting in smaller crystallite sizes and larger surface areas. These nanocomposites displayed greater photocatalytic activity than both P25 and undoped TiO_2 microspheres. The mechanism involves the migration of photogenerated electrons to the Au nanoparticles, which are then transferred to oxygen molecules adsorbed on the TiO_2 surface. As with Ag, Au forms a Schottky barrier at the metal-semiconductor junction, effectively separating the positively charged holes in TiO_2's valence band from the electrons in the Au nanoparticles, preventing their recombination. This was confirmed

through photoluminescence spectra, where the Au-TiO_2 nanocomposite exhibited lower intensity compared to P25, indicating higher photocatalytic efficiency. However, while an increase in the atomic percentage of Au initially boosts photocatalytic performance, beyond a certain threshold, it decreases due to the formation of Au nanoparticles that act as recombination centers for electron-hole pairs [86].

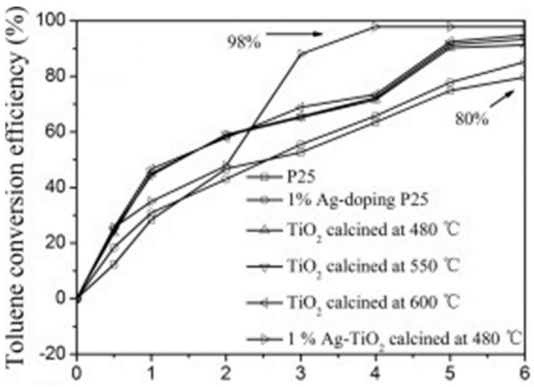

Figure 7. Degradation of toluene using Ag-doped TiO_2, pure TiO_2, P25, and Ag-doped P25 [142].

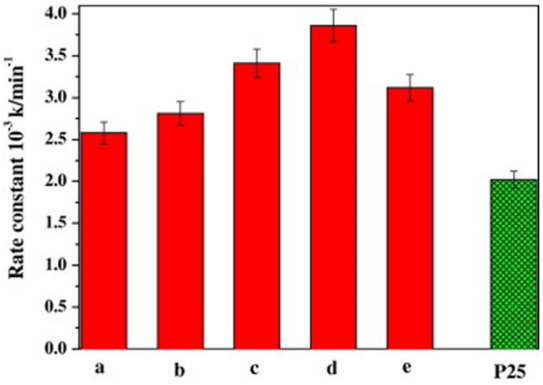

Figure 8. Reaction rate constants of TiO_2 (a), Au–TiO_2 containing various amounts of Au (b–e) and P25 [86].

Platinum is another widely studied noble metal dopant, particularly in Pt/TiO_2 photocatalysts, known for its high stability, pollutant removal efficiency, and regenerability. TiO_2 facilitates the dispersion of Pt active sites, enhancing pollutant adsorption (Figure 9) [143]. One study on Pt nanoparticles supported on faceted TiO_2 nanocrystals (Pt/TiO_2) for ethanol removal showed that Pt deposition increased TiO_2's adsorption capacity in the visible light range. Pt/TiO_2 exhibited superior photocatalytic activity, achieving a maximum ethanol conversion rate of 98%, compared to only 82% for undoped TiO_2. However, excessive deposition time led to larger Pt particles and the formation of aggregates due to the platinum reduction mechanism on TiO_2's surface. Pt nanoparticles nucleate on oxygen vacancies with high electron density, transferring photogenerated electrons from TiO_2 to the Pt nuclei, leading to an electron density increase. This nucleation process limits the formation of new nuclei, causing Pt particle growth and aggregation [144].

Recently, rare earth metals (RE) such as Nd, Ce, and Ln have been utilized as dopants to enhance photocatalytic performance. The incorporation of these metals into photocatalysts introduces intermediate energy levels within the band gap, facilitating the transfer of photogenerated electrons. This reduces charge carrier recombination and improves photocatalysis. Additionally, RE dopants can alter phase structures, increase surface area, and modify surface morphology, thereby enhancing light absorption and enabling photocatalytic reactions under visible light. Doping with rare earth materials can also inhibit

the anatase-to-rutile phase transition in TiO_2, and increase its surface area. Notably, the inhibitory effect on phase transition becomes more pronounced with the ionic radius of the RE metal, leading to distinct RE-TiO_2 phases [145].

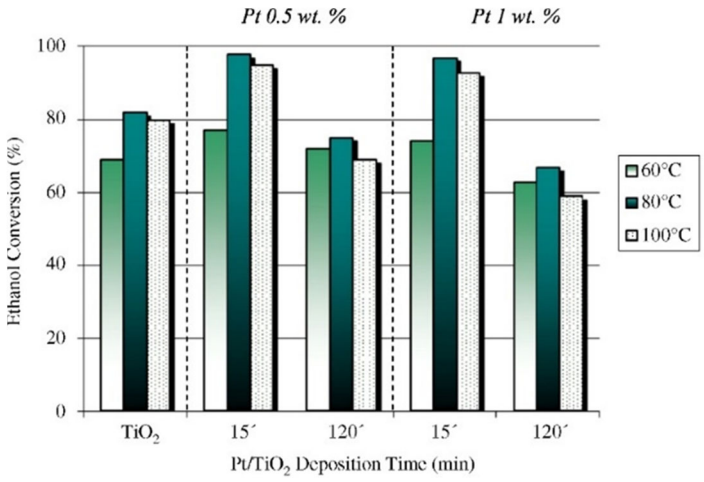

Figure 9. Ethanol conversion using TiO_2 and Pt-doped TiO_2 composed of different amounts of Pt [144].

For instance, Ce-doping of P25 has been shown to increase the photocatalytic oxidation rate of benzene, ethylbenzene, and m-xylene under UV radiation at specific reactor concentrations (Figure 10). In the case of benzene, the maximum conversion rate increased from 10 to 22.3 ppmv/min with Ce-doped P25. Similarly, for ethylbenzene removal, the maximum conversion rate rose from about 8 to 29 ppmv/min. Furthermore, P25/Ce demonstrated a higher conversion rate for benzene and ethylbenzene removal compared to P25/Pt and P25/Fe. This increased photocatalytic efficiency is attributed to the presence of cerium species on the photocatalyst's surface, which create vacancies, charge disparities, and unsaturated chemical bonds. These factors result in increased chemisorbed oxygen on the surface, enhancing photocatalytic oxidation.

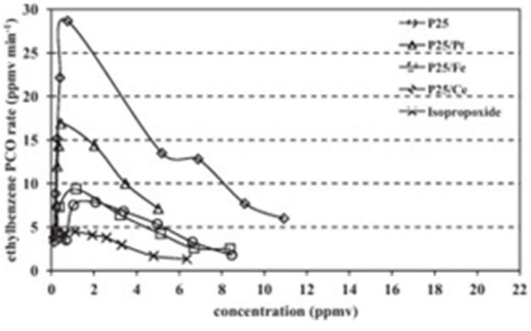

(**a**)

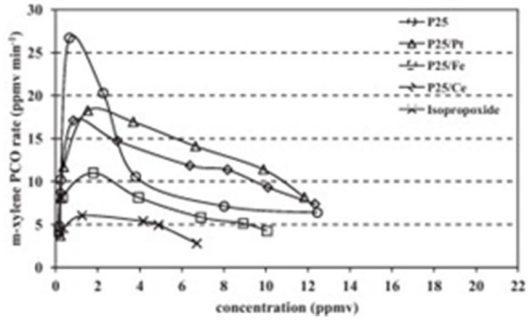

(**b**)

Figure 10. *Cont.*

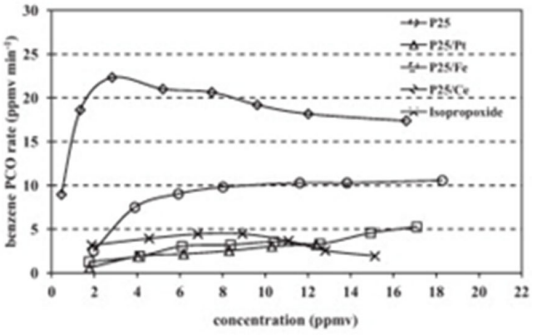

(**c**)

Figure 10. Photocatalytic oxidation rates of ethylbenzene (**a**), m-xylene (**b**), and benzene (**c**) using various photocatalysts [146].

In another study (Figure 11) [147], the photocatalytic activity of P25 doped with Eu, La, Y, and Ce under visible light was evaluated and compared with undoped P25. The undoped photocatalyst exhibited a conversion rate of 23 ppm/h for the transformation of isopropanol to acetone. In contrast, samples doped with Eu, La, and Y showed maximum conversion rates of 27, 32, and 21 ppm/h, respectively. However, the Ce-doped samples did not show any photocatalytic activity due to low concentrations of hydroxyl groups adsorbed on the surface and reduced specific surface area caused by synthesis conditions. The enhanced photocatalytic activity in the other RE-doped samples can be explained by the increase in the specific surface area induced by the dopants. Indeed, samples with larger surface areas exhibited higher photocatalytic oxidation rates for pollutants. Additionally, RE metals like Eu, La, and Y increase charge carrier separation and reduce recombination rates, further boosting photocatalytic activity.

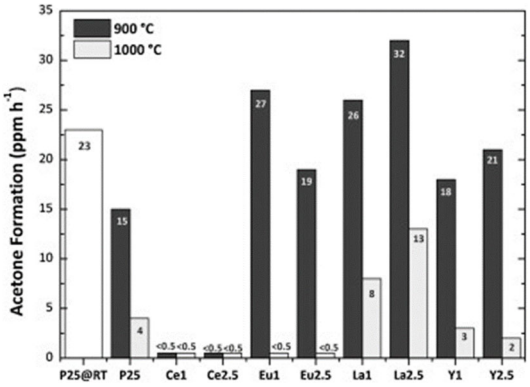

Figure 11. Photocatalytic activity of P25 and TiO_2 doped with various rare earth metals [147].

Interestingly, the concentration of RE dopants does not affect all photocatalysts uniformly. Samples of $Ti_{1-x}RE_xO_2$ were prepared with two different dopant concentrations (x = 0.01 and 0.025 mol). For La-TiO_2 and Y-TiO_2, higher dopant concentrations resulted in increased photocatalytic activity, with rates of 32 and 21 ppm/h, respectively. However, for Eu-TiO_2, increasing the dopant concentration caused the photocatalytic activity to drop to 19 ppm/h.

Despite the high photocatalytic efficiency of noble metal- and rare earth metal-doped photocatalysts, their high cost has led to the increased use of more affordable transition metals. Transition metals such as Mn, Cu, Co, Fe, Al, and Ni have been extensively studied as dopants for TiO_2 semiconductors. These dopants enhance charge carrier separation, reducing the recombination of electron-hole pairs and improving photocatalytic performance. However, if the dopant concentration exceeds an optimal threshold, it can disrupt

the catalyst's crystallinity and act as a recombination center, reducing overall photocatalytic efficiency. Different transition metals have unique optimal concentrations, meaning the impact on pollutant removal efficiency varies. Additionally, even with the same dopant amount, particle size and morphology of the photocatalysts can differ. After doping, the particle size of TiO_2 typically increases due to metal-induced agglomeration, with noticeable differences between samples [129].

Iron is frequently used as a dopant for TiO_2 photocatalysts because of its ability to enhance charge carrier separation and reduce recombination rates. It also induces a bathochromic shift, extending the applications of TiO_2 photocatalysts into the visible light range. Due to the similar ionic radii of Fe^{3+} and Ti^{4+}, iron cations substitute into TiO_2's lattice. Iron doping also catalyzes the anatase-to-rutile phase transition. Research on Fe-doped TiO_2 has demonstrated high photocatalytic efficiency for toluene degradation under visible light. The 0.7% Fe/TiO_2 sample exhibited a maximum degradation rate of 96.5% (Figure 12). Higher Fe concentrations resulted in increased recombination rates, lowering photocatalytic efficiency. This was confirmed by photoluminescence spectra, where the 0.7% Fe/TiO_2 sample showed lower intensity than other doped TiO_2 samples. Furthermore, Fe doping improved pore volume and specific surface area [128].

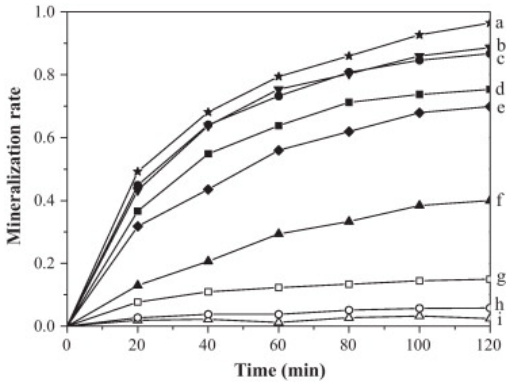

Figure 12. Mineralization rate of toluene using Fe-doped TiO_2 containing various amounts of Fe (a–f), TiO_2 (g), and no catalyst (h) under visible light and one sample of Fe-doped TiO_2 in dark (i) [128].

In another study [129] (Figure 13), the photocatalytic activity of TiO_2 doped with various transition metals (Mn, Co, Cu, Ni, and Fe) for benzene degradation was compared. Doped TiO_2 particles were significantly larger than undoped TiO_2, leading to lower specific surface areas. Metal doping likely blocked photocatalyst pores and/or catalyzed particle growth, increasing the samples' specific surface area. Additionally, the fractions of anatase and rutile in the samples revealed that metal doping accelerated the anatase-to-rutile conversion. Under vacuum ultraviolet (VUV) radiation, photocatalytic efficiency followed this order: $Mn/TiO_2 > Co/TiO_2 > Ni/TiO_2 > P25 > Cu/TiO_2 >$ anatase $TiO_2 > Fe/TiO_2$. The higher efficiency of Mn/TiO_2 and Co/TiO_2 aligns with the fact that MnO_x and CoO_x oxides have a strong ability to generate reactive oxygen species (ROS), which can oxidize benzene and boost photocatalytic efficiency.

Further research explored the photocatalytic degradation of acetaldehyde under visible and UV light using Mn/TiO_2, Co/TiO_2, and $Mn/Co/TiO_2$. These photocatalysts removed approximately 49%, 28%, and 74% of formaldehyde under visible light, respectively, and 57%, 71%, and 91% under UV light (Figure 14). The results, particularly for Mn/Co co-doped TiO_2, were significantly higher than those for undoped TiO_2. UV-vis adsorption spectra demonstrated that doped and co-doped TiO_2 had higher light absorption efficiency under visible light compared to undoped TiO_2, with $Mn/Co/TiO_2$ showing the highest absorption capacity. However, despite high removal rates, only Mn/TiO_2 exhib-

ited photocatalytic activity. Photocatalytic efficiency in metal-doped TiO_2 under visible light depends not only on adsorption properties but also on recombination rates. Thus, Co/TiO_2 and $Mn/Co/TiO_2$ showed no photocatalytic activity, even with excellent visible light absorption [88].

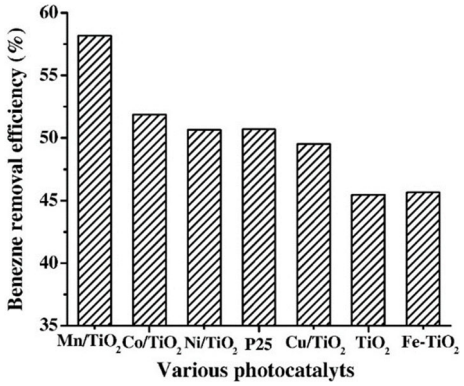

Figure 13. Benzene removal using P25, TiO_2, and TiO_2 doped with various metals [129].

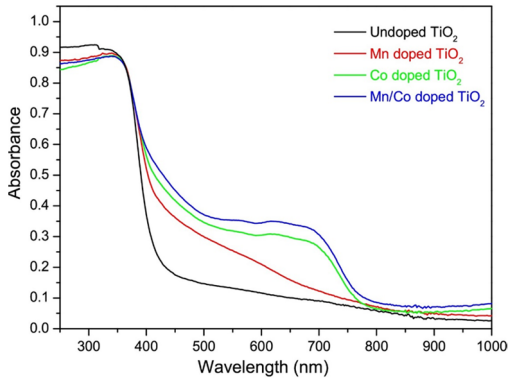

Figure 14. UV–vis absorption spectra of Mn/TiO_2, Co/TiO_2, $Mn/Co/TiO_2$, and un-doped TiO_2 samples [88].

In addition to metal doping, the use of non-metal anions such as C, N, F, and S for doping TiO_2 has been investigated to enhance the photocatalytic oxidation of pollutants. Both metal and non-metal dopants modify the electronic structure of TiO_2 by introducing new intermediate states in its band gap. Non-metal dopants create new levels near the valence band of TiO_2 and do not function as charge carriers, which is a significant limitation of metal doping. This characteristic makes non-metal doping advantageous. The introduction of new levels in the band gap narrows it, allowing non-metal dopants to expand TiO_2's adsorption capacity in the visible light range. These dopants replace oxygen in the TiO_2 lattice, and the resulting oxygen vacancies can serve as recombination centers for charge carriers, reducing photocatalytic efficiency [80]. Moreover, non-metal doping can enhance the durability and stability of the photocatalysts [141].

Nitrogen-doped TiO_2 has been particularly studied for its high stability, similar atomic radius to oxygen, and lower ionization energy compared to other non-metal dopants [80]. For example, the photocatalytic degradation of p-xylene has been explored using Ultra Small Porous Nitrogen-doped Titanium Dioxide (USPNT) under simulated indoor illumination. This photocatalyst achieved a maximum degradation rate of 94.4% for p-xylene removal under low-power daylight conditions, whereas P25 reached only 38% (Figure 15). USPNT demonstrated high crystallinity, which contributes to its enhanced photocatalytic activity. Furthermore, photoluminescence spectra revealed that the USPNT sample exhibited significantly lower photoluminescence intensity and, consequently, a much lower

recombination rate compared to P25. The intermediate levels introduced by N-doping act as hole reservoirs, promoting charge carrier separation and enhancing photocatalytic efficiency [85].

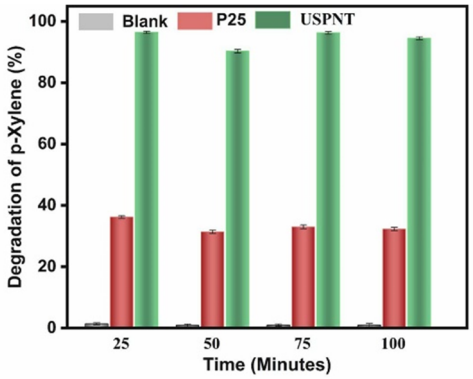

Figure 15. Degradation of p-xylene using P25 and USPNT [85].

Carbon doping in TiO_2 photocatalysts (Figure 16) [148] can also improve photocatalytic activity by stabilizing the anatase phase and enhancing pollutant adsorption on the TiO_2 surface. The introduction of C can improve the conductivity of TiO_2, increasing the charge transfer rate from the bulk to the surface. Research comparing the photocatalytic activity for methylene blue degradation among C-doped TiO_2, N-doped TiO_2, and C and N co-doped TiO_2 revealed that doping limits the growth of TiO_2 crystallites. UV-vis adsorption spectra indicated an increase in visible light adsorption capacity compared to undoped TiO_2. The degradation rates increased in the following order: undoped TiO_2 < N-TiO_2 < C-TiO_2 < C-N-TiO_2. Thus, TiO_2 doping enhances photocatalytic activity due to the presence of C and N atoms that facilitate electron transfer, with co-doped TiO_2 exhibiting the highest photocatalytic activity due to the synergistic effects of the two dopants.

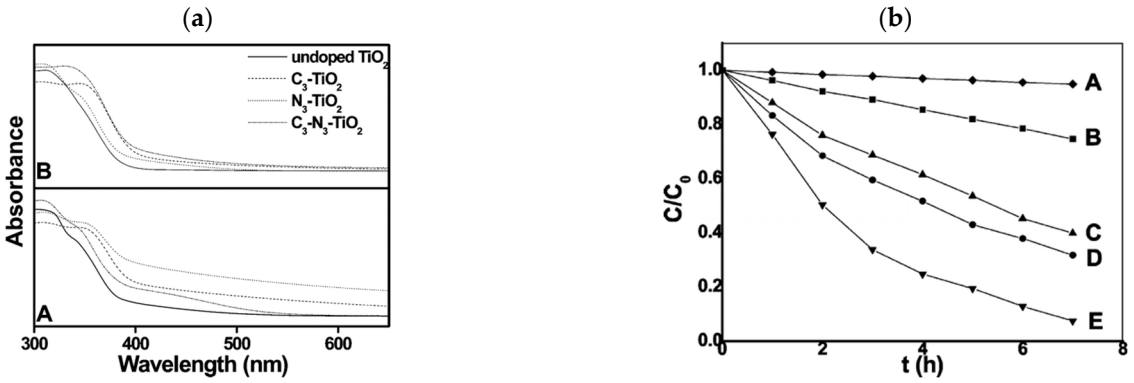

Figure 16. (**a**) UV-vis absorption spectra of undoped TiO_2, N-TiO_2, C-TiO_2, and C-N-TiO_2 calcinated at (A) 400 and (B) 500 °C. (**b**) Degradation of methylene blue using no catalyst (A), undoped TiO_2 (B), N-TiO_2 (C), C-TiO_2 (D), and C-N-TiO_2 (E) [148].

6. Carbon-Based Nanomaterials

Carbon-based nanomaterials can enhance the photocatalytic oxidation of pollutants due to their high adsorption capacity [149]. The ability to absorb pollutants on the surfaces of carbon-based photocatalysts is influenced by the physical and chemical properties of the nanomaterials, such as specific surface area, pore structure, and surface characteristics. Adsorption also depends on the target pollutant; specifically, carbon-based nanomaterials

exhibit a high affinity for volatile organic compounds (VOCs) due to various interactions, including coordination bonds, hydrogen bonding, and electrostatic interactions [150].

Additionally, carbon-based nanomaterials can reduce the recombination rate by forming heterojunctions, acting as charge mediators, and enhancing charge mobility. Typically, these nanomaterials are coupled with semiconductors like TiO_2 to improve the photocatalytic oxidation of pollutants by leveraging their high specific surface area and minimizing charge carrier recombination [151]. Structures such as activated carbon, carbon nanotubes, and reduced graphene oxide can absorb a broad spectrum of light, increasing the generation of electron-hole pairs at lower energy levels than a pristine photocatalyst and narrowing the band gap. This results in higher photocatalytic activity and potential applications under visible light.

Recently, research on carbon-based nanomaterials has surged, particularly focusing on carbon nanotubes and graphene oxides, which are among the most extensively studied. However, other carbon-based adsorbents (OCBAs) have also been investigated for pollutant removal (Figure 17) [152].

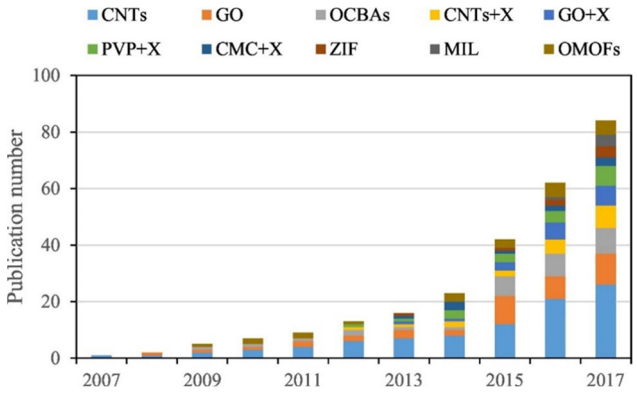

Figure 17. Number of studies about nanoadsorbents for pollutant removal during 2007–2017 [152].

6.1. Activated Carbons

Activated carbons (AC) are widely used in photocatalysis as adsorbents for pollutants, owing to their high specific surface area, substantial pore volume, low cost, defect-rich morphology, and excellent adsorption capacity [153]. ACs exhibit a higher affinity for non-polar molecules, attributed to their carbon-rich conjugated surface structure, which has a non-polar nature. They demonstrate significant adsorption efficiency for volatile organic compounds (VOCs), even at low pollutant concentrations. However, their efficiency in removing high concentrations of VOCs is limited by factors such as desorption and flammability [154,155].

The adsorption force—the force required to release the adsorbate trapped in the pores—increases as pore dimensions decrease [156]. Initially, pollutant adsorption occurs in the micropores, where the adsorption force is strongest, before progressing to larger pores. The adsorption capacity of ACs increases rapidly at first but slows down as saturation approaches. Notably, the adsorption capacity does not necessarily correlate with specific surface area and pore volume; thus, these metrics alone do not determine adsorption effectiveness. For instance, a well-organized arrangement of micropores enhances the diffusion of adsorbate compounds [157], thereby increasing the overall adsorption capacity. Additionally, the size of the adsorbate affects the adsorption characteristics of ACs with varying pore structures. While an adsorbate can enter larger pores, excessively large pore sizes can weaken the adsorption potential. For example, with toluene as a target pollutant, mesoporous volume plays a crucial role in adsorption capacity, which increases as mesoporous volume rises [158].

In photocatalytic applications, ACs are often coupled with semiconductors like TiO_2 to enhance photocatalytic efficiency by acting as both a support material and an adsorbent. Furthermore, activated carbons can be doped with metal oxides to improve their affinity and adsorption of both polar and non-polar VOCs by increasing the number of functional groups on their surfaces. However, desorption of pollutants from AC pores may occur due to competition from other compounds that exhibit stronger adsorption forces [159].

6.2. Activated Carbon Fibers

Activated carbon fibers (ACFs) exhibit superior adsorption kinetics and enhanced mass transfer rates compared to activated carbons (ACs), owing to their fibrous morphology and the organized arrangement of micropores [160]. ACFs are derived from organic precursor fibers through pyrolysis and activation with H_2O and CO_2, and they have been effectively utilized as adsorbents or substrates for removing indoor pollutants in air filters. While ACFs have lower adsorption efficiency for polar volatile organic compounds (VOCs), their adsorption properties can be improved through surface modification and coupling with other semiconductors. However, the production cost of ACFs is higher due to the expensive organic precursors, which limits their applications [155,160].

ACFs possess a hydrophobic nature, resulting in a greater adsorption affinity for non-polar and weakly polar VOCs [161]. They are particularly effective for removing high concentrations of VOCs in humid conditions, as they do not strongly interact with water molecules. The hydrophobicity of ACFs can be modified by introducing oxygen-containing functional groups onto the fibers or by applying metal oxides to their surfaces. Such modifications enhance their adsorption capacity for target pollutants [155]. Pollutants are initially adsorbed onto the ACFs and subsequently transferred to the photocatalyst. ACFs can also adsorb and re-adsorb intermediates and by-products, increasing their retention time and facilitating the desired reactions. This process leads to a higher degradation rate of the target pollutant, reduces competition for adsorption sites, and minimizes the release of by-products [162].

The role of ACFs as an adsorbent in TiO_2 photocatalysts has been demonstrated in studies focusing on the photocatalytic removal of methyl ethyl ketone (Figure 18). Specifically, the use of ACFs as support materials for TiO_2 resulted in a significant increase in the adsorption capacity for methyl ethyl ketone, achieving 100% breakthrough after 15 to 19 h. This enhancement in adsorption properties is attributed to the microporous structure, large surface area, and pore volume of ACFs. The adsorption of various compounds is also influenced by van der Waals interactions and interactions with functional groups on the ACF surfaces. In this context, π-π interactions and donor-acceptor complexes are the predominant mechanisms for the adsorption of VOCs.

6.3. Carbon Nanotubes

The applications of carbon nanotubes (CNTs) for the removal of indoor pollutants have been extensively studied due to their thermal and mechanical stability, hydrophobicity, and hollow structure, which contribute to a large surface area. CNTs also exhibit high electrical conductivity and structural tunability; however, their high production costs limit their use in photocatalysis. The adsorption capacity of CNTs is influenced by several factors. Notably, there is a direct correlation between the diameter of the nanotubes and their adsorption affinity for volatile organic compounds (VOCs). Research has demonstrated that CNTs possess a higher affinity for slightly polar molecules such as acetone, toluene, and methanol. Additionally, the electrical charge of CNTs can affect their adsorption capacity towards various pollutants [155].

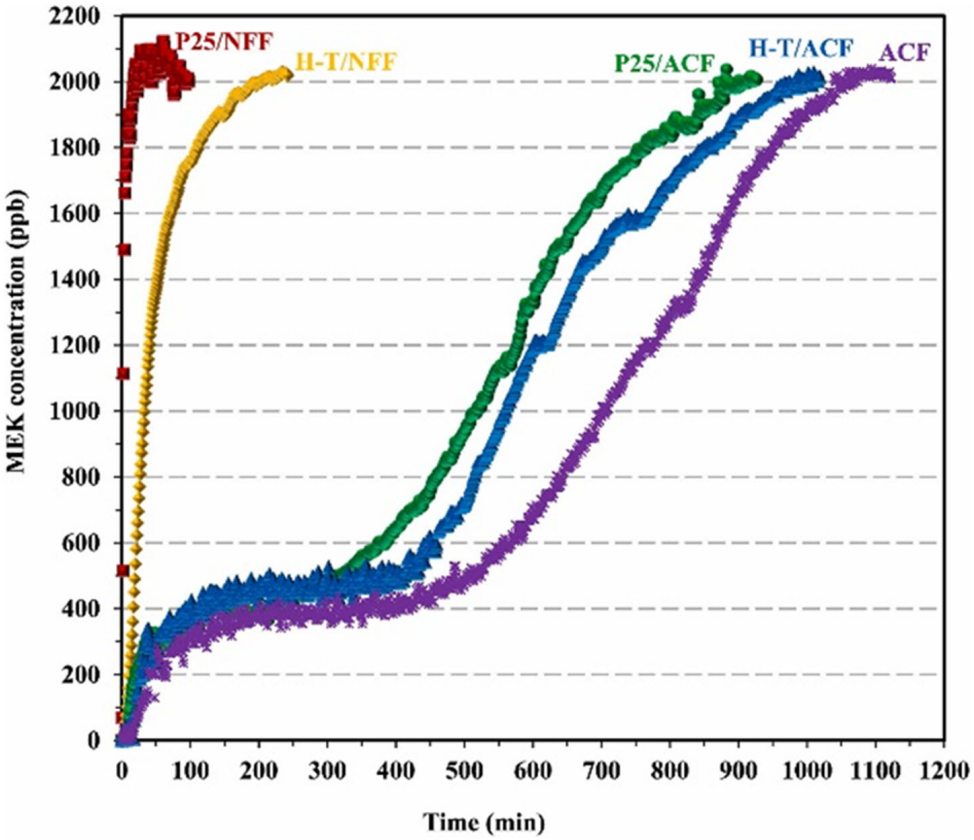

Figure 18. Adsorption of methyl ethyl ketone using various photocatalytic air filters [162].

When coupled with photocatalysts, CNTs serve two primary roles: they act as photosensitizers and function as electron sinks, facilitating the transfer of electrons to adsorbed pollutant molecules. These actions enhance the photocatalytic activity of the semiconductor, leading to increased degradation of pollutants [141].

In a study examining TiO_2/CNT composites for the photocatalytic removal of acetone (Figure 19) [163], it was found that introducing CNTs into the photocatalyst resulted in higher photocatalytic activity for certain samples compared to P25. Specifically, increasing the amount of CNTs in the composite led to a reduction in anatase crystallite size, an increase in the anatase content, and a decrease in brookite content within the TiO_2. These changes contributed to enhanced photocatalytic efficiency. However, it was also observed that the introduction of CNTs negatively impacted the adsorption properties of TiO_2 under UV light when the amount of CNTs exceeded the optimum level. Interestingly, some samples exhibited higher photocatalytic activity compared to the TiO_2/AC composite, despite CNTs having a lower surface area than activated carbon [163].

The presence of CNTs in the composite can also alter the morphology of TiO_2. Specifically, an increase in CNT content results in a transition from spherical particles to agglomerated particles and ultimately to bulk structures. Furthermore, photoluminescence spectra indicated that the TiO_2/CNT composites exhibited lower photoluminescence intensity than untreated TiO_2, suggesting a reduced rate of charge carrier recombination. As the CNT content in the TiO_2/CNT composites increased, the photoluminescence intensity for the various samples decreased [163].

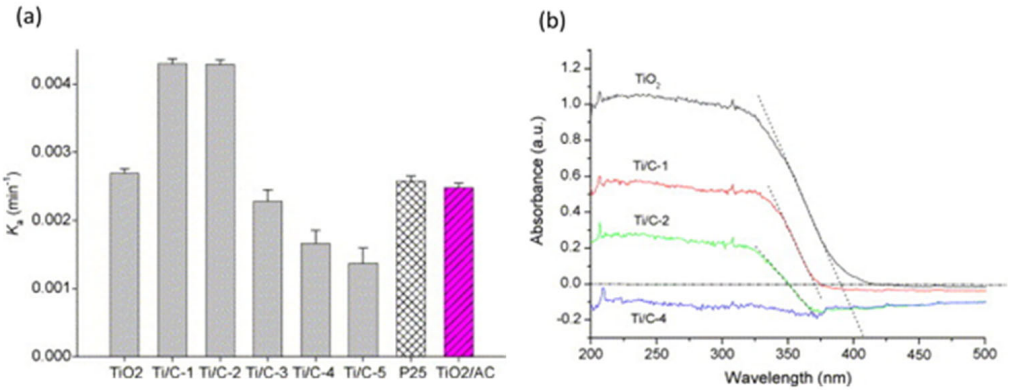

Figure 19. (**a**) Photocatalytic activity of TiO_2, TiO_2/CNT with various molar ratio, P25 and TiO_2/AC, and (**b**) UV–vis spectra of TiO_2 and TiO_2/CNT with various molar ratio [163].

6.4. Graphene

Recently, graphene has gained significant attention in photocatalytic oxidation for the removal of pollutants. It has been demonstrated that graphene possesses excellent adsorption capacity and can extend the light absorption range, thereby enhancing the photocatalytic activity of TiO_2 [90]. Graphene has a high affinity for pollutants, particularly polar volatile organic compounds (VOCs), along with a large surface area, chemical and thermal stability, and a robust pore structure. Due to its electronically conductive two-dimensional structure, graphene acts as a sink for accepting and transporting photogenerated electrons to the photocatalyst. The conduction band energy of most semiconductors is typically more negative than the low Fermi level of graphene (E = −0.08 V) [164]. Consequently, when graphene is coupled with a semiconductor, photogenerated electrons are rapidly transferred from the conduction band of the photocatalyst to graphene. Additionally, graphene exhibits high charge carrier mobility, allowing electrons to move swiftly [165]. This characteristic makes graphene an effective electron acceptor and mediator, reducing charge carrier recombination and enhancing photocatalytic activity [166].

Recently, graphene-derived materials such as graphene oxide (GO) [167] and reduced graphene oxide (rGO) [168] have been studied for their advantageous properties. Unlike hydrophobic graphene, GO contains functional groups, including carboxyl (COOH) and hydroxyl (OH), enabling efficient interaction with various compounds through covalent [169] and non-covalent bonding [170]. The band structure of GO is linked to its degree of oxidation and can be altered using different synthesis methods. rGO is prepared by chemically or thermally treating GO to remove surface functional groups, resulting in a material with a high surface area and a significant affinity for non-polar VOCs due to its hydrophobic nature. rGO can also be modified to increase its pore volume, thereby enhancing its adsorption capacity.

In a study [90] (Figure 20), rGO/TiO_2 exhibited remarkable photocatalytic activity under visible light for the degradation of formaldehyde. The introduction of rGO into the photocatalyst led to better dispersion of TiO_2 nanoparticles, which typically tend to aggregate. Analysis of UV-visible adsorption spectra revealed that the incorporation of rGO into the photocatalyst improved its adsorption properties in the visible light range. The rGO/TiO_2 composite demonstrated higher photocatalytic efficiency for formaldehyde removal under visible light compared to untreated TiO_2 and rGO. This high photocatalytic efficiency can be attributed to the conductive properties of rGO, which facilitate the rapid transfer of photogenerated electrons from the valence band of TiO_2 to electron acceptors within the rGO structure. The enhanced electron transfer leads to an increased lifetime of the photogenerated charge carriers, resulting in improved photocatalytic activity [90].

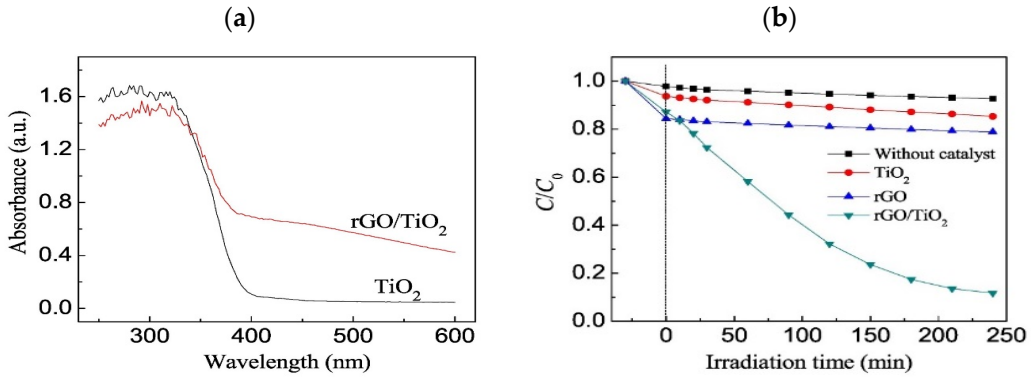

Figure 20. (**a**) UV–vis absorption spectra of TiO_2 and rGO/TiO_2 and (**b**) degradation of formaldehyde using no catalyst, TiO_2, rGO, and rGO/TiO_2 [90].

6.5. Graphitic Carbon Nitrides

Graphitic carbon nitride (g-C_3N_4) is a carbon-based two-dimensional conjugated polymer that has recently gained attention in photocatalysis. Although it has a relatively low specific surface area and a limited porous structure, its adsorption properties can be enhanced through modifications with metal oxides that increase its surface area [155]. g-C_3N_4 is a semiconductor with an energy band gap of 2.7 eV, featuring conduction band and valence band potentials of −0.85 eV and 1.85 eV, respectively [171]. When exposed to radiation with sufficient energy, it can photogenerate electron and hole pairs. Due to its excellent stability, metal-free composition, and environmental friendliness, g-C_3N_4 is utilized as a photocatalyst for the removal of volatile organic compounds (VOCs). However, its photocatalytic activity is hindered by a low density of active sites and low charge carrier mobility, which leads to a high recombination rate of electron-hole pairs [172].

To enhance the adsorption and photocatalytic efficiency of g-C_3N_4, various strategies have been explored, including doping [173], surface modifications [174], and the creation of heterojunctions with other semiconductors [175]. For instance, a composite photocatalyst combining g-C_3N_4, TiO_2, and waste zeolites has been synthesized for the photocatalytic removal of formaldehyde (Figure 21) [95]. In this study, it was observed that the emission peak of g-C_3N_4 in the photoluminescence spectrum is intense and broad, indicating rapid charge carrier recombination. However, when combined with TiO_2 and waste zeolites, the photoluminescence intensity of these samples decreases significantly and experiences a blue shift, likely due to enhanced contact with TiO_2.

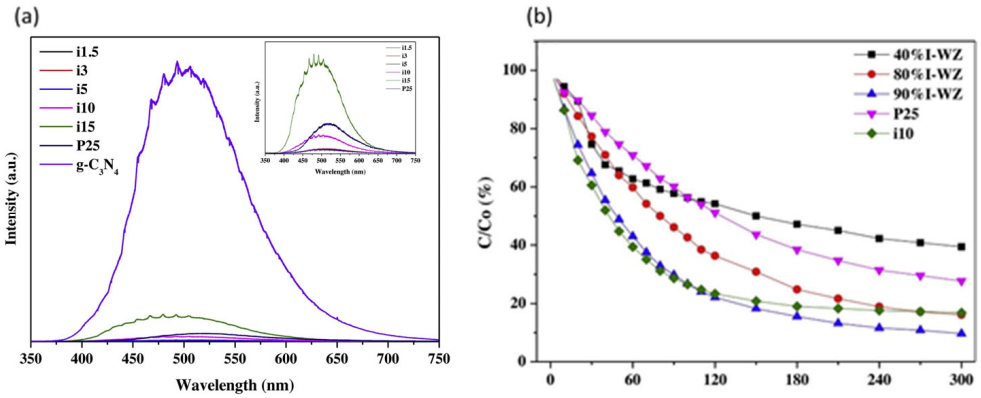

Figure 21. (**a**) Photoluminescence spectra of g-C_3N_4-TiO_2 with various amounts of g-C_3N_4, P25, and g-C3N4 and (**b**) degradation of formaldehyde using g-C_3N_4-TiO_2/waste zeolites with various amount of g-C_3N_4, P25 and a sample of g-C_3N_4/TiO_2 [95].

Furthermore, it was noted that the total pore volume and micropore volume of the samples slightly increase as the amount of g-C_3N_4 in the composite increases, probably due to the formation of low-density g-C_3N_4 on TiO_2. Under visible light, photogenerated electrons in g-C_3N_4 are transferred to the conduction band of TiO_2 through a heterojunction, reducing the charge carrier recombination rate and increasing photocatalytic activity. The photogenerated electrons in the conduction band of TiO_2 react with oxygen molecules to form reactive oxygen species (ROS), while the photogenerated holes in the valence band of g-C_3N_4 react with water molecules to produce hydroxyl (·OH) radicals. The photocatalytic degradation of formaldehyde was investigated, revealing that most of the prepared samples exhibited higher photocatalytic activity compared to P25 [95].

6.6. Carbon Dots

Carbon dots (CDs) are zero-dimensional carbon-based nanomaterials that have recently gained attention in photocatalysis due to their non-toxicity, low cost, electron conductivity, and excellent photostability [176]. When coupled with other materials, CDs can provide highly selective adsorption sites for photocatalytic processes. Additionally, the electronic structure of CDs allows them to act as electron donors or acceptors after photoexcitation, resulting in enhanced electron transmission, photochemical stability, and tunable optical properties. The incorporation of CDs into semiconductor photocatalysts can narrow the band gap and expand their adsorption capacity in the visible light range. Research on the use of CDs for the photocatalytic reduction of carbon dioxide [177], volatile organic compounds (VOCs) [178], and other pollutants has significantly increased in recent years. To improve their properties, CDs have undergone doping, and composite formation to create heterojunctions and surface modifications with various functional groups. This class of carbon-based nanomaterials includes carbon quantum dots and graphitic carbon nitride quantum dots, each with distinct chemical properties and structures [87].

Carbon quantum dots (CQDs) are ultra-small nanoparticles with diameters less than 10 nm, exhibiting the electronic properties of carbon nanomaterials and the optical characteristics of quantum dots [179]. The integration of CQDs into semiconductor photocatalysts can enhance their photocatalytic activity through various mechanisms, including photosensitization [180], increased adsorption of VOCs, electron mediation [181], and reduction of band gap energy. Furthermore, the surface of CQDs is rich in functional groups containing oxygen, which contributes to their water solubility [182].

Recently (Figure 22), graphitic carbon nitride quantum dots (CNQDs) have been synthesized and combined with TiO_2 to improve the photocatalytic performance of this material under visible light and enhance the efficiency of surface charge carrier transfer. For example, a study on CNQDs in situ-modified TiO_2 inverse opal [183] demonstrated superior photocatalytic efficiency in the degradation of toluene compared to conventional inverse opal TiO_2, P25, and bulk TiO_2. The photoluminescence spectrum of the CNQDs in situ-modified TiO_2 inverse opal showed lower intensity than that of inverse opal TiO_2 and bulk TiO_2, indicating a reduction in the charge carrier recombination rate due to the introduction of CNQDs. Notably, the CNQDs in situ-modified TiO_2 inverse opal achieved a toluene removal rate of 95%, surpassing the degradation rates of inverse opal TiO_2 (88%), P25 (77%), and bulk TiO_2 (60%) [183].

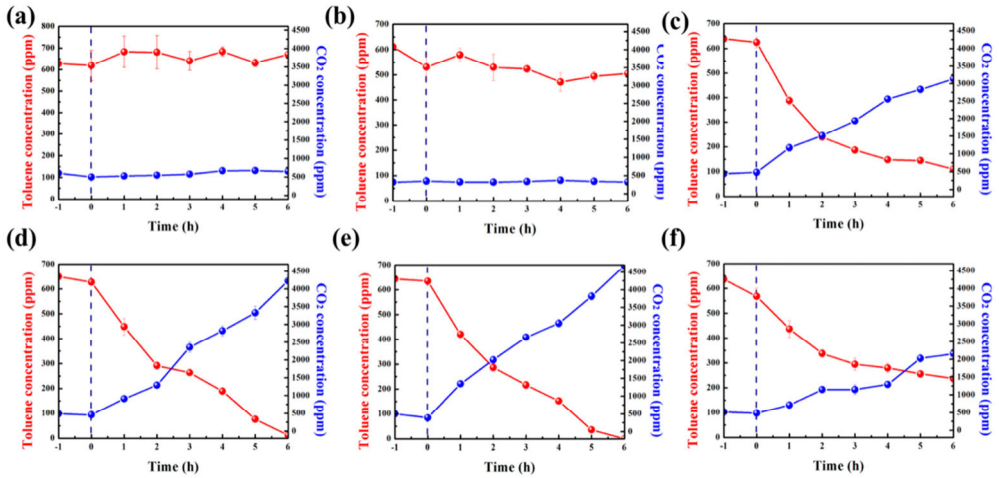

Figure 22. Conversion of toluene and concentration of CO_2 using no catalyst (**a**) and TCN IO (**b**) in dark; bulk-TiO_2 (**c**), inverse opal TiO_2 (TiO_2 IO) (**d**), CNDQs in situ-modified TiO_2 inverse opal (TCN IO) (**e**) and P25 (**f**) under irradiation [183].

7. Other Metal-Oxide Nanomaterials

Other than the most common titania-based and carbon-based nanomaterials, various materials such as metal oxides have been used in photocatalysis. Research about the least common nanomaterials especially ZnO [184] and WO_3 [185] have increased in recent years.

7.1. ZnO-Based

Zinc oxide (ZnO) has been known for centuries, primarily as a pigment and additive in products like ceramics, paints, and ointments. Its photochemical properties, however, began to gain attention in the early 20th century when scientists first observed its semiconducting and photoactive behaviors.

The development of solid-state physics, in the 1930s, led to the discovery of the semiconducting nature of ZnO. Its wide bandgap (~3.37 eV) and high exciton binding energy (~60 meV) made it a subject of interest for electronic and optical applications. Early photocatalytic studies were primarily focused on understanding its photoconductivity and interaction with ultraviolet (UV) light. These investigations laid the groundwork for using ZnO in photochemical reactions.

ZnO gained more importance in photocatalysis during the 1970s and 1980s, driven by the global energy crisis and increased environmental concerns. Researchers were exploring photocatalytic water splitting and pollutant degradation as solutions to energy and environmental challenges.

Nowadays, ZnO is one of the most extensively studied nanomaterials for photocatalysis, owing to its excellent photocatalytic, electrical, and optical properties [186]. ZnO wide band gap limits its adsorption capacity in the visible light range, thus constraining its application as a photocatalyst in indoor environments. To enhance its visible light adsorption properties, ZnO can be modified using dopants [187] or combined with other semiconductors to form composites [188]. Due to its polar nature, ZnO promotes rapid separation and transfer of photogenerated charge carriers. When irradiated with UV light, ZnO generates photogenerated electron centers (Zn^+) and hole centers (O^-) [189].

Research has examined the degradation of formaldehyde using a photocatalytic ZnO air filter, both with and without UV light irradiation [190]. Notably, the ZnO filter exhibited a higher formaldehyde removal efficiency without UV light. When irradiated with UV light, photogenerated electron-hole pairs react with H_2O molecules to form hydroxyl ions, leading to the photocatalytic adsorption and degradation of formaldehyde. However, under UV radiation, fewer pollutant molecules are adsorbed on the surface of the ZnO

filter, resulting in lower removal efficiency. Conversely, the ZnO filter without UV light demonstrates higher removal efficiency due to its greater adsorption capacity, as more formaldehyde molecules are captured on its surface in the presence of condensed H_2O, given formaldehyde's hydrophilic nature [190].

In another study [191] (Figure 23), ZnO nanorods (ZnO-NRs) were synthesized through hydrothermal growth of ZnO nanoparticles and assessed for the photocatalytic degradation of formaldehyde. These ZnO-NRs were incorporated into the nanofibrils of a polytetrafluoroethylene (PTFE) membrane (ZnO-NRs@PTFE), commonly used for air purification. The ZnO-NRs@PTFE filter achieved a formaldehyde removal rate of 53%, while the PTFE membrane alone exhibited no formaldehyde removal. Furthermore, the deposition of silver (Ag) nanoparticles on the ZnO nanorods improved photocatalytic removal, reaching a maximum degradation rate of 60%. The enhanced photocatalytic activity of the ZnO-NRs@PTFE filter can be attributed to the increased specific surface area of the membrane and the reduced spacing between its fibrils due to the presence of ZnO nanorods. Additionally, Ag nanoparticles act as electron traps, promoting charge carrier separation and decreasing the recombination rate [191].

As mentioned earlier, ZnO can be doped to enhance its adsorption properties under visible light. For instance, a study synthesized nitrogen-doped (N-doped) ZnO micropolyhedrons to evaluate their photocatalytic activity toward formaldehyde degradation (Figure 23B) [192]. The UV-visible adsorption spectra indicated that the introduction of nitrogen atoms as dopants in ZnO significantly improved the photocatalyst's adsorption properties in the visible light range. The N-doped ZnO photocatalyst exhibited a degradation rate of approximately 85.6% for formaldehyde, outperforming both N-doped P25 and pure ZnO. The high photocatalytic activity of the N-doped ZnO catalyst can be attributed to three main factors: the enhanced adsorption capacity under visible light, the increased charge carrier transfer rate on the ZnO surface, and the enhanced separation of charge carriers due to the formation of an intermediate band in the ZnO band gap at around 1.3 eV above the valence band, induced by the introduction of nitrogen atoms.

When compared to most other photocatalytic materials, ZnO is more widely available, inexpensive, and easy to synthesize, making it an economically viable option for large-scale photocatalytic air purification systems. It can also be synthesized in various nanostructures (e.g., nanorods, nanowires, nanoparticles), which provide high surface areas and tunable properties for improved catalytic activity. Still, ZnO nanoparticles tend to aggregate, reducing their effective surface area and, consequently, their photocatalytic efficiency.

Over the years, ZnO has proven effective in decomposing a wide range of air pollutants, including VOCs, carbon monoxide (CO), and particulate matter, due to its strong oxidative properties. Moreover, ZnO has also demonstrated antimicrobial properties, making it useful in air filtration systems for controlling airborne pathogens.

ZnO primarily absorbs UV light, which constitutes only ~5% of the solar spectrum, limiting its effectiveness under natural sunlight. Extending its activity to the visible light range remains a significant challenge. Moreover, ZnO is prone to photocorrosion under prolonged light irradiation, particularly in humid conditions, which can degrade its structure and reduce long-term stability.

7.2. MnO_2-Based

Manganese dioxide (MnO_2) has long been known as a mineral, most notably as the naturally occurring pyrolusite. Its use has been common in batteries, ceramics, and as a catalyst in chemical processes, such as the oxidation of gases. Until the early 20th century, MO_2 was primarily seen as a material with industrial significance in oxidative reactions, rather than for photocatalysis. While titanium-based photocatalysts dominated

the early years of photocatalysis research, MnO_2 began to gain attention in the 1970s and 1980s as a potential material for oxidizing air pollutants under UV light. The real breakthrough for MnO_2-based photocatalysts in environmental applications came in the 1990s and early 2000s with the advent of nanotechnology. Research into nanomaterials had rapidly expanded during this period, and scientists began investigating how the unique properties of MnO_2 nanostructures could be exploited for photocatalysis.

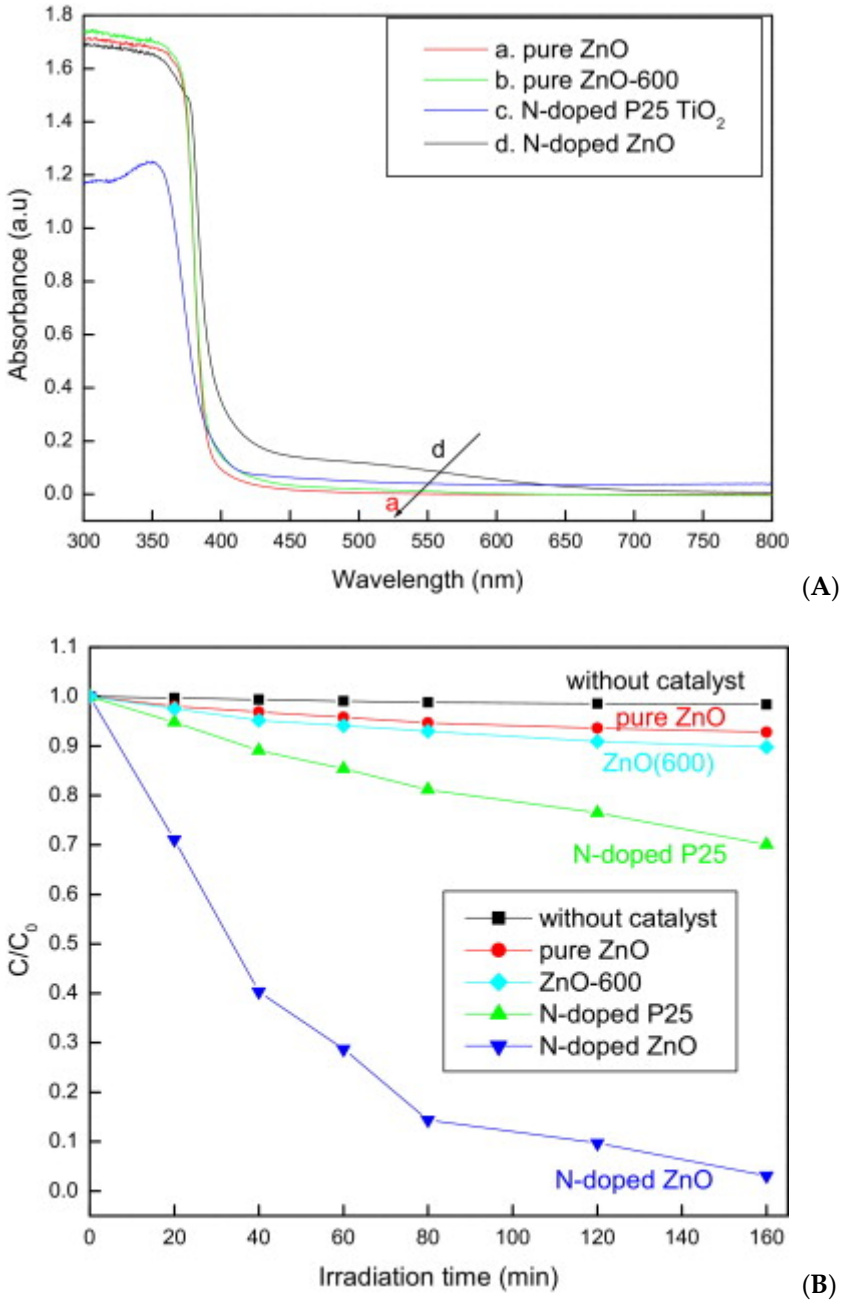

Figure 23. (**A**) UV–visible absorption spectra of various photocatalysts and (**B**) degradation of formaldehyde using various photocatalysts under visible-light irradiation [192].

Nowadays, manganese dioxide (MnO_2)-based nanomaterials have gained significant attention as alternatives to noble metal-based photocatalysts due to their advantageous properties. These materials are studied in photocatalysis because of their high specific surface area, pore characteristics, and oxygen storage potential. Additionally, MnO_2 is low-cost and environmentally compatible, making it an attractive option for various applications. This material exhibits significant photoadsorption properties for volatile organic

compounds (VOCs) and demonstrates an important photothermal effect. While MnO_2 shows high absorbance under UV and visible light irradiation, its adsorption properties are relatively lower in the near-infrared radiation range. The photocatalytic activity of MnO_2 can be further enhanced through doping or by forming junctions with other semiconductors [193].

Layered manganese oxide, commonly known as birnessite, has been extensively studied for the removal of formaldehyde [194]. This material has achieved a remarkable formaldehyde removal rate of up to 93%. Research indicates that H_2O molecules within birnessite enhance the adsorption of formaldehyde, with increased humidity levels (0% to 33% and then to 65%) positively affecting this process. However, at higher humidity levels of 92%, a decrease in the degradation rate was observed, likely due to competition between H_2O and formaldehyde for the active sites on the photocatalyst.

In another study (Figure 24) [193], a graphene-based MnO_2 composite (MnO_2-G) was evaluated for photocatalytic removal of formaldehyde under UV, visible, and infrared radiation. The MnO_2 exhibited superior formaldehyde removal capabilities compared to graphene, primarily due to its enhanced adsorption capacity; graphene was observed to desorb the pollutant instead. Notably, the graphene sample did not yield any CO_2, indicating that it only adsorbed the pollutant without facilitating its degradation. Conversely, the MnO_2-G composite demonstrated the highest photocatalytic activity for degrading formaldehyde, achieving a conversion rate of 80% into CO_2, significantly higher than that of MnO_2 alone. This enhancement in photocatalytic activity can be attributed to the synergistic photothermal effect between graphene and MnO_2, where photothermal energy is transferred from graphene to MnO_2, leveraging graphene's high conductivity. The combined photothermal effect and efficient electron transfer activate the active sites on MnO_2, facilitating the oxidation of the pollutant [193].

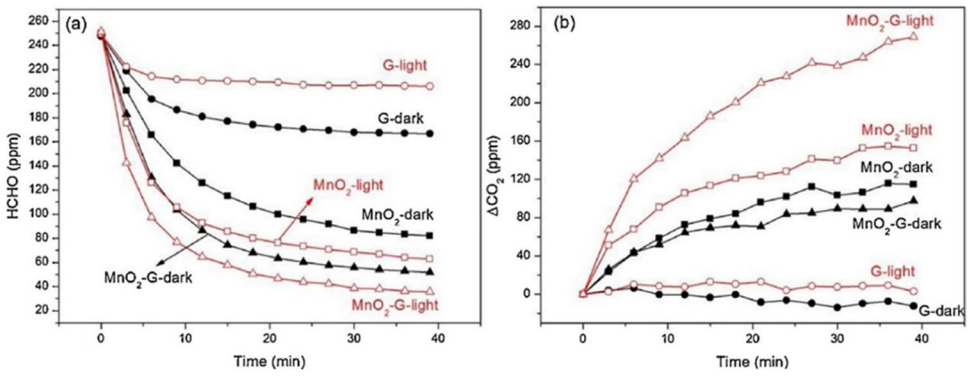

Figure 24. Removal of formaldehyde (**a**) and concentration of CO_2 (**b**) using MnO_2, graphene, and MnO_2-G with and without irradiation [193].

Apart from being low-cost and abundant, MnO_2 is a non-toxic, environmentally friendly material. It does not release harmful byproducts during photocatalytic reactions, which makes it an ideal choice for sustainable air pollution control technologies. Moreover, it shows good stability under various operating conditions, such as high humidity and temperature, which are typical in real-world air pollution environments.

Still, even if MnO_2 photocatalysts typically exhibit strong activity under UV light, like many other photocatalysts they are not very effective under visible light. This limits their efficiency under natural sunlight unless strategies to extend their activity into the visible spectrum are developed.

7.3. WO_3-Based

Tungsten trioxide (WO_3) was first identified in the 19th century and has long been known for its distinctive blue color and various industrial applications, such as in the production of catalysts and as a component in electrochromic devices. WO_3's photocatalytic properties, however, were not recognized until much later. Its potential for photocatalysis in environmental applications, especially for air pollution control, became an area of growing interest only in the late 20th century.

Early studies focused on WO_3's ability to degrade organic compounds under UV light, similar to other photocatalysts like TiO_2, but with the added benefit of WO_3's potential visible light activity.

WO_3-based nanomaterials have garnered attention in photocatalysis due to their narrow band gap of approximately 2.6 eV and the high oxidation capacity of their photogenerated holes, which can oxidize H_2O to O_2 [195]. WO_3 is frequently utilized as a co-catalyst to enhance the photocatalytic activity of other semiconductors because of its narrow band gap. The introduction of WO_3 can significantly improve the photocatalytic efficiency of the composite under visible light radiation due to the unique optical and electronic properties of the modified photocatalyst. Studies have shown that combining WO_3 with TiO_2 enhances photocatalytic activity under both UV and visible light. The conduction band of WO_3 is more positive than that of TiO_2, facilitating the transfer of photogenerated electrons from TiO_2 to WO_3 under UV light, thereby increasing the overall photocatalytic activity. Under visible light, only WO_3 is excited, allowing the adsorbed pollutant molecules on TiO_2 to react with the photogenerated charge carriers from WO_3. This synergistic effect between the two semiconductors significantly enhances the photocatalytic activity [195].

Research has examined the photocatalytic degradation of NO using WO_3/TiO_2 composites with varying proportions of TiO_2 under both visible light and UV radiation [195]. The results indicated that incorporating TiO_2 into the WO_3 photocatalyst increases the photocatalytic degradation of NO under both light conditions. The presence of TiO_2 likely promotes charge carrier separation due to the formation of a heterostructure, leading to enhanced photocatalytic activity. Specifically, the highest photocatalytic activity was observed with 70% TiO_2 under UV light and 80% TiO_2 under visible light. However, further increasing the TiO_2 content resulted in reduced photocatalytic activity, likely due to the formation of recombination centers [195].

In another study [120] (Figure 25), nanosheets of N-doped TiO_2/WO_3 (WO_3–N–TNSs) composites were synthesized with varying WO_3 content to investigate their photocatalytic degradation of vaporous hexane. The band gap of the samples was determined from UV-vis absorption spectra, revealing that the WO_3–N–TNS samples exhibited a significant increase in adsorption capacity with band gaps ranging from 2.75 to 2.91 eV, compared to N-TNS (3.08 eV) and undoped TNS (3.17 eV). It was also observed that increasing the WO_3 content resulted in greater visible light shifts in the WO_3–N–TNS samples.

These composites demonstrated higher photocatalytic efficiency compared to N-doped TNS (N–TNS) and undoped TNS, attributed to improved adsorption efficiency, enhanced charge carrier separation, and the combined effects of WO_3 and N doping. Photoluminescence spectra indicated a lower intensity for the WO_3–N–TNS samples compared to the others, suggesting a lower recombination rate. The optimal amount of WO_3 in this photocatalyst was determined based on trends in specific surface area and pore volume. Excess WO_3 in the photocatalyst likely partially blocked TNS pores or reduced the specific surface area of WO_3, leading to a decrease in the overall surface area of WO_3–N–TNS [120].

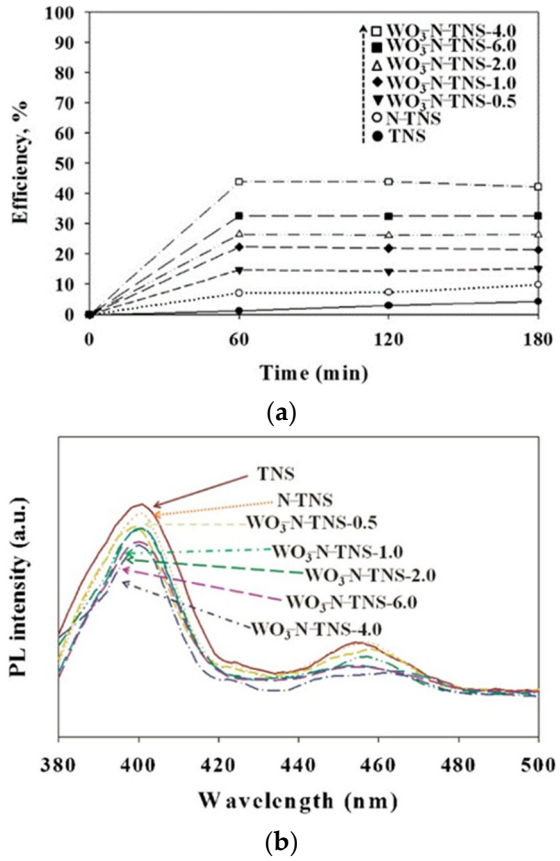

Figure 25. (**a**) Photocatalytic efficiency of hexane removal using TNS, N–TNS, and WO_3–N–TNSs containing various amounts of WO_3 and (**b**) photoluminescence spectra of TNS, N–TNS, and WO_3–N–TNSs containing various amount of WO_3 [120].

Apart from its visible light activity and effective pollutant degradation capabilities, WO_3 is a non-toxic, environmentally friendly material, making it a safe and sustainable option for air pollution control applications. It does not generate harmful byproducts during photocatalytic reactions, aligning with the principles of green chemistry. Moreover, tungsten is relatively abundant, and the cost of synthesizing WO_3 is lower compared to other advanced photocatalysts, making it an economically viable material for large-scale environmental applications.

On the other hand, WO_3 photocatalytic efficiency is somehow limited under low light intensity, as it requires a certain threshold of energy to activate. Moreover, WO_3-based photocatalysts can be sensitive to environmental conditions such as humidity and temperature. High humidity can lead to the formation of hydrated tungsten oxides, which can alter the material's photocatalytic properties.

7.4. CeO_2-Based

Cerium oxide (CeO_2), commonly referred to as ceria, is a p-type semiconductor that serves as an effective photocatalyst due to its chemical stability, low toxicity, affordability, high adsorption capacity under UV radiation, and impressive photocatalytic activity.

The compound was first identified in the early 19th century and gained early industrial significance for applications in catalysis, particularly in automotive catalytic converters. Its redox-active nature, where cerium can exist in both +3 and +4 oxidation states, made CeO_2 a valuable catalyst for various reactions, but its photocatalytic properties were not extensively studied until later. in the late 1990s and early 2000s. Early studies identified CeO_2's ability to generate reactive oxygen species (ROS), such as hydroxyl radicals (·OH),

under UV light, similar to more conventional photocatalysts like TiO_2. This opened up new avenues for using CeO_2 in photocatalytic air purification, especially for degrading volatile organic compounds (VOCs), nitrogen oxides (NOx), and ozone (O_3).

When combined with an n-type semiconductor, CeO_2 displays photocatalytic properties comparable to those of the widely used TiO_2. However, its photocatalytic applications are restricted by a wide band gap, a high charge carrier recombination rate, and a low charge transfer rate. To enhance its functionality, CeO_2 has been coupled with other semiconductors to form composites that narrow its band gap. Furthermore, CeO_2 can improve the stability of the catalysts it is combined with, possesses a substantial oxygen storage capacity, and can effectively release and store oxygen to drive photocatalytic reactions [143]. CeO_2 has a stable fluorite structure containing both Ce^{4+} and Ce^{3+} ions, which can lead to the creation of oxygen vacancies. The introduction of metal heteroatoms as dopants can further promote the formation of these vacancies [196] (Figure 26).

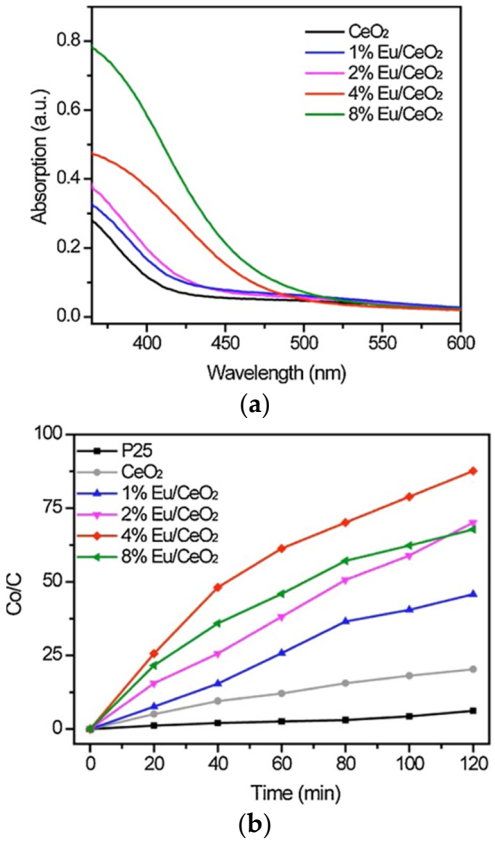

Figure 26. (**a**) UV–vis spectra of CeO_2 and Eu/CeO_2 containing different amounts of Eu and (**b**) photocatalytic degradation of formaldehyde using P25, CeO_2, and Eu/CeO_2 containing different amounts of Eu [196].

One study investigated a photocatalyst composed of CeO_2 and $BiVO_4$ (CeO_2-$BiVO_4$) coupled through a heterojunction to assess its photocatalytic degradation of formaldehyde under visible light [197]. This coupling resulted in a narrowing of the CeO_2 band gap and an enhancement of its photocatalytic activity. UV-vis adsorption spectra revealed that the introduction of $BiVO_4$ significantly increased CeO_2's adsorption in the visible range. Additionally, the photoluminescence intensity of the composite was lower than that of pure CeO_2 and $BiVO_4$, indicating a reduced charge carrier recombination rate [197].

The CeO_2-$BiVO_4$ composite demonstrated a maximum formaldehyde degradation of 78%, outperforming both pure CeO_2 and $BiVO_4$. The optimal ratio of the two photocatalysts was determined to be 4:1 for CeO_2-$BiVO_4$ [197].

In another study, the photocatalytic activity of europium-doped CeO_2 nanosheets was examined for formaldehyde degradation. Different amounts of Eu were used to dope CeO_2, enhancing defects on its surface and promoting the formation of oxygen vacancies. UV-vis adsorption spectra indicated that the visible range adsorption increased with higher Eu concentrations, with all Eu/CeO_2 samples showing superior adsorption compared to undoped CeO_2. The Eu/CeO_2 samples exhibited significantly greater photocatalytic activity than both undoped CeO_2 and P25 (Figure 26). Notably, the 4% Eu/CeO_2 sample exhibited the highest photocatalytic activity, with an 80% increase in degradation rate compared to undoped CeO_2 and P25. However, an excessive amount of Eu led to an abundance of oxygen vacancies, which can facilitate charge carrier recombination, thereby reducing photocatalytic activity. The enhanced photocatalytic degradation of formaldehyde by the Eu/CeO_2 samples was attributed to an increase in specific surface area and improved adsorption capacity.

Cerium oxide is known for its unique redox behavior, where cerium can switch between Ce^{3+} and Ce^{4+} oxidation states. This redox flexibility facilitates the generation of reactive oxygen species (ROS), such as hydroxyl radicals (·OH), which are highly effective in degrading a variety of air pollutants, including VOCs, NOx, and ozone. CeO_2 is also highly stable under a range of environmental conditions, including exposure to UV light, high temperatures, and humidity. This stability ensures that CeO_2-based photocatalysts maintain their effectiveness over extended periods, making them ideal for real-world applications in air purifiers and outdoor environments. Cerium is a relatively abundant element compared to other rare earth metals, and CeO_2 is inexpensive to synthesize. This makes CeO_2-based photocatalysts a cost-effective option for large-scale air pollution remediation applications. Still, CeO_2's ability to capture visible light remains relatively limited in its unmodified form. To enhance its performance under natural sunlight or artificial light, CeO_2 typically needs to be modified through doping with other metals or by combining it with other photocatalysts, making the process more expensive and more likely to pose environmental risks such as leaching.

8. CdS-Based Nanomaterials

Cadmium sulfide (CdS) is a semiconductor material that has been studied since the late 19th century, primarily for its optical properties, such as its distinct yellow color. In the early 20th century, CdS was known for its use in photoconductors and light-emitting devices. The photocatalytic properties of CdS began to be explored more actively in the 1970s. The recognition that semiconductors could drive photocatalytic reactions, particularly the decomposition of water into hydrogen and oxygen under UV light, led to increased interest in CdS as a photocatalyst for environmental applications. In the early 1990s, researchers began examining CdS for its ability to degrade organic pollutants and reduce carbon dioxide.

As a semiconductor with a band gap of approximately 2.4 eV, CdS can absorb visible light effectively [198]. The conduction band of CdS is less positive than those of other typical semiconductors, such as TiO_2 and ZnO, enabling heterojunction formation with these semiconductors to facilitate efficient transfer of photogenerated electrons across their electronic bands. However, CdS is susceptible to photo-corrosion, degrading into sulfur and cadmium ions, which diminishes its photocatalytic performance [199]. To mitigate this issue, CdS is often combined with other semiconductors to reduce the degradation [199,200].

In one study [201], CdS-TiO_2 photocatalysts supported on fiberglass cloth (FGC) were evaluated for benzene degradation, with varying CdS nanoparticle concentrations. UV-Vis absorption spectra revealed that higher CdS concentrations increased the adsorption capacity of CdS-TiO_2 photocatalysts. Photocatalytic benzene removal was tested under both

UV-Vis and visible light. Under UV-Vis radiation (Figure 27a), increased CdS nanoparticle content initially enhanced photocatalytic activity, peaking at 0.005 M with a degradation efficiency of 92.8%. Beyond this concentration, activity declined. Under visible light (Figure 27b), all CdS-TiO_2 samples outperformed TiO_2 alone, with optimal CdS concentration at 0.005 M, achieving a maximum degradation efficiency of 32.7%. The activity was lower under visible light as only CdS could photogenerate electrons in this range. Since the conduction band of CdS is positioned below that of TiO_2, electron transfer from CdS to TiO_2 is facilitated, while holes accumulate at the CdS valence band, enhancing charge separation and photocatalytic efficiency. Excessive CdS, however, can create recombination centers, reducing the activity [201] (Figure 27).

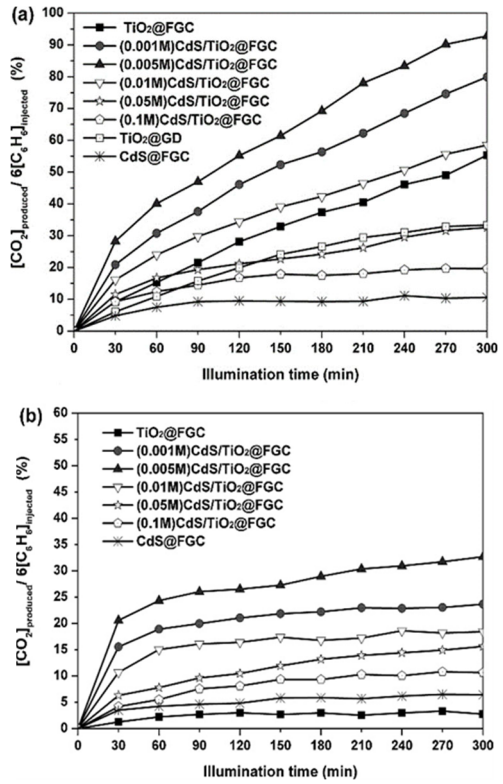

Figure 27. Photocatalytic efficiency for the degradation of benzene using TiO_2@FGC, CdS@FGC, and CdS/TiO_2@FGC containing different amounts of CdS under UV–visible (**a**) and visible light (**b**) irradiation [201].

Another investigation synthesized TiO_2 shells on CdS nanorods (CdS@TiO_2) to study phenol degradation under visible light [202]. All CdS@TiO_2 samples exhibited superior photocatalytic efficiency compared to untreated CdS, with the optimal configuration using 2 mL of titanium tetrabutoxide as the Ti precursor. The enhanced efficiency was attributed to the effective heterojunction between CdS and TiO_2, promoting charge separation. Photoluminescence measurements confirmed this by showing reduced intensity in CdS@TiO_2 samples, indicative of a lower recombination rate for charge carriers [202].

Compared to other high-performance photocatalysts like platinum or other noble metal-based materials, CdS is relatively inexpensive to synthesize, but cadmium is a toxic heavy metal, and CdS-based photocatalysts could pose environmental and health risks if not handled or disposed of properly. CdS tends to undergo photocorrosion under UV irradiation, which limits its long-term stability and photocatalytic efficiency. This degradation occurs due to the dissolution of Cd^{2+} ions from the material's surface. The potential leaching of cadmium ions into the environment raises concerns, especially in

long-term applications, making it necessary to address these issues through encapsulation or composite strategies.

9. Metal-Organic Frameworks

Metal-organic frameworks (MOFs) represent a unique class of materials composed of metal ions or clusters coordinated to organic ligands, forming a highly porous three-dimensional structure. Their exceptional surface area, tunable pore sizes, and chemical versatility make them highly attractive for various photocatalytic applications. The porous nature of MOFs allows for the efficient adsorption of reactants, while their intrinsic properties can be engineered by altering the metal centers or organic linkers, enabling tailored photocatalytic performance [203].

Research on MOFs started in the 1990s when researchers synthesized highly porous materials like MOF-5, developed by Omar M. Yaghi in 1999. The focus during this period was primarily on their gas storage and separation capabilities. However, the highly ordered structures and tunable pore sizes of MOFs hinted at their potential for other catalytic processes, including photocatalysis. A breakthrough occurred when researchers identified the potential of using organic ligands in MOFs as light-harvesting centers. By tailoring the conjugation of the ligands or incorporating metal-organic chromophores, MOFs could be engineered to exhibit strong visible light absorption, expanding their utility in solar-driven processes.

Metal-Organic Frameworks (MOFs) can exhibit photocatalytic properties, but their intrinsic efficiency often requires enhancement through functionalization. Certain MOFs, particularly those with metal centers like Ti [204], Zr [205], and Fe [206] and organic linkers capable of absorbing UV or visible light, can act as photocatalysts on their own; however, they are typically limited by the rapid recombination of electron-hole pairs. To improve their photocatalytic performance, MOFs are commonly functionalized or modified. Techniques include doping with metals or non-metals, such as Ti or graphitic carbon nitride [207], to enhance light absorption and facilitate electron transfer, or incorporating semiconductor nanoparticles like TiO_2 [208] or ZnO [209] to utilize their photoactive properties while retaining the high porosity of MOFs. Additionally, modifications to organic linkers can extend light absorption toward the visible range and introduce active sites for desired reactions. In essence, although MOFs have inherent photocatalytic potential, functionalization is frequently necessary to maximize their efficiency and make them more competitive with traditional photocatalysts [210].

The potential applications of MOFs in photocatalysis are diverse and promising. They have been extensively studied for environmental remediation [203], particularly in the degradation of organic pollutants and dyes under visible light [211]. Additionally, MOFs are being explored for hydrogen production [212] through photocatalytic water splitting and for carbon dioxide reduction into useful chemicals, offering a pathway to address global energy and environmental challenges. Recent advancements in the synthesis and functionalization of MOFs have expanded their applicability, making them a compelling choice for future photocatalytic technologies. As research progresses, MOFs are likely to play a significant role in developing sustainable photocatalytic systems for various industrial and environmental applications (Table 4).

When compared to competitor photocatalytical materials, MOF possesses a higher surface area (up to 7000 m^2/g) and porosity, allowing for enhanced adsorption of reactant molecules. Moreover, their modular design allows for better control of bandgap, light adsorption, and overall catalytic activity. This means that, for example, MOFs can be engineered to absorb visible light by incorporating photoactive organic ligands or metal

centers, making them highly efficient for solar-driven photocatalytic processes or that they can be tuned to target specific pollutants or be focused on the conversion of CO_2.

Table 4. Common MOF in photocatalysis, structures, and examples of their applications.

MOF Name	Structure	Applications	References
MOF-5	Composed of zinc oxide clusters and terephthalate linkers	Photocatalytic degradation of organic pollutants	[213]
ZIF-8	Zinc imidazolate framework with a sodalite topology	CO_2 conversion, degradation of pollutants	[214–216]
MIL-125	Titanium-based framework with a paddle-wheel structure	Photocatalytic degradation of dyes and pollutants	[217,218]
UiO-66	Zirconium-based with a octahedral topology	Photocatalytic degradation of dyes and pollutants	[219]
NH2-MIL-125	Amino-functionalized variant of MIL-125	Photocatalytic degradation of dyes and pollutants	[220,221]
ZIF-67	Cobalt imidazolate framework	Photocatalytic degradation of dyes and pollutants	[222,223]
MOF-808	Zirconium-based with a fcu topology	Photocatalytic CO_2 reduction, degradation of pollutants	[224,225]
MIL-53	The MIL-53 structure consists of inorganic [M-OH] chains, which are connected to four neighboring inorganic chains by therephthalate-based linker molecules	Photocatalytic degradation of dyes and pollutants	[226–228]
Cu-BTC	Copper-based with a three-dimensional structure	Photocatalytic degradation of pollutants	[229]

Despite the advantages, the large-scale use of MOFs is limited by various factors, including their limited thermal, chemical, and photostability, especially under harsh environmental conditions. Moreover, the synthesis of MOFs requires complex procedures, high costs, and strict conditions, making large-scale production more challenging. The low quantum efficiency of many MOFs, due to limited photon utilization, remains also a significant challenge in competing with traditional photocatalysts for large-scale applications.

10. Perovskite Nanomaterials

The study of perovskite materials for photocatalysis began gaining significant attention in the early 2000s, but the broader interest in perovskites dates back to their discovery in the 19th century and their initial use in electronic and optical applications in the 20th century. The turning point for perovskites in photocatalysis occurred after 2010, following the surge of interest in perovskite-based solar cells. Research into perovskites for photocatalysis began with studies of metal oxide-based perovskites, such as barium titanate ($BaTiO_3$) and strontium titanate ($SrTiO_3$). These materials demonstrated potential for applications like water splitting and pollutant degradation, though their UV-light activation limited broader applications. The breakthrough in hybrid perovskite materials like methylammonium lead halides (e.g., $CH_3NH_3PbI_3$) for solar cells sparked an explosion of research into their optical and electronic properties. Soon after, their potential for photocatalysis, particularly under visible light, was explored.

In the mid-2010s, researchers began optimizing perovskite materials for photocatalytic applications, focusing on improving their stability, charge carrier dynamics, and scalability. This period also saw the exploration of lead-free and fully inorganic perovskites to address toxicity and stability challenges.

Perovskite photocatalytic nanomaterials have emerged as an innovative class of materials in the field of photocatalysis, particularly due to their unique crystal structure, which enables remarkable light absorption and efficient charge carrier dynamics. These materials, characterized by the general formula ABX_3, where A and B are cations and X represents an

anion, can be composed of a variety of elements, allowing for tunable properties and enhanced photocatalytic performance. Perovskites can exist in both organic-inorganic hybrid forms and fully inorganic forms, with notable examples including methylammonium lead halides ($MAPbX_3$) [230] and barium titanate ($BaTiO_3$) [231].

The structure of perovskites facilitates efficient charge separation and transport, which minimizes recombination losses and enhances the overall photocatalytic activity. Furthermore, the tunability of perovskite materials allows for optimization of their bandgap, enabling them to effectively harness solar energy for various photocatalytic processes [232].

Perovskite photocatalytic nanomaterials have shown great potential in a range of applications (Table 5). One of the most significant is in the area of environmental remediation, where they can effectively degrade organic pollutants, including dyes and pharmaceuticals, through photocatalytic oxidation. Additionally, they are being actively researched for applications in hydrogen production through water splitting, offering an efficient pathway for solar-to-hydrogen conversion. The ability of perovskites to facilitate carbon dioxide reduction into valuable fuels and chemicals further highlights their versatility and potential impact in addressing energy sustainability and environmental challenges. With ongoing advancements in synthesis methods and material engineering, perovskite photocatalytic nanomaterials are poised to play a pivotal role in future photocatalytic applications.

Table 5. Common perovskites in photocatalysis, structures, and examples of their applications.

Perovskite Material	Structure	Applications	References
$CH_3NH_3PbI_3$	Organometal halide perovskite with a cubic structure	CO_2 reduction	[233,234]
$CsPbBr_3$	Inorganic perovskite with a cubic lattice	Photocatalytic degradation of organic pollutants, CO_2 reduction	[235,236]
$MAPbBr_3$	Methylammonium lead bromide with a tetragonal structure	Photocatalytic CO_2 reduction, dye degradation	[237–239]
$Cs_2AgBiBr_6$	Layered perovskite structure	Photocatalytic hydrogen production	[240]
$BaTiO_3$	Classic perovskite structure	Photocatalytic degradation of pollutants, CO_2 reduction	[241,242]
$SrTiO_3$	Titanium-based perovskite	CO_2 reduction, degradation of pollutants	[243–245]
$KTaO_3$	Potassium tantalate perovskite	Photocatalytic degradation of pollutants	[246–248]
$LaTiO_3$	Lanthanum titanate perovskite	Photocatalytic degradation of pollutants	[249,250]
$MAPbI_3$	Doped organometal halide perovskite	Photocatalytic degradation of pollutants	[239,251]

Perovskite materials exhibit excellent light-harvesting capabilities due to their tunable bandgap and high absorption coefficients, making them highly efficient under visible light. This gives them an advantage over traditional photocatalysts like TiO_2, which primarily rely on UV light for activation. The crystal structure of perovskites facilitates efficient charge separation and transport, reducing electron-hole recombination. This leads to enhanced photocatalytic activity compared to other materials with less efficient charge dynamics. Moreover, perovskites can be engineered with a wide variety of compositions (organic-inorganic hybrids, all-inorganic) to tailor properties such as bandgap, stability, and catalytic efficiency. This tunability is more versatile compared to fixed-structure materials like TiO_2 or ZnO.

Many perovskites can be synthesized using relatively low-temperature and solution-based methods, making them more cost-effective and scalable compared to some metal oxide-based photocatalysts.

One of the most significant drawbacks of perovskites, particularly hybrid organic-inorganic forms, is their susceptibility to degradation under environmental conditions such as moisture, UV light, and high temperatures. This is a critical limitation compared to more robust materials like TiO_2 and ZnO. Moreover, many high-performance perovskites,

such as lead-based halide perovskites, pose environmental and health risks due to their lead content, and the decomposition of hybrid perovskites can release harmful byproducts, including organic residues, which may offset the environmental benefits of their use. This limits their applicability unless non-toxic alternatives are developed.

Additionally, while laboratory-scale synthesis is relatively straightforward, scaling up the production of perovskite materials for commercial applications remains challenging, especially while maintaining performance and stability.

11. Transition Metal Dichalcogenides

Transition metal dichalcogenides (TMDs) have been studied since the mid-20th century, primarily for their unique electronic, optical, and mechanical properties. These materials are represented by the chemical formula MX_2, where "M" is a transition metal (e.g., Mo, W, Ti) and "X" is a chalcogen (S, Se, or Te). TMDs consist of layered structures where transition metal atoms are sandwiched between two layers of chalcogen atoms, forming weakly bonded van der Waals layers, which can be exfoliated into two-dimensional (2D) sheets. Early works focused on bulk materials like molybdenum disulfide (MoS_2) and tungsten disulfide (WS_2), particularly for their potential as solid lubricants due to their layered, easily sheared structures. Interest in TMDs expanded during the 1970s and 1980s, driven by their potential as semiconductors for photovoltaic and optoelectronic applications. Researchers discovered that certain TMDs, such as MoS_2 and WSe_2, exhibit direct or indirect bandgaps depending on their thickness, making them attractive for light-harvesting applications. Their catalytic properties, particularly in hydrogen evolution reactions, also gained attention during this period.

The isolation of graphene in 2004 reignited interest in layered materials, including TMDs. Researchers began investigating their 2D forms, discovering that monolayer TMDs exhibit unique properties distinct from their bulk counterparts. For example, monolayer MoS_2 transitions from an indirect bandgap (bulk) to a direct bandgap (~1.8 eV), making it highly efficient for optoelectronic devices.

TMDs have shown great promise in various photocatalytic applications (Table 6). One of the most notable is in hydrogen production, where materials like MoS_2 and WS_2 have demonstrated significant capabilities for photocatalytic water splitting. They can also efficiently degrade organic pollutants, such as dyes and volatile organic compounds (VOCs), through photocatalytic oxidation processes. Additionally, TMDs are being explored for carbon dioxide reduction, where they can convert CO_2 into valuable hydrocarbons, highlighting their potential in addressing both energy and environmental challenges.

Table 6. Common TMDs materials in photocatalysis, structures, and examples of their applications.

TMD Material	Structure	Applications	References
MoS_2	Layered structure with a hexagonal crystal lattice	CO_2 reduction, degradation of pollutants	[252–255]
WS_2	Layered structure similar to MoS_2	CO_2 reduction, degradation of pollutants	[256–258]
TiS_2	Layered structure with a distorted octahedral coordination	Photocatalytic degradation of pollutants	[259,260]
$MoSe_2$	Layered structure with hexagonal symmetry	CO_2 reduction, degradation of pollutants	[261–263]
WSe_2	Layered structure with hexagonal lattice	CO_2 reduction, degradation of pollutants	[264,265]
ReS_2	Layered structure with hexagonal symmetry	CO_2 reduction, degradation of pollutants	[266]
ZrS_2	Layered structure with hexagonal symmetry	Organic pollutant degradation	[267–269]
VS_2	Layered structure with a distorted octahedral coordination	Dye degradation	[270,271]
SnS_2	Layered structure with hexagonal symmetry	Photocatalytic degradation of pollutants	[271,272]

The layered structure of TMDs, especially in their exfoliated 2D form, provides an extremely high surface area, increasing the number of active sites available for photocat-

alytic reactions. This enhances their ability to interact with and degrade air pollutants like volatile organic compounds (VOCs) and nitrogen oxides (NO_x). Moreover, TMDs exhibit strong absorption across a broad spectrum of light, including visible light. This property enables the efficient generation of electron-hole pairs for photocatalytic activity.

Many TMDs, such as MoS_2 and WS_2, are also chemically stable under ambient conditions and resistant to oxidation. This makes them durable in environmental applications, including prolonged exposure to polluted air and light irradiation.

Recent advances in synthesis methods, such as chemical vapor deposition (CVD) and hydrothermal techniques, allow for relatively scalable and controllable production of TMDs, making them more accessible for large-scale applications than other competitors.

TMDs often suffer from rapid recombination of photogenerated electron-hole pairs, which can limit their photocatalytic efficiency. Strategies like doping or forming heterojunctions are often required to mitigate this issue, but this adds additional complications to the process. Moreover, the efficiency of TMDs as photocatalytic materials relies mainly on their structure, and obtaining defect-free monolayers can be challenging, particularly for large-scale productions. Moreover, certain TMDs, particularly in their 2D form, can degrade under prolonged light irradiation or in reactive environments. For instance, photoinduced oxidation or sulfide leaching may occur in materials like MoS_2, reducing their long-term stability. Moreover, potentially toxic metals like Mo or W can be leached into the environment following TMDs' degradation.

12. Applications

Photocatalytic nanomaterials are actively finding roles in practical applications for VOC removal, especially in air purification systems that target pollutants in both indoor and outdoor environments. Titanium dioxide (TiO_2) is widely applied in consumer-grade air purifiers, HVAC systems, and surface coatings due to its ability to break down VOCs like formaldehyde, benzene, and toluene under light exposure. TiO_2-coated surfaces are increasingly used in hospitals, schools, and public spaces to maintain clean air quality, as these coatings can continuously degrade airborne VOCs in the presence of light. Advances in TiO_2 modification, including doping with metals or integrating with visible-light-responsive semiconductors, have expanded its use indoors where natural light is limited. This has led to the commercialization of visible-light active TiO_2 products, such as wall and ceiling panels, that actively reduce VOC concentrations in residential and office spaces, directly addressing air quality issues without requiring complex machinery.

Carbon-based materials, such as graphene and carbon nanotubes (CNTs), are used to enhance the performance of air purification devices and VOC capture systems. These materials, when combined with other photocatalysts, improve charge separation and increase the surface area available for VOC adsorption and degradation. Carbon-TiO_2 composites are now featured in advanced air purifier filters, providing a dual-function system that captures VOCs effectively while degrading them through photocatalysis. Graphene-based photocatalytic filters are also gaining traction in HVAC systems for commercial buildings, airports, and malls, where large volumes of air need to be processed continuously. This application is especially valuable for reducing indoor pollution levels in high-traffic areas where VOC levels can accumulate due to limited ventilation. Additionally, CdS-based composites, while less common due to stability issues, have found niche applications in industrial VOC treatment, such as air scrubbers for chemical processing plants where CdS's visible-light activation can be efficiently used under controlled conditions.

More advanced materials like metal-organic frameworks (MOFs), perovskites, and transition metal dichalcogenides (TMDs) are pushing the boundaries of photocatalytic air purification technology. MOFs, with their high porosity and tunability, are being devel-

oped into filters and adsorbents tailored for high-performance VOC removal, especially in environments with sensitive air quality requirements like museums, archives, or pharmaceutical facilities. MOF-coated air filters can target specific VOCs based on the framework's design, offering highly selective purification for applications where traditional filters may fall short. Perovskites, known for their excellent light absorption, are being tested in photocatalytic coatings for outdoor building facades and public infrastructure to combat urban pollution by degrading VOCs emitted from traffic and industry. Although their practical application is still limited due to stability challenges, perovskite-based photocatalysts could soon contribute significantly to air quality management in urban areas. TMDs, such as MoS_2, are also being explored for industrial VOC treatment applications, where their strong visible-light absorption can be applied in large-scale photoreactors for factories or waste treatment facilities. By leveraging their high catalytic efficiency, TMD-based systems offer promising solutions for settings with high VOC emissions, providing cleaner air through enhanced photocatalytic degradation.

13. By-Products and Degradation in Photocatalysis

While the potential formation of by-products during photocatalytic reactions is acknowledged in the current study, a more detailed discussion is warranted. By-products, including secondary chemical intermediates and reaction products, can be generated depending on the nature of the substrate, catalyst, and reaction conditions. These by-products may affect the overall efficiency of the process, reduce selectivity, or introduce environmental and health risks [79].

In this context, potential by-products such as reactive oxygen species (ROS) [273], organic degradation products, and metal leaching from catalysts should be considered. ROS, such as hydroxyl radicals (·OH) and superoxide anions ($O_2 \cdot^-$), are often formed during photocatalysis and can lead to secondary oxidation products that may be toxic or difficult to remove. Organic substrates undergoing incomplete oxidation can produce intermediate compounds like aldehydes, ketones, or carboxylic acids, which could pose environmental hazards or interfere with the desired photocatalytic process.

Other examples of by-products include the formation of oxygenated species such as hydrogen peroxide (H_2O_2) from humid air, which, if not properly handled, can cause further degradation or undesired reactions [274]. In some photocatalytic processes, the photoreduction of substrates may lead to the production of toxic substances such as heavy metal ions or halogenated compounds when halide-containing substrates are used.

To mitigate the formation of undesired by-products, several strategies can be employed. First, optimizing reaction conditions such as light intensity and temperature can help control reaction pathways and reduce the formation of secondary products. Additionally, the use of more stable and selective photocatalysts [275,276], such as those with improved electronic properties or better surface characteristics, can help minimize side reactions.

The degradation of photocatalytic nanomaterials is another critical factor to consider, as it directly impacts the stability, reusability, and environmental implications of these systems [277]. Prolonged photocatalytic reactions or harsh operational conditions, such as exposure to intense light, high temperatures, or extreme pH, can lead to the breakdown or structural modification of nanomaterials [278]. This degradation often results in reduced photocatalytic efficiency over time and the release of nanoparticles or dissolved ions into the surrounding environment.

One of the most common risks associated with nanomaterial degradation is the leaching of metal ions from catalysts. For example, photocatalysts containing metals like titanium (Ti), zinc (Zn), or silver (Ag) may release these ions when exposed to reactive oxygen species (ROS), acidic or basic conditions, or prolonged irradiation [279]. The leached ions can have

toxic effects on aquatic ecosystems, as they may accumulate in organisms or interfere with biochemical pathways. In particular, silver ions (Ag^+) and zinc ions (Zn^{2+}) are known to exhibit cytotoxic effects, even at low concentrations, potentially posing risks to both environmental and human health.

In addition to metal leaching, the structural degradation of nanomaterials can lead to the generation of nanoscale fragments, including smaller nanoparticles or amorphous residues [280,281]. These fragments may exhibit different physicochemical properties compared to the original material, such as higher mobility or increased reactivity. For example, reduced particle size can enhance the penetration of nanoparticles into biological tissues, raising concerns about bioaccumulation and cytotoxicity. Studies have indicated that certain degraded nanomaterials can trigger oxidative stress, inflammation, or genotoxicity in living organisms, underscoring the need for a thorough assessment of their long-term environmental and biological impacts.

Another risk stems from surface modifications of nanomaterials due to photocorrosion or fouling. During photocatalysis, photoinduced reactions can alter the surface chemistry of catalysts, leading to the loss of active sites or the accumulation of contaminants. This not only diminishes the photocatalytic performance but may also promote the formation of unintended by-products, as fouled surfaces may catalyze unselective reactions. Furthermore, the altered surfaces of degraded nanomaterials could interact with biological membranes or macromolecules in unforeseen ways, introducing additional risks to ecosystems and human health.

14. Cost and Economic Feasibility

The integration of nanomaterials, particularly TiO_2-based catalysts, into photocatalytic air purification technologies offers significant potential to enhance indoor air quality. These materials are capable of degrading a wide range of pollutants, including volatile organic compounds (VOCs), bacteria, and particulate matter.

While the environmental and health benefits of improving indoor air quality are clear, the widespread adoption of photocatalytic air purification technologies faces several barriers, primarily cost and economic feasibility. For any technological advancement to transition from a research concept to a real-world application, a thorough economic evaluation is essential. This section explores the key factors influencing the cost of implementing nanomaterials in photocatalytic oxidation processes and provides a comprehensive analysis of their economic feasibility. However, it will not delve deeper into the detailed aspects of economic balance, such as return on investment (ROI), market dynamics, or cost-benefit optimization, as these topics require specialized expertise and would likely warrant a full paper dedicated to this subject [282]. Instead, the focus here is on the primary cost-related challenges and the general feasibility of incorporating nanomaterials into real-world applications.

14.1. Material Costs: Sourcing and Synthesis of Nanomaterials

The first and most immediate factor influencing the cost of nanomaterial-based photocatalysts is the synthesis and procurement of the materials themselves. Titanium dioxide (TiO_2), the most commonly used photocatalyst, is widely available and relatively inexpensive [283,284] compared to other nanomaterials such as carbon-based materials (e.g., graphene), and more exotic catalysts like CeO_2 [285]. However, the specific synthesis methods required to enhance the photocatalytic properties—such as doping TiO_2 with metals (e.g., silver or copper) or non-metals (e.g., nitrogen)—can increase costs significantly. These methods often require precise control of reaction conditions, advanced equipment, and the use of rare or expensive precursors. For example, doping with noble metals such

as platinum or palladium introduces high material costs, which could be prohibitive for large-scale applications [286].

Furthermore, the synthesis of carbon-based nanomaterials, which are increasingly being explored for their superior adsorption properties, results in higher costs due to the complexity of their production processes [287]. These materials are often produced via chemical vapor deposition or other high-temperature methods, which are energy-intensive and require significant technical expertise. In addition to raw material costs, the scale-up of production processes from laboratory to industrial scale often requires significant investment in infrastructure, which could further elevate costs.

14.2. Manufacturing and Processing Costs

Once the nanomaterials are synthesized, they must be incorporated into the photocatalytic system. This can be done through various methods such as coating materials on substrates, incorporating them into building materials like concrete, or producing them into ready-to-use filters and air purifiers. The manufacturing processes required for such integrations often involve specialized techniques like sol-gel methods, chemical vapor deposition, or electrospinning. These processes can be costly due to the need for advanced machinery, precise control over deposition parameters, and post-processing steps to ensure the stability and effectiveness of the photocatalytic coating.

In the case of integration into building materials (e.g., concrete, glass, or wallpaper), additional costs arise from the necessity to modify existing manufacturing processes to accommodate the nanomaterials. For example, incorporating TiO_2 nanoparticles into cement or concrete formulations may require the use of high-quality raw materials and advanced mixing techniques, which can increase the overall production cost of these building materials [288]. Moreover, incorporating photocatalytic materials into paints and coatings [105] requires careful consideration of the longevity and effectiveness of the material over time, adding to both the cost and complexity of production.

14.3. Operational and Maintenance Costs

While the use of photocatalytic materials in air purifiers, paints, and building materials has the potential to reduce energy consumption and maintenance requirements compared to traditional filtration systems, there are still operational costs to consider. For instance, photocatalytic oxidation processes require the presence of light to activate the photocatalyst. This means that in dark or low-light environments, supplementary lighting systems may be necessary to ensure that the photocatalysts remain active, adding to the operational energy cost. The energy efficiency of photocatalytic air purifiers, therefore, depends on the intensity and duration of light exposure, which can vary depending on the installation setting.

Furthermore, the longevity and effectiveness of the photocatalytic materials are critical for assessing long-term economic viability. Over time, photocatalysts may lose their activity due to factors such as particle agglomeration, surface poisoning, or deactivation [289]. This necessitates periodic maintenance, which may involve replacing or regenerating the photocatalytic materials. Regeneration techniques, such as heating or ultraviolet (UV) light treatment, may reduce the frequency of replacement but still incur additional operational costs. The cost of maintaining or replacing photocatalytic materials should be factored into the overall lifecycle cost analysis.

14.4. Cost-Benefit Analysis: Health and Environmental Impact

One of the major drivers for the adoption of nanomaterial-based photocatalytic air purification systems is the potential improvement in indoor air quality, which has direct and indirect economic benefits. By improving indoor air quality, photocatalytic systems

could help reduce the incidence of these health issues, thereby reducing healthcare costs and improving productivity, particularly in commercial and residential buildings.

Additionally, the environmental benefits of photocatalytic air purification systems, such as reducing the emission of volatile organic compounds (VOCs) and particulate matter, can also have long-term economic advantages. For example, reducing VOCs can lower the risk of environmental pollution and the associated costs of remediation. However, quantifying these benefits in monetary terms requires extensive research and data collection, which appears to not be available yet.

14.5. Commercialization Challenges

The commercialization of nanomaterial-based photocatalytic systems faces several challenges, including market competition, consumer acceptance, and regulatory hurdles. Although the demand for clean indoor air is high, many consumers are unaware of the benefits of photocatalytic air purifiers or are hesitant to adopt new technologies due to perceived high costs. In addition, regulatory standards for the safety and efficacy of nanomaterials in consumer products are still evolving. Manufacturers must comply with regulations concerning the use of nanomaterials, which may increase both the time and cost required to bring products to market.

The high initial investment required for developing commercial-grade photocatalytic air purifiers and building materials could also deter potential investors. To overcome this, manufacturers may need to partner with government agencies or research institutions to secure funding or subsidies, particularly in regions where air quality is a significant concern. This can help offset the high upfront costs and make the technology more accessible to a wider audience.

15. Future Developments

The future of photocatalytic nanomaterials for VOC removal lies in developing materials that are more efficient, durable, and tailored to specific environments and pollutants. One key area of development is the enhancement of visible-light-responsive photocatalysts, allowing them to operate effectively under ambient or indoor lighting conditions. Current research is focused on doping strategies, co-catalyst incorporation, and material hybridization to enable a wider range of nanomaterials—such as TiO_2, CdS, and MOFs—to be responsive to visible light, which comprises the majority of natural light. For example, advanced TiO_2-based composites doped with elements like nitrogen, carbon, or sulfur are already showing promise for effective VOC degradation under visible light, which could lead to energy-efficient air purifiers suitable for residential and commercial use.

Another promising development is the design of multifunctional photocatalysts that go beyond mere VOC degradation, enabling simultaneous antibacterial activity, odor elimination, and even CO_2 reduction in indoor spaces. This multifunctionality could be achieved by integrating different types of photocatalysts, such as combining TiO_2 with silver nanoparticles for antibacterial properties or coupling MOFs with perovskites for CO_2 capture and VOC degradation. These systems could be applied in "smart" coatings and filters for buildings, which not only remove harmful VOCs but also respond dynamically to other pollutants and pathogens, adapting to real-time air quality demands.

Stability and environmental sustainability are additional challenges that future developments aim to address, particularly with newer materials like perovskites and TMDs, which can suffer from stability issues under long-term exposure to light and humidity. Researchers are exploring encapsulation techniques and protective coatings that maintain the photocatalytic activity of these materials while extending their operational life, making them more viable for real-world applications. This work could open the door for high-

performance perovskite and TMD-based photocatalytic materials to be widely adopted for outdoor air purification, targeting urban pollution sources such as vehicle emissions and industrial VOCs.

Finally, scalability and real-time monitoring will play crucial roles in the future adoption of photocatalytic systems for air purification on a larger scale. Advanced manufacturing techniques, such as 3D printing and roll-to-roll processing, are making it possible to fabricate large-scale photocatalytic materials with precise structural control. These methods could lead to the widespread implementation of photocatalytic coatings on building facades and public infrastructure. Coupled with IoT (Internet of Things) technology, photocatalytic systems of the future could feature real-time monitoring and adaptive responses to VOC levels, automatically adjusting performance based on air quality data.

16. Conclusions

Photocatalytic nanomaterials have demonstrated significant potential for VOC removal, offering promising solutions to improve air quality across a wide range of applications. Materials like TiO_2, carbon-based nanocomposites, MOFs, and emerging semiconductors such as perovskites and TMDs provide various advantages, from stability to responsiveness under visible light. Research in this field has advanced the efficiency of these materials, allowing for targeted applications, including air purification systems, surface coatings, and industrial air treatment. However, several challenges remain, especially around the stability of certain photocatalysts (such as perovskites and CdS), the limited visible-light responsiveness of conventional catalysts, and the need to balance performance with environmental sustainability. Despite these issues, the progress in doping, hybridization, and surface modifications suggests a promising future where these materials could be further optimized for both effectiveness and durability.

Looking forward, the development of multifunctional photocatalysts capable of degrading VOCs while simultaneously capturing CO_2, neutralizing pathogens, or even providing self-cleaning functions, presents an exciting frontier for the field. Advanced composite materials combining, for instance, TiO_2 with silver for antibacterial effects, or MOFs with engineered porosity for VOC selectivity, could transform indoor and outdoor air purification approaches. Further work on real-time responsive systems will also enhance the applicability of photocatalytic nanomaterials in smart cities, where sensor-linked adaptive air purification could respond dynamically to changing pollution levels. Additionally, implementing scalable fabrication methods and environmentally friendly synthesis will be crucial to bringing these materials from the laboratory to real-world applications at scale.

In summary, photocatalytic nanomaterials represent a crucial advancement in air purification technology, addressing pressing environmental needs in both urban and industrial settings. As research continues to push the boundaries of these materials' capabilities, we move closer to a future where air quality can be continuously monitored and improved through advanced, sustainable technologies. Addressing current limitations in stability, efficiency under visible light, and environmental impact will be essential to realize the full potential of these systems, making them integral to next-generation pollution control and environmental health solutions.

17. Limitations of This Review

One of the key limitations of this study is the lack of consideration regarding legal and environmental regulations surrounding the use of nanomaterials, particularly in consumer products or closed environments. While this review focuses on the photocatalytic potential of nanomaterials, the safety and regulatory frameworks provided by authorities such as the European Union (EU), the World Health Organization (WHO), and the Environmental

Protection Agency (EPA) play a crucial role in determining the feasibility of implementing these technologies in real-world applications. The complexity of these regulations, combined with the evolving understanding of nanomaterial toxicity and environmental impact, is an area that requires expertise beyond the scope of this study.

Another limitation of this study is the absence of detailed comparative data, such as tables or graphs, that compare the performance of various nanomaterials under identical conditions. While the review aims to present the most adequate and comparable data available from existing studies, the reality is that different materials have been tested under highly variable conditions, such as differing light intensities, humidity levels, and pollutant concentrations. Due to these disparities, it would be impractical to generate new, standardized data for all materials solely for the purpose of this review.

A further limitation of this study is the lack of consideration for real-world conditions of use for photocatalytic nanomaterials. While laboratory tests are crucial for understanding the fundamental photocatalytic properties of these materials, they often do not accurately replicate the complex environmental conditions found in residential or commercial buildings, such as varying temperatures, air circulation, or pollutant concentrations. These factors can significantly influence the effectiveness of photocatalysis in practical applications. It is important to note that while we possess real-world data for a few materials, the vast majority of the solutions reviewed in this article are still under development.

Author Contributions: Conceptualization, E.G.; methodology, E.G. and A.D.S.; validation, P.B., A.M., P.P. and R.T.; resources, E.G. and E.M.; writing—original draft preparation, E.G. and A.D.S.; writing—review and editing, E.G., A.D.S. and E.M.; visualization, A.D.S.; supervision, E.M.; project administration, E.G. All authors have read and agreed to the published version of the manuscript.

Funding: This research received no external founding.

Conflicts of Interest: The authors declare no conflicts of interest.

Abbreviations

AC	Activated Carbons
ACF	Activated Carbon Fibers
AOP	Advanced Oxidation Process
CNQDs	Graphitic Carbon Nitride Quantum Dots
CQDs	Carbon Quantum Dots
GO	Graphene Oxide
HVAC	Heating, Ventilation, and Air Conditioning
IAQ	Indoor Air Quality
IoT	Internet of Things
IR	Infrared
MOFs	Metal-Organic Frameworks
PM	Particulate Matter
PTFE	Polytetrafluoroethylene
RE	Rare Earth
ROI	Return of Investment
ROS	Reactive Oxygen Species
rGO	Reduced Graphene Oxide
SBS	Sick Building Syndrome
TMD	Transition Metal Dichalcogenides
TNT	TiO_2 Nanotubes
USPNT	Uniformly Structured Photocatalytic Nanotubes
UV	Ultraviolet
VOCs	Volatile Organic Compounds

References

1. Farrow, A.; Taylor, H.; Golding, J. Time Spent in the Home by Different Family Members. *Environ. Technol.* **1997**, *18*, 605–613. [CrossRef]
2. Tham, K.W. Indoor Air Quality and Its Effects on Humans—A Review of Challenges and Developments in the Last 30 Years. *Energy Build.* **2016**, *130*, 637–650. [CrossRef]
3. Brown, S.K.; Sim, M.R.; Abramson, M.J.; Gray, C.N. Concentrations of Volatile Organic Compounds in Indoor Air—A Review. *Indoor Air* **1994**, *4*, 123–134. [CrossRef]
4. Salonen, H.; Salthammer, T.; Morawska, L. Human Exposure to NO_2 in School and Office Indoor Environments. *Environ. Int.* **2019**, *130*, 104887. [CrossRef] [PubMed]
5. Ramli, N.A.; Md Yusof, N.F.F.; Shith, S.; Suroto, A. Chemical and Biological Compositions Associated with Ambient Respirable Particulate Matter: A Review. *Water Air Soil Pollut.* **2020**, *231*, 120. [CrossRef]
6. Guo, K.; Qian, H.; Zhao, D.; Ye, J.; Zhang, Y.; Kan, H.; Zhao, Z.; Deng, F.; Huang, C.; Zhao, B.; et al. Indoor Exposure Levels of Bacteria and Fungi in Residences, Schools, and Offices in China: A Systematic Review. *Indoor Air* **2020**, *30*, 1147–1165. [CrossRef]
7. Yassin, M.F.; Almouqatea, S. Assessment of Airborne Bacteria and Fungi in an Indoor and Outdoor Environment. *Int. J. Environ. Sci. Technol.* **2010**, *7*, 535–544. [CrossRef]
8. Daisey, J.M.; Angell, W.J.; Apte, M.G. Indoor Air Quality, Ventilation and Health Symptoms in Schools: An Analysis of Existing Information. *Indoor Air* **2003**, *13*, 53–64. [CrossRef] [PubMed]
9. Madureira, J.; Paciência, I.; Rufo, J.; Ramos, E.; Barros, H.; Teixeira, J.P.; de Oliveira Fernandes, E. Indoor Air Quality in Schools and Its Relationship with Children's Respiratory Symptoms. *Atmos. Environ.* **2015**, *118*, 145–156. [CrossRef]
10. de Magalhães Rios, J.L.; Boechat, J.L.; Gioda, A.; dos Santos, C.Y.; de Aquino Neto, F.R.; e Silva, J.R.L. Symptoms Prevalence among Office Workers of a Sealed versus a Non-Sealed Building: Associations to Indoor Air Quality. *Environ. Int.* **2009**, *35*, 1136–1141. [CrossRef]
11. Saffell, J.; Nehr, S. Improving Indoor Air Quality through Standardization. *Standards* **2023**, *3*, 240–267. [CrossRef]
12. Li, Y.-W.; Ma, W.-L. Photocatalytic Oxidation Technology for Indoor Air Pollutants Elimination: A Review. *Chemosphere* **2021**, *280*, 130667. [CrossRef] [PubMed]
13. Maggos, T.; Bartzis, J.G.; Liakou, M.; Gobin, C. Photocatalytic Degradation of NOx Gases Using TiO_2-Containing Paint: A Real Scale Study. *J. Hazard. Mater.* **2007**, *146*, 668–673. [CrossRef]
14. Yu, Y.; Zhang, P.; Guo, L.; Chen, Z.; Wu, Q.; Ding, Y.; Zheng, W.; Cao, Y. The Design of TiO_2 Nanostructures (Nanoparticle, Nanotube, and Nanosheet) and Their Photocatalytic Activity. *J. Phys. Chem. C* **2014**, *118*, 12727–12733. [CrossRef]
15. Li, Z.; Li, K.; Du, P.; Mehmandoust, M.; Karimi, F.; Erk, N. Carbon-Based Photocatalysts for Hydrogen Production: A Review. *Chemosphere* **2022**, *308*, 135998. [CrossRef] [PubMed]
16. Lee, K.M.; Lai, C.W.; Ngai, K.S.; Juan, J.C. Recent Developments of Zinc Oxide Based Photocatalyst in Water Treatment Technology: A Review. *Water Res.* **2016**, *88*, 428–448. [CrossRef]
17. Dutta, V.; Sharma, S.; Raizada, P.; Thakur, V.K.; Khan, A.A.P.; Saini, V.; Asiri, A.M.; Singh, P. An Overview on WO_3 Based Photocatalyst for Environmental Remediation. *J. Environ. Chem. Eng.* **2021**, *9*, 105018. [CrossRef]
18. Ghaffarianhoseini, A.; AlWaer, H.; Omrany, H.; Ghaffarianhoseini, A.; Alalouch, C.; Clements-Croome, D.; Tookey, J. Sick Building Syndrome: Are We Doing Enough? *Archit. Sci. Rev.* **2018**, *61*, 99–121. [CrossRef]
19. Redlich, C.A.; Sparer, J.; Cullen, M.R. Sick-Building Syndrome. *Lancet* **1997**, *349*, 1013–1016. [CrossRef]
20. Burge, P.S. Sick Building Syndrome. *Occup. Environ. Med.* **2004**, *61*, 185–190. [CrossRef] [PubMed]
21. Apte, M.G.; Daisey, J.M. VOCs and "Sick Building Syndrome": Application of a New Statistical Approach for SBS Research to US EPA BASE Study Data. *Proc. Indoor Air* **1999**, *99*, 1–141.
22. Kemp, P.C.; Dingle, P.; Neumeister, H.G. Particulate Matter Intervention Study: A Causal Factor of Building-Related Symptoms in an Older Building. *Indoor Air* **1998**, *8*, 153–171. [CrossRef]
23. Niza, I.L.; De Souza, M.P.; Da Luz, I.M.; Broday, E.E. Sick Building Syndrome and Its Impacts on Health, Well-Being and Productivity: A Systematic Literature Review. *Indoor Built Environ.* **2024**, *33*, 218–236. [CrossRef]
24. Haghighat, F.; Huang, H. Integrated IAQ Model for Prediction of VOC Emissions from Building Material. *Build. Environ.* **2003**, *38*, 1007–1017. [CrossRef]
25. Uhde, E.; Salthammer, T. Impact of Reaction Products from Building Materials and Furnishings on Indoor Air Quality—A Review of Recent Advances in Indoor Chemistry. *Atmos. Environ.* **2007**, *41*, 3111–3128. [CrossRef]
26. Mjörnell, K.; Johansson, D.; Bagge, H. The Effect of High Occupancy Density on IAQ, Moisture Conditions and Energy Use in Apartments. *Energies* **2019**, *12*, 4454. [CrossRef]
27. Kamaruzzaman, S.N.; Sabrani, N.A. The Effect of Indoor Air Quality (IAQ) towards Occupants' Psychological Performance in Office Buildings. *J. Des. Built* **2011**, *4*, 49–61.

28. Reynolds, S.J.; Black, D.W.; Borin, S.S.; Breuer, G.; Burmeister, L.F.; Fuortes, L.J.; Smith, T.F.; Stein, M.A.; Subramanian, P.; Thorne, P.S.; et al. Indoor Environmental Quality in Six Commercial Office Buildings in the Midwest United States. *Appl. Occup. Environ. Hyg.* **2001**, *16*, 1065–1077. [CrossRef]
29. Wang, Y.; Cao, Y.; Liu, B.; Liu, J.; Yang, Y.; Yu, Q. An Evaluation Index for the Control Effect of the Local Ventilation Systems on Indoor Air Quality in Industrial Buildings. *Build. Simul.* **2016**, *9*, 669–676. [CrossRef]
30. Schito, E.; Testi, D.; Grassi, W. A Proposal for New Microclimate Indexes for the Evaluation of Indoor Air Quality in Museums. *Buildings* **2016**, *6*, 41. [CrossRef]
31. Al-Rajhi, S.; Ramaswamy, M.; Al-Jahwari, F. IAQ in Hospitals—Better Health through Indoor Air Quality Awareness. 2010. Available online: https://www.semanticscholar.org/paper/IAQ-in-Hospitals-Better-Health-through-Indoor-Air-Ramaswamy-Al-Jahwari/eaa33ee9711998cd83b25cf083546a120939a69a (accessed on 3 February 2025).
32. Korsavi, S.S.; Montazami, A.; Mumovic, D. Indoor Air Quality (IAQ) in Naturally-Ventilated Primary Schools in the UK: Occupant-Related Factors. *Build. Environ.* **2020**, *180*, 106992. [CrossRef]
33. Jeon, B.-I.; Kwak, M.-J.; Kang, S.-H.; Kim, J.-C.; Yun, H.-J.; Kim, H.-H. Development of IAQ Index for Indoor Air Quality in City Buses. *J. Environ. Health Sci.* **2020**, *46*, 444–456.
34. Lenzuni, P.; del Gaudio, M.; Freda, D. Indoor Air Quality Aboard Italian High-Speed Trains. In Proceedings of the 7th International Ergonomics Conference—Ergonomics, Zadar, Croatia, 13–16 June 2018; pp. 13–16.
35. Janczewski, J.N. IAQ on Passenger Planes. 1999. Available online: https://www.aivc.org/sites/default/files/airbase_12452.pdf (accessed on 3 February 2025).
36. Pandey, P.; Yadav, R. A Review on Volatile Organic Compounds (VOCs) as Environmental Pollutants: Fate and Distribution. *Int. J. Plant Environ.* **2018**, *4*, 14–26. [CrossRef]
37. Forbes, S.L.; Perrault, K.A.; Stefanuto, P.-H.; Nizio, K.D.; Focant, J.-F. Comparison of the Decomposition VOC Profile during Winter and Summer in a Moist, Mid-Latitude (Cfb) Climate. *PLoS ONE* **2014**, *9*, e113681. [CrossRef]
38. Norbäck, D.; Björnsson, E.; Janson, C.; Widström, J.; Boman, G. Asthmatic Symptoms and Volatile Organic Compounds, Formaldehyde, and Carbon Dioxide in Dwellings. *Occup. Environ. Med.* **1995**, *52*, 388–395. [CrossRef]
39. Loomis, D.; Guyton, K.Z.; Grosse, Y.; El Ghissassi, F.; Bouvard, V.; Benbrahim-Tallaa, L.; Guha, N.; Vilahur, N.; Mattock, H.; Straif, K. Carcinogenicity of Benzene. *Lancet Oncol.* **2017**, *18*, 1574–1575. [CrossRef]
40. Ross, D. Metabolic Basis of Benzene Toxicity. *Eur. J. Haematol.* **1996**, *57*, 111–118. [CrossRef] [PubMed]
41. Goldstein, B.D. Benzene Toxicity. *Occup. Med.* **1988**, *3*, 541–554.
42. Bove, K.E. Ethylene Glycol Toxicity. *Am. J. Clin. Pathol.* **1966**, *45*, 46–50. [CrossRef] [PubMed]
43. Cox, R.D.; Phillips, W.J. Ethylene Glycol Toxicity. *Mil. Med.* **2004**, *169*, 660–663. [CrossRef] [PubMed]
44. Iqbal, A.; Glagola, J.J.; Nappe, T.M. Ethylene Glycol Toxicity. In *StatPearls*; StatPearls Publishing: Treasure Island, FL, USA, 2019.
45. Bernardini, L.; Barbosa, E.; Charão, M.F.; Brucker, N. Formaldehyde Toxicity Reports from in Vitro and in Vivo Studies: A Review and Updated Data. *Drug Chem. Toxicol.* **2022**, *45*, 972–984. [CrossRef] [PubMed]
46. Heck, D.A.; Casanova, M.; Starr, T.B. Formaldehyde Toxicity—New Understanding. *Crit. Rev. Toxicol.* **1990**, *20*, 397–426. [CrossRef] [PubMed]
47. Loomis, T.A. Formaldehyde Toxicity. *Arch. Pathol. Lab. Med.* **1979**, *103*, 321–324. [PubMed]
48. Lieber, C.S. Metabolic Effects of Acetaldehyde. *Biochem. Soc. Trans.* **1988**, *16*, 241–247. [CrossRef]
49. Woutersen, R.A.; Appelman, L.M.; Van Garderen-Hoetmer, A.; Feron, V.J. Inhalation Toxicity of Acetaldehyde in Rats. III. Carcinogenicity Study. *Toxicology* **1986**, *41*, 213–231. [CrossRef]
50. Brecher, A.S.; Hellman, K.; Basista, M.H. A Perspective on Acetaldehyde Concentrations and Toxicity in Man and Animals. *Alcohol* **1997**, *14*, 493–496. [CrossRef] [PubMed]
51. Burek, J.D.; Nitschke, K.D.; Bell, T.J.; Wackerle, D.L.; Childs, R.C.; Beyer, J.E.; Dittenber, D.A.; Rampy, L.W.; McKenna, M.J. Methylene Chloride: A Two-Year Inhalation Toxicity and Oncogenicity Study in Rats and Hamsters. *Fundam. Appl. Toxicol.* **1984**, *4*, 30–47. [CrossRef] [PubMed]
52. Nitschke, K.D.; Burek, J.D.; Bell, T.J.; Kociba, R.J.; Rampy, L.W.; McKenna, M.J. Methylene Chloride: A 2-Year Inhalation Toxicity and Oncogenicity Study in Rats. *Fundam. Appl. Toxicol.* **1988**, *11*, 48–59. [CrossRef]
53. Rioux, J.P.; Myers, R.A. Methylene Chloride Poisoning: A Paradigmatic Review. *J. Emerg. Med.* **1988**, *6*, 227–238. [CrossRef]
54. Kobayashi, S.; Hutcheon, D.E.; Regan, J. Cardiopulmonary Toxicity of Tetrachloroethylene. *J. Toxicol. Environ. Health* **1982**, *10*, 23–30. [CrossRef] [PubMed]
55. Guyton, K.Z.; Hogan, K.A.; Scott, C.S.; Cooper, G.S.; Bale, A.S.; Kopylev, L.; Barone, S.; Makris, S.L.; Glenn, B.; Subramaniam, R.P.; et al. Human Health Effects of Tetrachloroethylene: Key Findings and Scientific Issues. *Environ. Health Perspect.* **2014**, *122*, 325–334. [CrossRef] [PubMed]
56. Seeber, A. Neurobehavioral Toxicity of Long-Term Exposure to Tetrachloroethylene. *Neurotoxicology Teratol.* **1989**, *11*, 579–583. [CrossRef] [PubMed]

57. von Oettingen, W.F.; Neal, P.A.; Donahue, D.D. The Toxicity and Potential Dangers of Toluene: Preliminary Report. *J. Am. Med. Assoc.* **1942**, *118*, 579–584. [CrossRef]
58. Demır, M.; Cicek, M.; Eser, N.; Yoldaş, A.; Sısman, T. Effects of Acute Toluene Toxicity on Different Regions of Rabbit Brain. *Anal. Cell. Pathol.* **2017**, *2017*, 2805370. [CrossRef] [PubMed]
59. Cohr, K.-H.; Stokholm, J. Toluene: A Toxicologic Review. *Scand. J. Work Environ. Health* **1979**, *5*, 71–90. [CrossRef]
60. Niaz, K.; Bahadar, H.; Maqbool, F.; Abdollahi, M. A Review of Environmental and Occupational Exposure to Xylene and Its Health Concerns. *EXCLI J.* **2015**, *14*, 1167. [PubMed]
61. Langman, J.M. Xylene: Its Toxicity, Measurement of Exposure Levels, Absorption, Metabolism and Clearance. *Pathology* **1994**, *26*, 301–309. [CrossRef]
62. Kandyala, R.; Raghavendra, S.P.C.; Rajasekharan, S.T. Xylene: An Overview of Its Health Hazards and Preventive Measures. *J. Oral Maxillofac. Pathol.* **2010**, *14*, 1–5. [CrossRef] [PubMed]
63. Melnick, R.L.; Huff, J. 1,3-Butadiene: Toxicity and Carcinogenicity in Laboratory Animals and in Humans. In *Reviews of Environmental Contamination and Toxicology*; Ware, G.W., Ed.; Reviews of Environmental Contamination and Toxicology; Springer: New York, NY, USA, 1992; Volume 124, pp. 111–144. ISBN 978-1-4612-7700-2.
64. Christian, M.S. Review of Reproductive and Developmental Toxicity of 1, 3-Butadiene. *Toxicology* **1996**, *113*, 137–143. [CrossRef]
65. Owen, P.E.; Glaister, J.R.; Gaunt, I.F.; Pullinger, D.H. Inhalation Toxicity Studies With 1,3-Butadiene 3 Two Year Toxicity/Carcinogenicity Study in Rats. *Am. Ind. Hyg. Assoc. J.* **1987**, *48*, 407–413. [CrossRef]
66. Hardin, B.D. Reproductive Toxicity of the Glycol Ethers. *Toxicology* **1983**, *27*, 91–102. [CrossRef]
67. Hardin, B.D.; Goad, P.T.; Burg, J.R. Developmental Toxicity of Four Glycol Ethers Applied Cutaneously to Rats. *Environ. Health Perspect.* **1984**, *57*, 69–74. [CrossRef]
68. Staples, C.A.; Boatman, R.J.; Cano, M.L. Ethylene Glycol Ethers: An Environmental Risk Assessment. *Chemosphere* **1998**, *36*, 1585–1613. [CrossRef] [PubMed]
69. Kim, Y.W.; Kim, M.J.; Chung, B.Y.; Bang, D.Y.; Lim, S.K.; Choi, S.M.; Lim, D.S.; Cho, M.C.; Yoon, K.; Kim, H.S.; et al. Safety Evaluation And Risk Assessment Of *d*-Limonene. *J. Toxicol. Environ. Health Part B* **2013**, *16*, 17–38. [CrossRef] [PubMed]
70. Ravichandran, C.; Badgujar, P.C.; Gundev, P.; Upadhyay, A. Review of Toxicological Assessment of D-Limonene, a Food and Cosmetics Additive. *Food Chem. Toxicol.* **2018**, *120*, 668–680. [CrossRef] [PubMed]
71. Bernson, V.S.; Pettersson, B. The Toxicity of Menthol in Short-Term Bioassays. *Chem.-Biol. Interact.* **1983**, *46*, 233–246. [CrossRef] [PubMed]
72. Morrow, P.E. An Evaluation of Recent NOx Toxicity Data and an Attempt to Derive an Ambient Air Standard for NOx by Established Toxicological Procedures. *Environ. Res.* **1975**, *10*, 92–112. [CrossRef]
73. Tucki, K.; Mruk, R.; Orynycz, O.; Botwińska, K.; Gola, A.; Bączyk, A. Toxicity of Exhaust Fumes (CO, NOx) of the Compression-Ignition (Diesel) Engine with the Use of Simulation. *Sustainability* **2019**, *11*, 2188. [CrossRef]
74. Allen, B.W.; Demchenko, I.T.; Piantadosi, C.A. Two Faces of Nitric Oxide: Implications for Cellular Mechanisms of Oxygen Toxicity. *J. Appl. Physiol.* **2009**, *106*, 662–667. [CrossRef]
75. Zhao, J.; Yang, X. Photocatalytic Oxidation for Indoor Air Purification: A Literature Review. *Build. Environ.* **2003**, *38*, 645–654. [CrossRef]
76. Mamaghani, A.H.; Haghighat, F.; Lee, C.-S. Photocatalytic Oxidation Technology for Indoor Environment Air Purification: The State-of-the-Art. *Appl. Catal. B Environ.* **2017**, *203*, 247–269. [CrossRef]
77. Yu, Q.L.; Brouwers, H.J.H. Indoor Air Purification Using Heterogeneous Photocatalytic Oxidation. Part I: Experimental Study. *Appl. Catal. B Environ.* **2009**, *92*, 454–461. [CrossRef]
78. Ameta, R.; Ameta, S.C. *Photocatalysis: Principles and Applications*; CRC Press: Boca Raton, FL, USA, 2016.
79. Farhanian, D.; Haghighat, F. Photocatalytic Oxidation Air Cleaner: Identification and Quantification of by-Products. *Build. Environ.* **2014**, *72*, 34–43. [CrossRef]
80. Shayegan, Z.; Lee, C.-S.; Haghighat, F. TiO_2 Photocatalyst for Removal of Volatile Organic Compounds in Gas Phase–A Review. *Chem. Eng. J.* **2018**, *334*, 2408–2439. [CrossRef]
81. Moser, J.; Grätzel, M.; Gallay, R. Inhibition of Electron-Hole Recombination in Substitutionally Doped Colloidal Semiconductor Crystallites. *Helv. Chim. Acta* **1987**, *70*, 1596–1604. [CrossRef]
82. Liqiang, J.; Yichun, Q.; Baiqi, W.; Shudan, L.; Baojiang, J.; Libin, Y.; Wei, F.; Honggang, F.; Jiazhong, S. Review of Photoluminescence Performance of Nano-Sized Semiconductor Materials and Its Relationships with Photocatalytic Activity. *Sol. Energy Mater. Sol. Cells* **2006**, *90*, 1773–1787. [CrossRef]
83. Zhang, W.; Huang, W.; Wu, B.; Yang, J.; Jin, J.; Zhang, S. Excitonic Effect in MOFs-Mediated Photocatalysis: Phenomenon, Characterization Techniques and Regulation Strategies. *Coord. Chem. Rev.* **2023**, *491*, 215235. [CrossRef]
84. Li, Q.; Anpo, M.; Wang, X. Application of Photoluminescence Spectroscopy to Elucidate Photocatalytic Reactions at the Molecular Level. *Res. Chem. Intermed.* **2020**, *46*, 4325–4344. [CrossRef]

85. Parasuraman, V.; Sekar, P.P.; Lee, H.; Sheraz, M.; Ly, H.N.; Azizar, G.A.B.; Hong, J.W.; Lee, W.R.; Kim, S. Photocatalytic Self-Cleaning Eco-Friendly Paint: A Unique Approach for Efficient Indoor Air Pollutant Removal and Surface Disinfection. *Constr. Build. Mater.* **2024**, *412*, 134671. [CrossRef]
86. Yu, J.; Yue, L.; Liu, S.; Huang, B.; Zhang, X. Hydrothermal Preparation and Photocatalytic Activity of Mesoporous Au–TiO_2 Nanocomposite Microspheres. *J. Colloid Interface Sci.* **2009**, *334*, 58–64. [CrossRef]
87. Yu, Z.; Li, F.; Xiang, Q. Carbon Dots-Based Nanocomposites for Heterogeneous Photocatalysis. *J. Mater. Sci. Technol.* **2024**, *175*, 244–257. [CrossRef]
88. Karafas, E.S.; Romanias, M.N.; Stefanopoulos, V.; Binas, V.; Zachopoulos, A.; Kiriakidis, G.; Papagiannakopoulos, P. Effect of Metal Doped and Co-Doped TiO_2 Photocatalysts Oriented to Degrade Indoor/Outdoor Pollutants for Air Quality Improvement. A Kinetic and Product Study Using Acetaldehyde as Probe Molecule. *J. Photochem. Photobiol. A Chem.* **2019**, *371*, 255–263. [CrossRef]
89. Lyu, J.; Zhu, L.; Burda, C. Considerations to Improve Adsorption and Photocatalysis of Low Concentration Air Pollutants on TiO_2. *Catal. Today* **2014**, *225*, 24–33. [CrossRef]
90. Yu, L.; Wang, L.; Sun, X.; Ye, D. Enhanced Photocatalytic Activity of rGO/TiO_2 for the Decomposition of Formaldehyde under Visible Light Irradiation. *J. Environ. Sci.* **2018**, *73*, 138–146. [CrossRef] [PubMed]
91. Korologos, C.A.; Philippopoulos, C.J.; Poulopoulos, S.G. The Effect of Water Presence on the Photocatalytic Oxidation of Benzene, Toluene, Ethylbenzene and m-Xylene in the Gas-Phase. *Atmos. Environ.* **2011**, *45*, 7089–7095. [CrossRef]
92. Takeuchi, M.; Deguchi, J.; Sakai, S.; Anpo, M. Effect of H_2O Vapor Addition on the Photocatalytic Oxidation of Ethanol, Acetaldehyde and Acetic Acid in the Gas Phase on TiO_2 Semiconductor Powders. *Appl. Catal. B Environ.* **2010**, *96*, 218–223. [CrossRef]
93. Kotzias, D.; Binas, V.; Kiriakidis, G. Smart Surfaces: Heterogeneous Photo-Catalysis on TiO_2 Based Coatings for De-Pollution Purposes in Indoor and Outdoor Environments. *Top Catal* **2020**, *63*, 875–881. [CrossRef]
94. Liu, R.; Wang, J.; Zhang, J.; Xie, S.; Wang, X.; Ji, Z. Honeycomb-like Micro-Mesoporous Structure TiO_2/Sepiolite Composite for Combined Chemisorption and Photocatalytic Elimination of Formaldehyde. *Microporous Mesoporous Mater.* **2017**, *248*, 234–245. [CrossRef]
95. Liu, S.-H.; Lin, W.-X. A Simple Method to Prepare G-C_3N_4-TiO_2/Waste Zeolites as Visible-Light-Responsive Photocatalytic Coatings for Degradation of Indoor Formaldehyde. *J. Hazard. Mater.* **2019**, *368*, 468–476. [CrossRef] [PubMed]
96. Hussain, M.; Russo, N.; Saracco, G. Photocatalytic Abatement of VOCs by Novel Optimized TiO_2 Nanoparticles. *Chem. Eng. J.* **2011**, *166*, 138–149. [CrossRef]
97. Li, J.-J.; Cai, S.-C.; Yu, E.-Q.; Weng, B.; Chen, X.; Chen, J.; Jia, H.-P.; Xu, Y.-J. Efficient Infrared Light Promoted Degradation of Volatile Organic Compounds over Photo-Thermal Responsive Pt-rGO-TiO_2 Composites. *Appl. Catal. B Environ.* **2018**, *233*, 260–271. [CrossRef]
98. Ollis, D.F.; Pelizzetti, E.; Serpone, N. Photocatalyzed Destruction of Water Contaminants. *Environ. Sci. Technol.* **1991**, *25*, 1522–1529. [CrossRef]
99. Yaghoubi, H.; Li, Z.; Chen, Y.; Ngo, H.T.; Bhethanabotla, V.R.; Joseph, B.; Ma, S.; Schlaf, R.; Takshi, A. Toward a Visible Light-Driven Photocatalyst: The Effect of Midgap-States-Induced Energy Gap of Undoped TiO_2 Nanoparticles. *ACS Catal.* **2015**, *5*, 327–335. [CrossRef]
100. Paramasivam, I.; Jha, H.; Liu, N.; Schmuki, P. A Review of Photocatalysis Using Self-organized TiO_2 Nanotubes and Other Ordered Oxide Nanostructures. *Small* **2012**, *8*, 3073–3103. [CrossRef] [PubMed]
101. Jiang, Z.; Sun, W.; Miao, W.; Yuan, Z.; Yang, G.; Kong, F.; Yan, T.; Chen, J.; Huang, B.; An, C.; et al. Living Atomically Dispersed Cu Ultrathin TiO_2 Nanosheet CO_2 Reduction Photocatalyst. *Adv. Sci.* **2019**, *6*, 1900289. [CrossRef] [PubMed]
102. Samsudin, E.M.; Abd Hamid, S.B. Effect of Band Gap Engineering in Anionic-Doped TiO_2 Photocatalyst. *Appl. Surf. Sci.* **2017**, *391*, 326–336. [CrossRef]
103. Zaleska, A. Doped-TiO_2: A Review. *Recent Pat. Eng.* **2008**, *2*, 157–164. [CrossRef]
104. Jimmy, C.Y.; Yu, J.; Ho, W.; Zhao, J. Light-Induced Super-Hydrophilicity and Photocatalytic Activity of Mesoporous TiO_2 Thin Films. *J. Photochem. Photobiol. A Chem.* **2002**, *148*, 331–339.
105. Bersch, J.D.; Flores-Colen, I.; Masuero, A.B.; Dal Molin, D.C. Photocatalytic TiO_2-Based Coatings for Mortars on Facades: A Review of Efficiency, Durability, and Sustainability. *Buildings* **2023**, *13*, 186. [CrossRef]
106. Ayati, A.; Ahmadpour, A.; Bamoharram, F.F.; Tanhaei, B.; Mänttäri, M.; Sillanpää, M. A Review on Catalytic Applications of Au/TiO_2 Nanoparticles in the Removal of Water Pollutant. *Chemosphere* **2014**, *107*, 163–174. [CrossRef]
107. Wang, D.; Liu, Y.; Yu, B.; Zhou, F.; Liu, W. TiO_2 Nanotubes with Tunable Morphology, Diameter, and Length: Synthesis and Photo-Electrical/Catalytic Performance. *Chem. Mater.* **2009**, *21*, 1198–1206. [CrossRef]
108. Wan, J.; Chen, W.; Jia, C.; Zheng, L.; Dong, J.; Zheng, X.; Wang, Y.; Yan, W.; Chen, C.; Peng, Q.; et al. Defect Effects on TiO_2 Nanosheets: Stabilizing Single Atomic Site Au and Promoting Catalytic Properties. *Adv. Mater.* **2018**, *30*, 1705369. [CrossRef]
109. Zhao, Y.; Zhang, X.; Zhai, J.; He, J.; Jiang, L.; Liu, Z.; Nishimoto, S.; Murakami, T.; Fujishima, A.; Zhu, D. Enhanced Photocatalytic Activity of Hierarchically Micro-/Nano-Porous TiO_2 Films. *Appl. Catal. B Environ.* **2008**, *83*, 24–29. [CrossRef]

110. Padayachee, D.; Mahomed, A.S.; Singh, S.; Friedrich, H.B. Effect of the TiO_2 Anatase/Rutile Ratio and Interface for the Oxidative Activation of *n*-Octane. *ACS Catal.* **2020**, *10*, 2211–2220. [CrossRef]
111. Carp, O.; Huisman, C.L.; Reller, A. Photoinduced Reactivity of Titanium Dioxide. *Prog. Solid State Chem.* **2004**, *32*, 33–177. [CrossRef]
112. Raj, K.; Viswanathan, B. Effect of Surface Area, Pore Volume and Particle Size of P25 Titania on the Phase Transformation of Anatase to Rutile. 2009. Available online: https://nopr.niscpr.res.in/handle/123456789/6124 (accessed on 3 February 2025).
113. Verbruggen, S.W. TiO_2 Photocatalysis for the Degradation of Pollutants in Gas Phase: From Morphological Design to Plasmonic Enhancement. *J. Photochem. Photobiol. C Photochem. Rev.* **2015**, *24*, 64–82. [CrossRef]
114. Wu, A.; Wang, D.; Wei, C.; Zhang, X.; Liu, Z.; Feng, P.; Ou, X.; Qiang, Y.; Garcia, H.; Niu, J. A Comparative Photocatalytic Study of TiO_2 Loaded on Three Natural Clays with Different Morphologies. *Appl. Clay Sci.* **2019**, *183*, 105352. [CrossRef]
115. Mavrikos, A.; Papoulis, D.; Todorova, N.; Papailias, I.; Trapalis, C.; Panagiotaras, D.; Chalkias, D.A.; Stathatos, E.; Gianni, E.; Somalakidi, K. Synthesis of Zn/Cu Metal Ion Modified Natural Palygorskite Clay–TiO_2 Nanocomposites for the Photocatalytic Outdoor and Indoor Air Purification. *J. Photochem. Photobiol. A Chem.* **2022**, *423*, 113568. [CrossRef]
116. Zhang, Z.; Wang, C.-C.; Zakaria, R.; Ying, J.Y. Role of Particle Size in Nanocrystalline TiO_2-Based Photocatalysts. *J. Phys. Chem. B* **1998**, *102*, 10871–10878. [CrossRef]
117. Xiao, J.; Peng, T.; Li, R.; Peng, Z.; Yan, C. Preparation, Phase Transformation and Photocatalytic Activities of Cerium-Doped Mesoporous Titania Nanoparticles. *J. Solid State Chem.* **2006**, *179*, 1161–1170. [CrossRef]
118. Antonio, J.T.; Cortes-Jacome, M.A.; Orozco-Cerros, S.L.; Montiel-Palacios, E.; Suarez-Parra, R.; Angeles-Chavez, C.; Navarete, J.; López-Salinas, E. Assessing Optimal Photoactivity on Titania Nanotubes Using Different Annealing Temperatures. *Appl. Catal. B Environ.* **2010**, *100*, 47–54. [CrossRef]
119. Weon, S.; Choi, E.; Kim, H.; Kim, J.Y.; Park, H.-J.; Kim, S.; Kim, W.; Choi, W. Active {001} Facet Exposed TiO_2 Nanotubes Photocatalyst Filter for Volatile Organic Compounds Removal: From Material Development to Commercial Indoor Air Cleaner Application. *Environ. Sci. Technol.* **2018**, *52*, 9330–9340. [CrossRef] [PubMed]
120. Lee, J.Y.; Jo, W.-K. Heterojunction-Based Two-Dimensional N-Doped TiO_2/WO_3 Composite Architectures for Photocatalytic Treatment of Hazardous Organic Vapor. *J. Hazard. Mater.* **2016**, *314*, 22–31. [CrossRef]
121. Xu, F. Review of Analytical Studies on TiO_2 Nanoparticles and Particle Aggregation, Coagulation, Flocculation, Sedimentation, Stabilization. *Chemosphere* **2018**, *212*, 662–677. [CrossRef] [PubMed]
122. Reddy, E.P.; Davydov, L.; Smirniotis, P. TiO_2-Loaded Zeolites and Mesoporous Materials in the Sonophotocatalytic Decomposition of Aqueous Organic Pollutants: The Role of the Support. *Appl. Catal. B Environ.* **2003**, *42*, 1–11. [CrossRef]
123. Xia, X.-H.; Jia, Z.-J.; Yu, Y.; Liang, Y.; Wang, Z.; Ma, L.-L. Preparation of Multi-Walled Carbon Nanotube Supported TiO_2 and Its Photocatalytic Activity in the Reduction of CO_2 with H_2O. *carbon* **2007**, *45*, 717–721. [CrossRef]
124. Guirado-López, R.A.; Sánchez, M.; Rincón, M.E. Interaction of Acetone Molecules with Carbon-Nanotube-Supported TiO_2 Nanoparticles: Possible Applications as Room Temperature Molecular Sensitive Coatings. *J. Phys. Chem. C* **2007**, *111*, 57–65. [CrossRef]
125. Poolwong, J.; Kiatboonyarit, T.; Achiwawanich, S.; Butburee, T.; Khemthong, P.; Kityakarn, S. Three-Dimensional Hierarchical Porous TiO_2 for Enhanced Adsorption and Photocatalytic Degradation of Remazol Dye. *Nanomaterials* **2021**, *11*, 1715. [CrossRef]
126. Greco, E.; Ciliberto, E.; Cirino, A.M.E.; Capitani, D.; Di Tullio, V. A New Preparation of Doped Photocatalytic TiO_2 Anatase Nanoparticles: A Preliminary Study for the Removal of Pollutants in Confined Museum Areas. *Appl. Phys. A* **2016**, *122*, 530. [CrossRef]
127. Shon, H.; Phuntsho, S.; Okour, Y.; Cho, D.-L.; Kim, K.S.; Li, H.-J.; Na, S.; Kim, J.B.; Kim, J.-H. Visible Light Responsive Titanium Dioxide (TiO_2). *Appl. Chem. Eng.* **2008**, *19*, 1–16.
128. Sun, S.; Ding, J.; Bao, J.; Gao, C.; Qi, Z.; Yang, X.; He, B.; Li, C. Photocatalytic Degradation of Gaseous Toluene on Fe-TiO_2 under Visible Light Irradiation: A Study on the Structure, Activity and Deactivation Mechanism. *Appl. Surf. Sci.* **2012**, *258*, 5031–5037. [CrossRef]
129. Huang, H.; Huang, H.; Zhang, L.; Hu, P.; Ye, X.; Leung, D.Y. Enhanced Degradation of Gaseous Benzene under Vacuum Ultraviolet (VUV) Irradiation over TiO_2 Modified by Transition Metals. *Chem. Eng. J.* **2015**, *259*, 534–541. [CrossRef]
130. Tan, Y.N.; Wong, C.L.; Mohamed, A.R. An Overview on the Photocatalytic Activity of Nano-Doped-TiO_2 in the Degradation of Organic Pollutants. *ISRN Mater. Sci.* **2011**, *2011*, 261219. [CrossRef]
131. Devi, L.G.; Kavitha, R. A Review on Plasmonic Metal TiO_2 Composite for Generation, Trapping, Storing and Dynamic Vectorial Transfer of Photogenerated Electrons across the Schottky Junction in a Photocatalytic System. *Appl. Surf. Sci.* **2016**, *360*, 601–622. [CrossRef]
132. Hernández, J.V.; Coste, S.; Murillo, A.G.; Romo, F.C.; Kassiba, A. Effects of Metal Doping (Cu, Ag, Eu) on the Electronic and Optical Behavior of Nanostructured TiO_2. *J. Alloys Compd.* **2017**, *710*, 355–363. [CrossRef]
133. Janisch, R.; Gopal, P.; Spaldin, N.A. Transition Metal-Doped TiO_2 and ZnO—Present Status of the Field. *J. Phys. Condens. Matter* **2005**, *17*, R657. [CrossRef]

134. Campet, G.; Verniolle, J.; Doumerc, J.-P.; Claverie, J. Photoelectronic Processes in Transition-Element Doped n-Type TiO_2 Electrodes. *Mater. Res. Bull.* **1980**, *15*, 1135–1141. [CrossRef]
135. Das, S.; Liu, D.; Park, J.B.; Hahn, Y.-B. Metal-Ion Doped p-Type TiO_2 Thin Films and Their Applications for Heterojunction Devices. *J. Alloys Compd.* **2013**, *553*, 188–193. [CrossRef]
136. Su, Y.; Deng, Y. Effect of Structure on the Photocatalytic Activity of Pt-Doped TiO_2 Nanotubes. *Appl. Surf. Sci.* **2011**, *257*, 9791–9795. [CrossRef]
137. Rusinque, B.; Escobedo, S.; de Lasa, H. Photoreduction of a Pd-Doped Mesoporous TiO_2 Photocatalyst for Hydrogen Production under Visible Light. *Catalysts* **2020**, *10*, 74. [CrossRef]
138. Ali, T.; Ahmed, A.; Alam, U.; Uddin, I.; Tripathi, P.; Muneer, M. Enhanced Photocatalytic and Antibacterial Activities of Ag-Doped TiO_2 Nanoparticles under Visible Light. *Mater. Chem. Phys.* **2018**, *212*, 325–335. [CrossRef]
139. Zhang, Y.; Hu, H.; Chang, M.; Chen, D.; Zhang, M.; Wu, L.; Li, X. Non-Uniform Doping Outperforms Uniform Doping for Enhancing the Photocatalytic Efficiency of Au-Doped TiO_2 Nanotubes in Organic Dye Degradation. *Ceram. Int.* **2017**, *43*, 9053–9059. [CrossRef]
140. Greco, E.; Balsamo, S.A.; Maccarrone, G.; Mello, D.; Ciliberto, E.; Shang, J.; Zhu, T. Gold-Core Lithium-Doped Titania Shell Nanostructures for Plasmon-Enhanced Visible Light Harvesting with Photocatalytic Activity. *J. Nanopart. Res.* **2020**, *22*, 164. [CrossRef]
141. Som, I.; Roy, M. Recent Development on Titania-Based Nanomaterial for Photocatalytic CO_2 Reduction: A Review. *J. Alloys Compd.* **2022**, *918*, 165533. [CrossRef]
142. Li, X.; Zou, X.; Qu, Z.; Zhao, Q.; Wang, L. Photocatalytic Degradation of Gaseous Toluene over Ag-Doping TiO_2 Nanotube Powder Prepared by Anodization Coupled with Impregnation Method. *Chemosphere* **2011**, *83*, 674–679. [CrossRef] [PubMed]
143. Vikrant, K.; Weon, S.; Kim, K.-H.; Sillanpää, M. Platinized Titanium Dioxide (Pt/TiO_2) as a Multi-Functional Catalyst for Thermocatalysis, Photocatalysis, and Photothermal Catalysis for Removing Air Pollutants. *Appl. Mater. Today* **2021**, *23*, 100993. [CrossRef]
144. Murcia, J.J.; Hidalgo, M.C.; Navío, J.A.; Vaiano, V.; Ciambelli, P.; Sannino, D. Ethanol Partial Photoxidation on Pt/TiO_2 Catalysts as Green Route for Acetaldehyde Synthesis. *Catal. Today* **2012**, *196*, 101–109. [CrossRef]
145. Yurtsever, H.A.; Çiftçioğlu, M. The Effect of Rare Earth Element Doping on the Microstructural Evolution of Sol-Gel Titania Powders. *J. Alloys Compd.* **2017**, *695*, 1336–1353. [CrossRef]
146. Korologos, C.A.; Nikolaki, M.D.; Zerva, C.N.; Philippopoulos, C.J.; Poulopoulos, S.G. Photocatalytic Oxidation of Benzene, Toluene, Ethylbenzene and m-Xylene in the Gas-Phase over TiO_2-Based Catalysts. *J. Photochem. Photobiol. A Chem.* **2012**, *244*, 24–31. [CrossRef]
147. Tobaldi, D.M.; Pullar, R.C.; Škapin, A.S.; Seabra, M.P.; Labrincha, J.A. Visible Light Activated Photocatalytic Behaviour of Rare Earth Modified Commercial TiO_2. *Mater. Res. Bull.* **2014**, *50*, 183–190. [CrossRef]
148. Chen, D.; Jiang, Z.; Geng, J.; Wang, Q.; Yang, D. Carbon and Nitrogen Co-Doped TiO_2 with Enhanced Visible-Light Photocatalytic Activity. *Ind. Eng. Chem. Res.* **2007**, *46*, 2741–2746. [CrossRef]
149. Liu, D.; Gu, W.; Zhou, L.; Wang, L.; Zhang, J.; Liu, Y.; Lei, J. Recent Advances in MOF-Derived Carbon-Based Nanomaterials for Environmental Applications in Adsorption and Catalytic Degradation. *Chem. Eng. J.* **2022**, *427*, 131503. [CrossRef]
150. Nawaz, F.; Ali, M.; Ahmad, S.; Yong, Y.; Rahman, S.; Naseem, M.; Hussain, S.; Razzaq, A.; Khan, A.; Ali, F. Carbon Based Nanocomposites, Surface Functionalization as a Promising Material for VOCs (Volatile Organic Compounds) Treatment. *Chemosphere* **2024**, *364*, 143014. [CrossRef] [PubMed]
151. Hossen, M.A.; Ikreedeegh, R.R.; Abd Aziz, A.; Zerga, A.Y.; Tahir, M. Carbon-Based Nanomaterials (CNMs) Modified TiO_2 Nanotubes (TNTs) Photo-Driven Catalysts for Sustainable Energy and Environmental Applications: A Comprehensive Review. *J. Environ. Chem. Eng.* **2024**, *364*, 114088. [CrossRef]
152. Zhao, L.; Deng, J.; Sun, P.; Liu, J.; Ji, Y.; Nakada, N.; Qiao, Z.; Tanaka, H.; Yang, Y. Nanomaterials for Treating Emerging Contaminants in Water by Adsorption and Photocatalysis: Systematic Review and Bibliometric Analysis. *Sci. Total Environ.* **2018**, *627*, 1253–1263. [CrossRef] [PubMed]
153. Velo-Gala, I.; López-Peñalver, J.J.; Sánchez-Polo, M.; Rivera-Utrilla, J. Activated Carbon as Photocatalyst of Reactions in Aqueous Phase. *Appl. Catal. B Environ.* **2013**, *142*, 694–704. [CrossRef]
154. Zanella, O.; Tessaro, I.C.; Féris, L.A. Desorption- and Decomposition-Based Techniques for the Regeneration of Activated Carbon. *Chem. Eng. Technol.* **2014**, *37*, 1447–1459. [CrossRef]
155. Ahmad, A.; Ali, M.; Al-Sehemi, A.G.; Al-Ghamdi, A.A.; Park, J.-W.; Algarni, H.; Anwer, H. Carbon-Integrated Semiconductor Photocatalysts for Removal of Volatile Organic Compounds in Indoor Environments. *Chem. Eng. J.* **2023**, *452*, 139436. [CrossRef]
156. Muzarpar, M.S.; Leman, A.M.; Maghpor, N.; Hassan, N.N.M.; Misdana, N. The Adsorption Mechanism of Activated Carbon and Its Application-A Review. *Int. J. Adv. Technol. Mech. Mechatron. Mater.* **2020**, *1*, 118–124. [CrossRef]

157. Zhang, W.; Cheng, H.; Niu, Q.; Fu, M.; Huang, H.; Ye, D. Microbial Targeted Degradation Pretreatment: A Novel Approach to Preparation of Activated Carbon with Specific Hierarchical Porous Structures, High Surface Areas, and Satisfactory Toluene Adsorption Performance. *Environ. Sci. Technol.* **2019**, *53*, 7632–7640. [CrossRef]
158. Yang, X.; Yi, H.; Tang, X.; Zhao, S.; Yang, Z.; Ma, Y.; Feng, T.; Cui, X. Behaviors and Kinetics of Toluene Adsorption-Desorption on Activated Carbons with Varying Pore Structure. *J. Environ. Sci.* **2018**, *67*, 104–114. [CrossRef]
159. Suresh, S.; Bandosz, T.J. Removal of Formaldehyde on Carbon-Based Materials: A Review of the Recent Approaches and Findings. *Carbon* **2018**, *137*, 207–221. [CrossRef]
160. Hassan, M.F.; Sabri, M.A.; Fazal, H.; Hafeez, A.; Shezad, N.; Hussain, M. Recent Trends in Activated Carbon Fibers Production from Various Precursors and Applications—A Comparative Review. *J. Anal. Appl. Pyrolysis* **2020**, *145*, 104715. [CrossRef]
161. Mangun, C.L.; Yue, Z.; Economy, J.; Maloney, S.; Kemme, P.; Cropek, D. Adsorption of Organic Contaminants from Water Using Tailored ACFs. *Chem. Mater.* **2001**, *13*, 2356–2360. [CrossRef]
162. Mamaghani, A.H.; Haghighat, F.; Lee, C.-S. Effect of Titanium Dioxide Properties and Support Material on Photocatalytic Oxidation of Indoor Air Pollutants. *Build. Environ.* **2021**, *189*, 107518. [CrossRef]
163. Yu, Y.; Jimmy, C.Y.; Yu, J.-G.; Kwok, Y.-C.; Che, Y.-K.; Zhao, J.-C.; Ding, L.; Ge, W.-K.; Wong, P.-K. Enhancement of Photocatalytic Activity of Mesoporous TiO_2 by Using Carbon Nanotubes. *Appl. Catal. A Gen.* **2005**, *289*, 186–196. [CrossRef]
164. Gao, E.; Wang, W.; Shang, M.; Xu, J. Synthesis and Enhanced Photocatalytic Performance of Graphene-Bi_2WO_6 Composite. *Phys. Chem. Chem. Phys.* **2011**, *13*, 2887–2893. [CrossRef]
165. Buron, J.D.; Pizzocchero, F.; Jepsen, P.U.; Petersen, D.H.; Caridad, J.M.; Jessen, B.S.; Booth, T.J.; Bøggild, P. Graphene Mobility Mapping. *Sci. Rep.* **2015**, *5*, 12305. [CrossRef] [PubMed]
166. Yu, M.; Yuan, X.; Guo, J.; Tang, N.; Ye, S.; Liang, J.; Jiang, L. Selective Graphene-like Metal-Free 2D Nanomaterials and Their Composites for Photocatalysis. *Chemosphere* **2021**, *284*, 131254. [CrossRef] [PubMed]
167. Compton, O.C.; Nguyen, S.T. Graphene Oxide, Highly Reduced Graphene Oxide, and Graphene: Versatile Building Blocks for Carbon-Based Materials. *Small* **2010**, *6*, 711–723. [CrossRef] [PubMed]
168. Tarcan, R.; Todor-Boer, O.; Petrovai, I.; Leordean, C.; Astilean, S.; Botiz, I. Reduced Graphene Oxide Today. *J. Mater. Chem. C* **2020**, *8*, 1198–1224. [CrossRef]
169. Greco, E.; Shang, J.; Zhu, J.; Zhu, T. Synthesis of Polyacetylene-like Modified Graphene Oxide Aerogel and Its Enhanced Electrical Properties. *ACS Omega* **2019**, *4*, 20948–20954. [CrossRef] [PubMed]
170. Guo, S.; Garaj, S.; Bianco, A.; Ménard-Moyon, C. Controlling Covalent Chemistry on Graphene Oxide. *Nat. Rev. Phys.* **2022**, *4*, 247–262. [CrossRef]
171. Wen, J.; Xie, J.; Chen, X.; Li, X. A Review on G-C_3N_4-Based Photocatalysts. *Appl. Surf. Sci.* **2017**, *391*, 72–123. [CrossRef]
172. Fu, J.; Yu, J.; Jiang, C.; Cheng, B. g-C_3N_4-Based Heterostructured Photocatalysts. *Adv. Energy Mater.* **2018**, *8*, 1701503. [CrossRef]
173. Patnaik, S.; Sahoo, D.P.; Parida, K. Recent Advances in Anion Doped G-C_3N_4 Photocatalysts: A Review. *Carbon* **2021**, *172*, 682–711. [CrossRef]
174. Wang, Y.; Tan, G.; Dang, M.; Dong, S.; Liu, Y.; Liu, T.; Ren, H.; Xia, A.; Lv, L. Study on Surface Modification of G-C_3N_4 Photocatalyst. *J. Alloys Compd.* **2022**, *908*, 164507. [CrossRef]
175. Li, Y.; Zhou, M.; Cheng, B.; Shao, Y. Recent Advances in G-C_3N_4-Based Heterojunction Photocatalysts. *J. Mater. Sci. Technol.* **2020**, *56*, 1–17. [CrossRef]
176. Han, M.; Zhu, S.; Lu, S.; Song, Y.; Feng, T.; Tao, S.; Liu, J.; Yang, B. Recent Progress on the Photocatalysis of Carbon Dots: Classification, Mechanism and Applications. *Nano Today* **2018**, *19*, 201–218. [CrossRef]
177. Domingo-Tafalla, B.; Martínez-Ferrero, E.; Franco, F.; Palomares-Gil, E. Applications of Carbon Dots for the Photocatalytic and Electrocatalytic Reduction of CO_2. *Molecules* **2022**, *27*, 1081. [CrossRef] [PubMed]
178. Zhao, J.; Li, C.; Du, X.; Zhu, Y.; Li, S.; Liu, X.; Liang, C.; Yu, Q.; Huang, L.; Yang, K. Recent Progress of Carbon Dots for Air Pollutants Detection and Photocatalytic Removal: Synthesis, Modifications, and Applications. *Small* **2022**, *18*, 2200744. [CrossRef] [PubMed]
179. Lim, S.Y.; Shen, W.; Gao, Z. Carbon Quantum Dots and Their Applications. *Chem. Soc. Rev.* **2015**, *44*, 362–381. [CrossRef]
180. Sargin, I.; Yanalak, G.; Arslan, G.; Patir, I.H. Green Synthesized Carbon Quantum Dots as TiO_2 Sensitizers for Photocatalytic Hydrogen Evolution. *Int. J. Hydrog. Energy* **2019**, *44*, 21781–21789. [CrossRef]
181. Jia, J.; Jiang, C.; Zhang, X.; Li, P.; Xiong, J.; Zhang, Z.; Wu, T.; Wang, Y. Urea-Modified Carbon Quantum Dots as Electron Mediator Decorated g-C_3N_4/WO_3 with Enhanced Visible-Light Photocatalytic Activity and Mechanism Insight. *Appl. Surf. Sci.* **2019**, *495*, 143524. [CrossRef]
182. Dimos, K. Carbon Quantum Dots: Surface Passivation and Functionalization. *Curr. Org. Chem.* **2016**, *20*, 682–695. [CrossRef]
183. Yu, J.; Caravaca, A.; Guillard, C.; Vernoux, P.; Zhou, L.; Wang, L.; Lei, J.; Zhang, J.; Liu, Y. Carbon Nitride Quantum Dots Modified TiO_2 Inverse Opal Photonic Crystal for Solving Indoor Vocs Pollution. *Catalysts* **2021**, *11*, 464. [CrossRef]
184. Chen, X.; Wu, Z.; Liu, D.; Gao, Z. Preparation of ZnO Photocatalyst for the Efficient and Rapid Photocatalytic Degradation of Azo Dyes. *Nanoscale Res Lett* **2017**, *12*, 143. [CrossRef] [PubMed]

185. Szilágyi, I.M.; Fórizs, B.; Rosseler, O.; Szegedi, Á.; Németh, P.; Király, P.; Tárkányi, G.; Vajna, B.; Varga-Josepovits, K.; László, K. WO_3 Photocatalysts: Influence of Structure and Composition. *J. Catal.* **2012**, *294*, 119–127. [CrossRef]
186. Zheng, A.L.T.; Abdullah, C.A.C.; Chung, E.L.T.; Andou, Y. Recent Progress in Visible Light-Doped ZnO Photocatalyst for Pollution Control. *Int. J. Environ. Sci. Technol.* **2023**, *20*, 5753–5772. [CrossRef]
187. Samadi, M.; Zirak, M.; Naseri, A.; Khorashadizade, E.; Moshfegh, A.Z. Recent Progress on Doped ZnO Nanostructures for Visible-Light Photocatalysis. *Thin Solid Film.* **2016**, *605*, 2–19. [CrossRef]
188. Qin, R.; Meng, F.; Khan, M.W.; Yu, B.; Li, H.; Fan, Z.; Gong, J. Fabrication and Enhanced Photocatalytic Property of TiO_2-ZnO Composite Photocatalysts. *Mater. Lett.* **2019**, *240*, 84–87. [CrossRef]
189. Chen, D.; Wang, Z.; Ren, T.; Ding, H.; Yao, W.; Zong, R.; Zhu, Y. Influence of Defects on the Photocatalytic Activity of ZnO. *J. Phys. Chem. C* **2014**, *118*, 15300–15307. [CrossRef]
190. Tseng, C.-H.; Li, Z.; Shiue, A.; Chao, Y.-H.; Leggett, G. Evaluation of Foamed Nickel Photocatalytic Filters for an Air Cleaner on Removal of Formaldehyde in the Indoor Environment. *Optik* **2021**, *244*, 167550. [CrossRef]
191. Feng, S.; Li, D.; Low, Z.; Liu, Z.; Zhong, Z.; Hu, Y.; Wang, Y.; Xing, W. ALD-Seeded Hydrothermally-Grown Ag/ZnO Nanorod PTFE Membrane as Efficient Indoor Air Filter. *J. Membr. Sci.* **2017**, *531*, 86–93. [CrossRef]
192. Wu, C. Facile One-Step Synthesis of N-Doped ZnO Micropolyhedrons for Efficient Photocatalytic Degradation of Formaldehyde under Visible-Light Irradiation. *Appl. Surf. Sci.* **2014**, *319*, 237–243. [CrossRef]
193. Wang, J.; Zhang, G.; Zhang, P. Graphene-Assisted Photothermal Effect on Promoting Catalytic Activity of Layered MnO_2 for Gaseous Formaldehyde Oxidation. *Appl. Catal. B Environ.* **2018**, *239*, 77–85. [CrossRef]
194. Wang, J.; Zhang, P.; Li, J.; Jiang, C.; Yunus, R.; Kim, J. Room-Temperature Oxidation of Formaldehyde by Layered Manganese Oxide: Effect of Water. *Environ. Sci. Technol.* **2015**, *49*, 12372–12379. [CrossRef] [PubMed]
195. Luévano-Hipólito, E.; Martínez-De La Cruz, A.; López-Cuellar, E.; Yu, Q.L.; Brouwers, H.J.H. Synthesis, Characterization and Photocatalytic Activity of WO_3/TiO_2 for NO Removal under UV and Visible Light Irradiation. *Mater. Chem. Phys.* **2014**, *148*, 208–213. [CrossRef]
196. Huang, Y.; Long, B.; Tang, M.; Rui, Z.; Balogun, M.-S.; Tong, Y.; Ji, H. Bifunctional Catalytic Material: An Ultrastable and High-Performance Surface Defect CeO_2 Nanosheets for Formaldehyde Thermal Oxidation and Photocatalytic Oxidation. *Appl. Catal. B Environ.* **2016**, *181*, 779–787. [CrossRef]
197. Lu, C.-C.; Alshahrani, T.; Wu, R.-J.; Fegade, U.; Jethave, G.; Al-Ahmed, A.; Khan, F.; Kolate, S. Synthesis of CeO_2–$BiVO_4$ Nano Photocatalyst Material and Used for the Degradation of Gaseous Formaldehyde. *Opt. Mater.* **2023**, *144*, 114310. [CrossRef]
198. Kumar, S.; Bhattacharya, B. Variation of Band Gap in CdPbS with Composition Prepared by a Precipitation Technique. 2005. Available online: https://nopr.niscpr.res.in/handle/123456789/8844 (accessed on 3 February 2025).
199. Fermín, D.J.; Ponomarev, E.A.; Peter, L.M. A Kinetic Study of CdS Photocorrosion by Intensity Modulated Photocurrent and Photoelectrochemical Impedance Spectroscopy. *J. Electroanal. Chem.* **1999**, *473*, 192–203. [CrossRef]
200. Hernández-Torres, M.; Ojeda-Carrera, M.; Sánchez-Cantú, M.; Silva-González, N.; Gracia-Jiménez, J. CdS/TiO_2 Composite Films for Methylene Blue Photodecomposition under Visible Light Irradiation and Non-Photocorrosion of Cadmium Sulfide. *Chem. Pap.* **2014**, *68*, 1257–1264. [CrossRef]
201. Liu, Z.; Fang, P.; Wang, S.; Gao, Y.; Chen, F.; Zheng, F.; Liu, Y.; Dai, Y. Photocatalytic Degradation of Gaseous Benzene with CdS-Sensitized TiO_2 Film Coated on Fiberglass Cloth. *J. Mol. Catal. A Chem.* **2012**, *363*, 159–165. [CrossRef]
202. Dong, W.; Pan, F.; Xu, L.; Zheng, M.; Sow, C.H.; Wu, K.; Xu, G.Q.; Chen, W. Facile Synthesis of CdS@ TiO_2 Core–Shell Nanorods with Controllable Shell Thickness and Enhanced Photocatalytic Activity under Visible Light Irradiation. *Appl. Surf. Sci.* **2015**, *349*, 279–286. [CrossRef]
203. Wang, Q.; Gao, Q.; Al-Enizi, A.M.; Nafady, A.; Ma, S. Recent Advances in MOF-Based Photocatalysis: Environmental Remediation under Visible Light. *Inorg. Chem. Front.* **2020**, *7*, 300–339. [CrossRef]
204. Chen, J.; Cheng, F.; Luo, D.; Huang, J.; Ouyang, J.; Nezamzadeh-Ejhieh, A.; Khan, M.S.; Liu, J.; Peng, Y. Recent Advances in Ti-Based MOFs in Biomedical Applications. *Dalton Trans.* **2022**, *51*, 14817–14832. [CrossRef] [PubMed]
205. Bai, Y.; Dou, Y.; Xie, L.-H.; Rutledge, W.; Li, J.-R.; Zhou, H.-C. Zr-Based Metal–Organic Frameworks: Design, Synthesis, Structure, and Applications. *Chem. Soc. Rev.* **2016**, *45*, 2327–2367. [CrossRef] [PubMed]
206. Du, C.; Zhang, Y.; Zhang, Z.; Zhou, L.; Yu, G.; Wen, X.; Chi, T.; Wang, G.; Su, Y.; Deng, F. Fe-Based Metal Organic Frameworks (Fe-MOFs) for Organic Pollutants Removal via Photo-Fenton: A Review. *Chem. Eng. J.* **2022**, *431*, 133932. [CrossRef]
207. Kong, L.; Chen, Q.; Shen, X.; Xu, Z.; Xu, C.; Ji, Z.; Zhu, J. MOF Derived Nitrogen-Doped Carbon Polyhedrons Decorated on Graphitic Carbon Nitride Sheets with Enhanced Electrochemical Capacitive Energy Storage Performance. *Electrochim. Acta* **2018**, *265*, 651–661. [CrossRef]
208. Wang, C.-C.; Wang, X.; Liu, W. The Synthesis Strategies and Photocatalytic Performances of TiO_2/MOFs Composites: A State-of-the-Art Review. *Chem. Eng. J.* **2020**, *391*, 123601. [CrossRef]
209. Gupta, N.K.; Bae, J.; Kim, S.; Kim, K.S. Fabrication of Zn-MOF/ZnO Nanocomposites for Room Temperature H_2S Removal: Adsorption, Regeneration, and Mechanism. *Chemosphere* **2021**, *274*, 129789. [CrossRef] [PubMed]

210. Deng, X.; Li, Z.; García, H. Visible Light Induced Organic Transformations Using Metal-Organic-Frameworks (MOFs). *Chem. A Eur. J.* **2017**, *23*, 11189–11209. [CrossRef] [PubMed]
211. Xia, T.; Lin, Y.; Li, W.; Ju, M. Photocatalytic Degradation of Organic Pollutants by MOFs Based Materials: A Review. *Chin. Chem. Lett.* **2021**, *32*, 2975–2984. [CrossRef]
212. Wen, M.; Mori, K.; Kuwahara, Y.; An, T.; Yamashita, H. Design and Architecture of Metal Organic Frameworks for Visible Light Enhanced Hydrogen Production. *Appl. Catal. B Environ.* **2017**, *218*, 555–569. [CrossRef]
213. Yao, T.; Tan, Y.; Zhou, Y.; Chen, Y.; Xiang, M. Preparation of Core-Shell MOF-5/Bi_2WO_6 Composite for the Enhanced Photocatalytic Degradation of Pollutants. *J. Solid State Chem.* **2022**, *308*, 122882. [CrossRef]
214. Dai, H.; Yuan, X.; Jiang, L.; Wang, H.; Zhang, J.; Zhang, J.; Xiong, T. Recent Advances on ZIF-8 Composites for Adsorption and Photocatalytic Wastewater Pollutant Removal: Fabrication, Applications and Perspective. *Coord. Chem. Rev.* **2021**, *441*, 213985. [CrossRef]
215. Zhang, Z.; Xian, S.; Xi, H.; Wang, H.; Li, Z. Improvement of CO_2 Adsorption on ZIF-8 Crystals Modified by Enhancing Basicity of Surface. *Chem. Eng. Sci.* **2011**, *66*, 4878–4888. [CrossRef]
216. Abdelhamid, H.N. Zeolitic Imidazolate Frameworks (ZIF-8, ZIF-67, and ZIF-L) for Hydrogen Production. *Appl. Organom Chemis* **2021**, *35*, e6319. [CrossRef]
217. Rahmani, A.; Emrooz, H.B.M.; Abedi, S.; Morsali, A. Synthesis and Characterization of CdS/MIL-125 (Ti) as a Photocatalyst for Water Splitting. *Mater. Sci. Semicond. Process.* **2018**, *80*, 44–51. [CrossRef]
218. Kampouri, S.; Nguyen, T.N.; Spodaryk, M.; Palgrave, R.G.; Züttel, A.; Smit, B.; Stylianou, K.C. Concurrent Photocatalytic Hydrogen Generation and Dye Degradation Using MIL-125-NH_2 under Visible Light Irradiation. *Adv. Funct. Mater.* **2018**, *28*, 1806368. [CrossRef]
219. Gul Zaman, H.; Baloo, L.; Kutty, S.R.; Aziz, K.; Altaf, M.; Ashraf, A.; Aziz, F. Insight into Microwave-Assisted Synthesis of the Chitosan-MOF Composite: Pb(II) Adsorption. *Environ. Sci. Pollut. Res.* **2023**, *30*, 6216–6233. [CrossRef]
220. Ao, D.; Zhang, J.; Liu, H. Visible-Light-Driven Photocatalytic Degradation of Pollutants over Cu-Doped NH_2-MIL-125 (Ti). *J. Photochem. Photobiol. A Chem.* **2018**, *364*, 524–533. [CrossRef]
221. Solís, R.R.; Gómez-Avilés, A.; Belver, C.; Rodriguez, J.J.; Bedia, J. Microwave-Assisted Synthesis of NH_2-MIL-125 (Ti) for the Solar Photocatalytic Degradation of Aqueous Emerging Pollutants in Batch and Continuous Tests. *J. Environ. Chem. Eng.* **2021**, *9*, 106230. [CrossRef]
222. Yang, Z.; Xie, H.-S.; Lin, W.-Y.; Chen, Y.-W.; Teng, D.; Cong, X.-S. Enhanced Adsorption–Photocatalytic Degradation of Organic Pollutants via a ZIF-67-Derived Co–N Codoped Carbon Matrix Catalyst. *ACS Omega* **2022**, *7*, 40882–40891. [CrossRef] [PubMed]
223. Li, Y.; Jin, Z.; Zhao, T. Performance of ZIF-67–Derived Fold Polyhedrons for Enhanced Photocatalytic Hydrogen Evolution. *Chem. Eng. J.* **2020**, *382*, 123051. [CrossRef]
224. Karmakar, S.; Barman, S.; Rahimi, F.A.; Maji, T.K. Covalent Grafting of Molecular Photosensitizer and Catalyst on MOF-808: Effect of Pore Confinement toward Visible Light-Driven CO_2 Reduction in Water. *Energy Environ. Sci.* **2021**, *14*, 2429–2440. [CrossRef]
225. Luo, H.; Feng, M.; Wang, W.; Li, X.; Li, X.; Yang, S. CdS QDs Interspersed onto MOF-808 as Adsorptive Photocatalyst for Efficient Visible-Light Driven Degradation of Ciprofloxacin. *J. Alloys Compd.* **2024**, *988*, 174247. [CrossRef]
226. Jiao, Y.; Li, Z.; Ma, Y.; Zhou, G.; Wang, S.; Lu, G. The Studies on Gas Adsorption Properties of MIL-53 Series MOFs Materials. *AIP Adv.* **2017**, *7*, 085009. [CrossRef]
227. Du, J.-J.; Yuan, Y.-P.; Sun, J.-X.; Peng, F.-M.; Jiang, X.; Qiu, L.-G.; Xie, A.-J.; Shen, Y.-H.; Zhu, J.-F. New Photocatalysts Based on MIL-53 Metal–Organic Frameworks for the Decolorization of Methylene Blue Dye. *J. Hazard. Mater.* **2011**, *190*, 945–951. [CrossRef] [PubMed]
228. Gao, Y.; Li, S.; Li, Y.; Yao, L.; Zhang, H. Accelerated Photocatalytic Degradation of Organic Pollutant over Metal-Organic Framework MIL-53 (Fe) under Visible LED Light Mediated by Persulfate. *Appl. Catal. B Environ.* **2017**, *202*, 165–174. [CrossRef]
229. He, H.; Li, R.; Yang, Z.; Chai, L.; Jin, L.; Alhassan, S.I.; Ren, L.; Wang, H.; Huang, L. Preparation of MOFs and MOFs Derived Materials and Their Catalytic Application in Air Pollution: A Review. *Catal. Today* **2021**, *375*, 10–29. [CrossRef]
230. Mosconi, E.; Umari, P.; De Angelis, F. Electronic and Optical Properties of MAPbX 3 Perovskites (X= I, Br, Cl): A Unified DFT and GW Theoretical Analysis. *Phys. Chem. Chem. Phys.* **2016**, *18*, 27158–27164. [CrossRef] [PubMed]
231. Ray, S.K.; Cho, J.; Hur, J. A Critical Review on Strategies for Improving Efficiency of $BaTiO_3$-Based Photocatalysts for Wastewater Treatment. *J. Environ. Manag.* **2021**, *290*, 112679. [CrossRef] [PubMed]
232. Xiao, Z.; Zhou, Y.; Hosono, H.; Kamiya, T.; Padture, N.P. Bandgap Optimization of Perovskite Semiconductors for Photovoltaic Applications. *Chem. A Eur. J.* **2018**, *24*, 2305–2316. [CrossRef] [PubMed]
233. Li, P.; Lin, Y.; Ma, M.; Wang, Q.; Zhang, M.; Li, J.; Maheskumar, V.; Wang, Z.; Jiang, Z.; Zhang, R. Effect of Pressure on Photocatalytic Water Splitting Performance of Z-Scheme RP/CH3NH3PbI3 Perovskite Heterostructure. *Int. J. Hydrog. Energy* **2022**, *47*, 8091–8104. [CrossRef]
234. Bresolin, B.M. Synthesis and Performance of Metal-Halide Perovskites as New Visible Light Photocatalysts. 2021. Available online: https://lutpub.lut.fi/handle/10024/162090 (accessed on 3 February 2025).

235. Zhao, Y.; Wang, Y.; Liang, X.; Shi, H.; Wang, C.; Fan, J.; Hu, X.; Liu, E. Enhanced Photocatalytic Activity of Ag-$CsPbBr_3$/CN Composite for Broad Spectrum Photocatalytic Degradation of Cephalosporin Antibiotics 7-ACA. *Appl. Catal. B Environ.* **2019**, *247*, 57–69. [CrossRef]
236. Zhang, Z.; Li, L.; Jiang, Y.; Xu, J. Step-Scheme Photocatalyst of $CsPbBr_3$ Quantum Dots/BiOBr Nanosheets for Efficient CO_2 Photoreduction. *Inorg. Chem.* **2022**, *61*, 3351–3360. [CrossRef]
237. Zhou, D.-Y.; Su, W.-T.; Li, X.-Y.; Hong, T.; Pan, G.-Y.; Xu, M.-L.; Liu, F.-T.; Li, K. Self-Assembly of $MAPbBr_3$/Pb-MOF Heterostructures with Enhanced Photocatalytic CO_2 Reduction Performance and Stability. *J. Mater. Chem. C* **2023**, *11*, 15700–15705. [CrossRef]
238. Zhou, Z.; Xu, J.; Liu, Y.; Wei, C.; Zhang, H.; Wang, Q. Zn-Alloyed $MAPbBr_3$ Crystals with Improved Thermoelectric and Photocatalytic Properties. *Mater. Chem. Front.* **2021**, *5*, 8319–8332. [CrossRef]
239. Zhao, Z.; Wu, J.; Zheng, Y.-Z.; Li, N.; Li, X.; Ye, Z.; Lu, S.; Tao, X.; Chen, C. Stable Hybrid Perovskite MAPb $(I_{1-x}Br_x)_3$ for Photocatalytic Hydrogen Evolution. *Appl. Catal. B Environ.* **2019**, *253*, 41–48. [CrossRef]
240. He, Z.; Tang, Q.; Liu, X.; Yan, X.; Li, K.; Yue, D. Lead-Free $Cs_2AgBiBr_6$ Perovskite with Enriched Surface Defects for Efficient Photocatalytic Hydrogen Evolution. *Energy Fuels* **2021**, *35*, 15005–15009. [CrossRef]
241. Wang, B.; Yao, S.; Peng, Y.; Xu, Y. Toluene Removal over TiO_2-$BaTiO_3$ Catalysts in an Atmospheric Dielectric Barrier Discharge. *J. Environ. Chem. Eng.* **2018**, *6*, 3819–3826. [CrossRef]
242. Dasireddy, V.D.; Likozar, B. Photocatalytic CO_2 Reduction to Methanol over Bismuth Promoted $BaTiO_3$ Perovskite Nanoparticle Catalysts. *Renew. Energy* **2022**, *195*, 885–895. [CrossRef]
243. Shan, J.; Raziq, F.; Humayun, M.; Zhou, W.; Qu, Y.; Wang, G.; Li, Y. Improved Charge Separation and Surface Activation via Boron-Doped Layered Polyhedron $SrTiO_3$ for Co-Catalyst Free Photocatalytic CO_2 Conversion. *Appl. Catal. B Environ.* **2017**, *219*, 10–17. [CrossRef]
244. Mai, X.T.; Bui, D.N.; Pham, V.K.; Nguyen, T.H.L.; Nguyen, T.T.L.; Chau, H.D.; Tran, T.K.N. Effect of CuO Loading on the Photocatalytic Activity of $SrTiO_3$ for Hydrogen Evolution. *Inorganics* **2022**, *10*, 130. [CrossRef]
245. Chang, C.-W.; Hu, C. Graphene Oxide-Derived Carbon-Doped $SrTiO_3$ for Highly Efficient Photocatalytic Degradation of Organic Pollutants under Visible Light Irradiation. *Chem. Eng. J.* **2020**, *383*, 123116. [CrossRef]
246. Krukowska, A.; Trykowski, G.; Lisowski, W.; Klimczuk, T.; Winiarski, M.J.; Zaleska-Medynska, A. Monometallic Nanoparticles Decorated and Rare Earth Ions Doped $KTaO_3$/$K2Ta_2O_6$ Photocatalysts with Enhanced Pollutant Decomposition and Improved H_2 Generation. *J. Catal.* **2018**, *364*, 371–381. [CrossRef]
247. Sasahara, A.; Kimura, K.; Sudrajat, H.; Happo, N.; Hayashi, K.; Onishi, H. $KTaO_3$ Wafers Doped with Sr or La Cations for Modeling Water-Splitting Photocatalysts: 3D Atom Imaging around Doping Cations. *J. Phys. Chem. C* **2022**, *126*, 19745–19755. [CrossRef]
248. Różańska, A.; Namieśnik, J. $KTaO_3$ a Perovskite for Water and Air Treatment. *World Sci. News* **2017**, *75*, 73–80.
249. Dias, J.A.; Andrade, M.A.S.; Santos, H.L.S.; Morelli, M.R.; Mascaro, L.H. Lanthanum-Based Perovskites for Catalytic Oxygen Evolution Reaction. *ChemElectroChem* **2020**, *7*, 3173–3192. [CrossRef]
250. Zhang, L.; Nie, Y.; Hu, C.; Qu, J. Enhanced Fenton Degradation of Rhodamine B over Nanoscaled Cu-Doped $LaTiO_3$ Perovskite. *Appl. Catal. B Environ.* **2012**, *125*, 418–424. [CrossRef]
251. Wang, Q.; Ma, M.; Wu, X.; Qin, W. Comparison of Carrier Dynamic Behavior and Photocatalytic Molecular Oxygen Activation of Optimized $MAPbX_3$ (X = I, Br). *J. Environ. Chem. Eng.* **2020**, *8*, 104241. [CrossRef]
252. Yang, R.; Fan, Y.; Zhang, Y.; Mei, L.; Zhu, R.; Qin, J.; Hu, J.; Chen, Z.; Hau Ng, Y.; Voiry, D.; et al. 2D Transition Metal Dichalcogenides for Photocatalysis. *Angew. Chem.* **2023**, *135*, e202218016. [CrossRef]
253. Cao, Y. Roadmap and Direction toward High-Performance MoS_2 Hydrogen Evolution Catalysts. *ACS Nano* **2021**, *15*, 11014–11039. [CrossRef] [PubMed]
254. Singh, S.; Modak, A.; Pant, K.K.; Sinhamahapatra, A.; Biswas, P. MoS_2–Nanosheets-Based Catalysts for Photocatalytic CO_2 Reduction: A Review. *ACS Appl. Nano Mater.* **2021**, *4*, 8644–8667. [CrossRef]
255. Amaral, L.O.; Daniel-da-Silva, A.L. MoS_2 and MoS_2 Nanocomposites for Adsorption and Photodegradation of Water Pollutants: A Review. *Molecules* **2022**, *27*, 6782. [CrossRef] [PubMed]
256. Yuan, P.; Zhou, Q.; Hu, X. WS_2 Nanosheets at Noncytotoxic Concentrations Enhance the Cytotoxicity of Organic Pollutants by Disturbing the Plasma Membrane and Efflux Pumps. *Environ. Sci. Technol.* **2020**, *54*, 1698–1709. [CrossRef] [PubMed]
257. Ismail, P.M.; Ali, S.; Raziq, F.; Bououdina, M.; Abu-Farsakh, H.; Xia, P.; Wu, X.; Xiao, H.; Ali, S.; Qiao, L. Stable and Robust Single Transition Metal Atom Catalyst for CO_2 Reduction Supported on Defective WS_2. *Appl. Surf. Sci.* **2023**, *624*, 157073. [CrossRef]
258. Cheng, L.; Huang, W.; Gong, Q.; Liu, C.; Liu, Z.; Li, Y.; Dai, H. Ultrathin WS_2 Nanoflakes as a High-Performance Electrocatalyst for the Hydrogen Evolution Reaction. *Angew. Chem. Int. Ed.* **2014**, *53*, 7860–7863. [CrossRef]
259. Nguyen, T.P.; Choi, S.; Jeon, J.-M.; Kwon, K.C.; Jang, H.W.; Kim, S.Y. Transition Metal Disulfide Nanosheets Synthesized by Facile Sonication Method for the Hydrogen Evolution Reaction. *J. Phys. Chem. C* **2016**, *120*, 3929–3935. [CrossRef]

260. Telkhozhayeva, M.; Hirsch, B.; Konar, R.; Teblum, E.; Lavi, R.; Weitman, M.; Malik, B.; Moretti, E.; Nessim, G.D. 2D TiS_2 Flakes for Tetracycline Hydrochloride Photodegradation under Solar Light. *Appl. Catal. B Environ.* **2022**, *318*, 121872. [CrossRef]
261. Yang, S.; Shao, C.; Zhou, X.; Li, X.; Tao, R.; Li, X.; Liu, S.; Liu, Y. $MoSe_2/TiO_2$ Nanofibers for Cycling Photocatalytic Removing Water Pollutants under UV–Vis–NIR Light. *ACS Appl. Nano Mater.* **2020**, *3*, 2278–2287. [CrossRef]
262. Yin, Y.; Zhang, Y.; Gao, T.; Yao, T.; Zhang, X.; Han, J.; Wang, X.; Zhang, Z.; Xu, P.; Zhang, P.; et al. Synergistic Phase and Disorder Engineering in 1T-$MoSe_2$ Nanosheets for Enhanced Hydrogen-Evolution Reaction. *Adv. Mater.* **2017**, *29*, 1700311. [CrossRef]
263. Singh, A.; Rohilla, J.; Hassan, M.S.; Ingole, P.P.; Santra, P.K.; Ghosh, D.; Sapra, S. $MoSe_2$/SnS Nanoheterostructures for Water Splitting. *ACS Appl. Nano Mater.* **2022**, *5*, 4293–4304. [CrossRef]
264. Wang, Y.; Zhao, S.; Wang, Y.; Laleyan, D.A.; Wu, Y.; Ouyang, B.; Ou, P.; Song, J.; Mi, Z. Wafer-Scale Synthesis of Monolayer WSe_2: A Multi-Functional Photocatalyst for Efficient Overall Pure Water Splitting. *Nano Energy* **2018**, *51*, 54–60. [CrossRef]
265. Madkhali, O. WSe_2–PPy-Based Type-II Heterostructure for Efficient Photocatalytic Removal of Nitrofurazone. *Langmuir* **2024**, *40*, 18525–18534. [CrossRef] [PubMed]
266. Rahman, M.; Davey, K.; Qiao, S. Advent of 2D Rhenium Disulfide (ReS_2): Fundamentals to Applications. *Adv Funct Mater.* **2017**, *27*, 1606129. [CrossRef]
267. Krishnakumar, B.; Imae, T.; Miras, J.; Esquena, J. Synthesis and Azo Dye Photodegradation Activity of ZrS_2–ZnO Nano-Composites. *Sep. Purif. Technol.* **2014**, *132*, 281–288. [CrossRef]
268. Som, N.N.; Jha, P.K. Hydrogen Evolution Reaction of Metal Di-Chalcogenides: ZrS_2, $ZrSe_2$ and Janus ZrSSe. *Int. J. Hydrog. Energy* **2020**, *45*, 23920–23927. [CrossRef]
269. Singh, D.; Gupta, S.K.; Sonvane, Y.; Kumar, A.; Ahuja, R. 2D-HfS_2 as an Efficient Photocatalyst for Water Splitting. *Catal. Sci. Technol.* **2016**, *6*, 6605–6614. [CrossRef]
270. Cheng, J.; Jiang, H.; Cai, L.; Pan, F.; Shi, Y.; Wang, X.; Zhang, X.; Lu, S.; Yang, Y.; Li, L. Porous N-Doped C/VB-Group VS_2 Composites Derived from Perishable Garbage to Synergistically Solve the Environmental and Electromagnetic Pollution. *Chem. Eng. J.* **2023**, *457*, 141208. [CrossRef]
271. Zhong, X.; Tang, J.; Wang, J.; Shao, M.; Chai, J.; Wang, S.; Yang, M.; Yang, Y.; Wang, N.; Wang, S. 3D Heterostructured Pure and N-Doped $Ni3S_2/VS_2$ Nanosheets for High Efficient Overall Water Splitting. *Electrochim. Acta* **2018**, *269*, 55–61. [CrossRef]
272. Kovacic, M.; Papac, J.; Kusic, H.; Karamanis, P.; Bozic, A.L. Degradation of Polar and Non-Polar Pharmaceutical Pollutants in Water by Solar Assisted Photocatalysis Using Hydrothermal TiO_2-SnS_2. *Chem. Eng. J.* **2020**, *382*, 122826. [CrossRef]
273. Ma, H.-Y.; Zhao, L.; Guo, L.-H.; Zhang, H.; Chen, F.-J.; Yu, W.-C. Roles of Reactive Oxygen Species (ROS) in the Photocatalytic Degradation of Pentachlorophenol and Its Main Toxic Intermediates by TiO_2/UV. *J. Hazard. Mater.* **2019**, *369*, 719–726. [CrossRef]
274. Wang, W.-L.; Wu, Q.-Y.; Huang, N.; Xu, Z.-B.; Lee, M.-Y.; Hu, H.-Y. Potential Risks from UV/H_2O_2 Oxidation and UV Photocatalysis: A Review of Toxic, Assimilable, and Sensory-Unpleasant Transformation Products. *Water Res.* **2018**, *141*, 109–125. [CrossRef] [PubMed]
275. Fukuzumi, S.; Ohkubo, K. Selective Photocatalytic Reactions with Organic Photocatalysts. *Chem. Sci.* **2013**, *4*, 561–574. [CrossRef]
276. Lazar, M.A.; Daoud, W.A. Achieving Selectivity in TiO 2-Based Photocatalysis. *RSC Adv.* **2013**, *3*, 4130–4140. [CrossRef]
277. Mendoza-Sánchez, A.R.; Hernández-Rodríguez, Y.M.; Cigarroa-Mayorga, O.E. Degradation of ZnO Nanostructures Interface by Effect of Photocatalytic Activity in Methylene Blue. In Proceedings of the 2021 IEEE International Summer Power Meeting/International Meeting on Communications and Computing (RVP-AI/ROC&C), Acapulco, Mexico, 14–18 November 2021; pp. 1–5.
278. Abela, S.; Farrugia, C.; Xuereb, R.; Lia, F.; Zammit, E.; Rizzo, A.; Refalo, P.; Grech, M. Photocatalytic Activity of Titanium Dioxide Nanotubes Following Long-Term Aging. *Nanomaterials* **2021**, *11*, 2823. [CrossRef] [PubMed]
279. Jimenez-Relinque, E.; Grande, M.; Duran, T.; Castillo, Á.; Castellote, M. Environmental Impact of Nano-Functionalized Construction Materials: Leaching of Titanium and Nitrates from Photocatalytic Pavements under Outdoor Conditions. *Sci. Total Environ.* **2020**, *744*, 140817. [CrossRef]
280. Brovelli, C.; Crispino, M. Photocatalytic Suspension for Road Pavements: Investigation on Wearing and Contaminant Effects. *J. Mater. Civ. Eng.* **2013**, *25*, 548–554. [CrossRef]
281. Hassan, M.M.; Dylla, H.; Mohammad, L.N.; Rupnow, T. Evaluation of the Durability of Titanium Dioxide Photocatalyst Coating for Concrete Pavement. *Constr. Build. Mater.* **2010**, *24*, 1456–1461. [CrossRef]
282. Wei, Y.; Meng, H.; Wu, Q.; Bai, X.; Zhang, Y. TiO_2-Based Photocatalytic Building Material for Air Purification in Sustainable and Low-Carbon Cities: A Review. *Catalysts* **2023**, *13*, 1466. [CrossRef]
283. Sukawaputri, A.M.; Fauziah, I.A.N.; Lestari, I.P.; Arindita, N.P.Y.; Pratiwi, R.N.; Hofifah, S.N.; Nandiyanto, A.B.D. Economic Evaluation of the Production of Titanium Dioxide (TiO_2) Nanoparticles Using the Simple Aqueous Peroxo Route Method. *Int. J. Energetica* **2020**, *5*, 12–17.
284. Nandiyanto, A.B.D.; Ragadhita, H.N.P.R.; Soegoto, S.W. Cost Analysis and Economic Evaluation for TiO_2 Synthesis Using Sol-Gel Method. *Moroc. J. Chem.* **2022**, *10*, 13–21.

285. Montini, T.; Melchionna, M.; Monai, M.; Fornasiero, P. Fundamentals and Catalytic Applications of CeO_2-Based Materials. *Chem. Rev.* **2016**, *116*, 5987–6041. [CrossRef] [PubMed]
286. Michałek, T.; Hessel, V.; Wojnicki, M. Production, Recycling and Economy of Palladium: A Critical Review. *Materials* **2023**, *17*, 45. [CrossRef] [PubMed]
287. da Costa, G.M.; Hussain, C.M. Ethical, Legal, Social and Economics Issues of Graphene. In *Comprehensive Analytical Chemistry*; Elsevier: Amsterdam, The Netherlands, 2020; Volume 91, pp. 263–279.
288. Reches, Y. Nanoparticles as Concrete Additives: Review and Perspectives. *Constr. Build. Mater.* **2018**, *175*, 483–495. [CrossRef]
289. Seremak, W.; Jasiorski, M.; Baszczuk, A.; Winnicki, M. Durability Assessment of Low-Pressure Cold-Sprayed TiO_2 Photocatalytic Coatings: Photocatalytic and Mechanical Stability. *Surf. Coat. Technol.* **2025**, *497*, 131740. [CrossRef]